Turtles in silico: Using computational fluid dynamics to mechanistically niche model leatherback sea turtles.

Ву

Peter N. Dudley

A dissertation submitted in partial fulfillment of the requirements for the degree of

Doctor of Philosophy

(Zoology)

at the

UNIVERSITY OF WISCONSIN-MADISON

2014

Date of final oral examination: 5/15/2014

The dissertation is approved by the following members of the Final Oral Committee:

Warren Porter, Professor, Zoology Riccardo Bonazza, Professor, Engineering Physics

William Karasov, Professor, Department of Forest and Wildlife Ecology

Carol Lee, Professor, Zoology

Benjamin Zuckerberg, Assistant Professor, Department of Forest and Wildlife Ecology

Table of Contents

Dedicationii
Acknowledgementsiii
Abstractiv
General Introduction
Chapter 1 8
Figures
References
Chapter 2
Figures
References70
Chapter 3
Figures
References
Chapter 4
Figures
References
Conclusion
Appendix 1
Appendix 2

I dedicate this work to my parents, Brenda and John Dudley, who set me on a good course and helped guide me along the way.

I would first like to thank Warren Porter for taking a chance on a physicists/engineer with little biological background and allowing me to work in the field of ecology. I would also like to thank the members of my lab, Shu-Ping Huang, Stefanie Buxel-Florenzen, Megan Fitzpatrick, Paul Mathewson, Javier Velasco, and Jeremiah Yah, for help with manuscripts. Thank you to my committee members for being flexible and for insightful suggestions. Thanks to the zoology course coordinators for helping me teach efficiently. Special thanks to Samantha L. Greene for numerous helpful edits on this dissertation.

Abstract

To aid sea turtle conservation, academic literature and government publications state the need to predict future potential sea turtle nesting sites given different global warming scenarios. To accomplish this goal, managers will need to have a clear picture of how sea turtles respond to many combinations of climatic conditions across turtle migratory ranges and between terrestrial nesting sites and adjacent waters. Because global warming will create climatic combinations sea turtles do not currently encounter, assessing the sea turtle response is difficult and a mechanistic model may be the best approach. Our lab has successfully mechanistically niche mapped many terrestrial animals but not yet an aquatic species. As sea turtles are a marine species, the animal-fluid interactions make constructing a highly accurate mechanistic model complicated. The animal-fluid interaction not only affects the turtle's energy use (through thrust and drag) but also the heat transfer with its environment. To solve these issues we combine modern 3D design programs, computation fluid dynamic (CFD) software and in-house programs to construct a realistic, swimming leatherback sea turtle CFD simulation. These simulations allow us to analyze not only the animal-fluid interaction but also the turtle's internal heat transfer. We validate these models with data from the literature and flume and wind tunnel experiments. This simulation provides inputs for a mechanistic niche model, which can predict where leatherbacks can thermally persist both in water and on land. Thus with the niche model output, we can predict future potential nesting sites under different global warming scenarios. We show that global warming threatens leatherbacks with overheating, particularly in South East Asia. We also show that the impact may be less on leatherbacks that shift their nesting time or location or who are smaller. Methods such these

are important to produce accurate maps of regions that will become inhospitable to species under global warming conditions.

General Introduction

Throughout the next century, global warming will likely shift many species' ranges (Parmesan & Yohe 2003). In addition to causing these range shifts, global warming makes predicting species future ranges difficult because it introduces regionally novel sets of abiotic conditions. With these novel circumstances, forming an empirical niche map requires complex statistical methods and may still be inappropriate or inaccurate (Dormann 2007, Phillips et al. 2008). Under global warming conditions, a more appropriate niche mapping approach may be mapping the fundamental niche (Hutchinson 1957) using a biophysical mechanistic niche model. A biophysical model permits any combination of abiotic conditions, novel or otherwise, provided the model can accurately represent how they affect the organism (Kearney & Porter 2009).

While the biophysical niche model approach is successful with terrestrial animals (for example: Kearney, Phillips, Tracy, & Christian, 2008), it is more difficult to implement with aquatic organisms. The main reason for this difficulty is the strong link between heat transfer, metabolic rate and aquatic motion (Boisclair & Tang 1993) and the difficulty in measuring each of these. First, while it is possible to measure metabolic rate for some aquatic animals, it is difficult or impossible to measure it for others. Second, the complex interaction between thrust and drag on a deforming body makes it difficult to determine a moving animal's useful work (Schultz & Webb 2002). Finally, determining how rapidly a self-propelling, aquatic organism loses metabolic waste heat further complicates making a biophysical niche map.

Many methods attempt to address some of these difficulties. Trained live animals can fly/swim in a wind tunnel/flume or while tethered. The animals my wear pressure sensors

(Usherwood 2003, Blake & Chan 2007) or temperature sensors (Tieleman et al. 2003, Marom et al. 2006). There are also non-contact methods such as filming particle flow around an animal and calculating force with software (Drucker and Lauder '99), using cameras to measure reference point movement (Skrovan et al. '99; Tobalske, Peacock, and Dial '99), or using thermal cameras to measure temperature profiles (not possible for aquatic animals) (Ward et al. '99). In addition to logistical and ethical consideration of live animal trials, all these methods have limited resolution and cannot decouple thrust and drag. Modern computational fluid dynamics (CFD) could address many live animal experiments short falls while giving biophysical niche models necessary information to make accurate predictions.

CFD is now allowing researchers to measure drag (Pavlov & Rashad 2012) of static animals and even thrust and power of undulating swimmers (Liu et al. 1997). We use a novel CFD technique to not only measure the power and heat flux form 3D complex animal motion, but also to model animal internal heat transfer accounting for complex physiological issues such as an insulating layer's varying thickness, vasoconstriction and dilation, and counter current heat exchangers. We combine the data from our CDF model (power, heat transfer coefficients, infrared (IR) absorption and radiation, and internal temperature profiles) with global climate models (GCMs) to accurately predict regions within a marine animal's current marine and/or terrestrial range which may become inaccessible under global warming conditions. We examine potential shifts in reproduction time, range, as well as body geometry and size. To our knowledge, this is the first projection of the fundamental niche of an organism using this high level of accuracy, which can only come from CFD and numerical heat transfer models.

To conduct these simulations we chose leatherback sea turtle (*Dermochelys coriacea*) as the focal species. Leatherback sea turtles are the last remaining member of the 90 million year old family Dermochelyidae (Weems 1988). Tragically, they are critically endangered (Martinez 2011). Fishing bycatch (Spotila et al. 1996, Eckert 1997, Lewison et al. 2004), egg poaching (Kaplan 2005, Tapilatu & Tiwari 2007, Tomillo et al. 2008), beach development (Chan et al. 2007, Hernandez et al. 2007, Mazaris et al. 2009, Witherington et al. 2011), and pollution (Barreiros & Barcelos 2001, Bugoni et al. 2001, Mrosovsky et al. 2009) caused the 1980 global nesting population of 115,000 to decline to between 26,200 and 42,900 by 1996 (Spotila et al. 1996). Continued global warming will likely put additional pressure on future leatherback populations.

Adult leatherbacks are especially vulnerable to global warming because they are gigantotherms. Gigantotherms are poikilotherms whose activity and large body size elevates their body temperature considerably above ambient (as much as 18°C for leatherbacks (Bostrom & Jones 2007)) (Paladino et al. 1990). This gigantothermy allows leatherbacks to forage in cold northern waters (e.g. offshore of Nova Scotia, Canada), but also means that they can only persist in waters which can adequately cool them. Thus, a large increase in global temperatures may make tropical waters inhospitably warm for adults.

The leatherback's main prey item is gelatinous zooplankton. Fortunately for leatherbacks and unfortunately for humans, gelatinous zooplankton are increasing (Lilley et al. 2011) and most likely will continue to increase with more anthropogenic disturbance, warming and synergistic affects between the two (Purcell et al. 2007, Kirby et al. 2009). Thus, the leatherback's fundamental niche will likely not be resource-limited. Therefore, our

fundamental niche model will determine the acceptable thermal range of leatherbacks. While two studies have used empirical models to predict leatherback populations and nesting sites under global warming conditions (Saba et al. 2012, Pike 2013), ours is the first study to use a mechanistic model to fundamental niche maps of leatherbacks under global warming conditions.

References

- Barreiros JP, Barcelos J (2001) Plastic ingestion by a leatherback turtle (*Dermochelys coriacea*) from the Azores (NE Atlantic). Mar Pollut Bull 42:1196–1197
- Blake RW, Chan KHS (2007) Swimming in the upside down catfish synodontis nigriventris: It matters which way is up. J Exp Biol 210:2979–89
- Boisclair D, Tang M (1993) Empirical analysis of the influence of swimming pattern on the net energetic cost of swimming in fishes. J Fish Biol 42:169–183
- Bostrom BL, Jones DR (2007) Exercise warms adult leatherback turtles. Comp Biochem Physiol Part A Mol Integr Physiol 147:323–31
- Bugoni L, Krause L, Petryà MV (2001) Marine debris and human impacts on sea turtles in Southern Brazil. Mar Pollut Bull 42:1330–1334
- Chan SKF, Cheng IJ, Zhou T, Wang HJ (2007) A comprehensive overview of the population and conservation status of sea turtles in China. Chelonian Conserv Biol 6:185–198
- Dormann CF (2007) Promising the future? Global change projections of species distributions.

 Basic Appl Ecol 8:387–397
- Drucker E, Lauder G (1999) Locomotor forces on a swimming fish: Three-dimensional vortex wake dynamics quantified using digital particle image velocimetry. J Exp Biol 202:2393–2412
- Eckert SA (1997) Distant fisheries implicated in the loss of the worlds largest leatherback nesting population. Mar Turt Newsl 78:2–7
- Hernandez R, Buitrago J, Guada H, Hernandez-Hamon H, Llano M (2007) Nesting distribution and hatching success of the Leatherback, *Dermochelys coriacea*, in relation to human pressures at Playa Parguito, Margarita Island, Venezuela. Chelonian Conserv Biol 6:79–86
- Hutchinson EG (1957) Concluding remarks. In: Cold Spring Harbor Symposia on Quantitative Biology.p 415–42782
- Kaplan IC (2005) A risk assessment for Pacific leatherback turtles (*Dermochelys coriacea*). Can J Fish Aquat 1719:1710–1719
- Kearney M, Phillips B, Tracy C, Christian K (2008) Modelling species distributions without using species distributions: The cane toad in Australia under current and future climates. Ecography (Cop):1–12

- Kearney M, Porter W (2009) Mechanistic niche modelling: combining physiological and spatial data to predict species' ranges. Ecol Lett 12:334–50
- Kirby RR, Beaugrand G, Lindley JA (2009) Synergistic effects of climate and fishing in a marine ecosystem. Ecosystems 12:548–561
- Lewison RL, Freeman SA, Crowder LB (2004) Quantifying the effects of fisheries on threatened species: the impact of pelagic longlines on loggerhead and leatherback sea turtles. Ecol Lett 7:221–231
- Lilley MKS, Beggs SE, Doyle TK, Hobson VJ, Stromberg KHP, Hays GC (2011) Global patterns of epipelagic gelatinous zooplankton biomass. Mar Biol 158:2429–2436
- Liu H, Wassersug R, Kawachi K (1997) The three-dimensional hydrodynamics of tadpole locomotion. J Exp Biol 200:2807–19
- Marom S, Korine C, Wojciechowski MS, Tracy CR, Pinshow B (2006) Energy metabolism and evaporative water loss in the European free-tailed bat and Hemprich's long-eared bat (*Microchiroptera*): species sympatric in the Negev Desert. Physiol Biochem Zool 79:944–56
- Martinez S (2011) Dermochelys coriacea. IUCN Red List Threat Species
- Mazaris AD, Matsinos G, Pantis JD (2009) Evaluating the impacts of coastal squeeze on sea turtle nesting. Ocean Coast Manag 52:139–145
- Mrosovsky N, Ryan GD, James MC (2009) Leatherback turtles: the menace of plastic. Mar Pollut Bull 58:287–9
- Paladino FV, O'Connor MP, Spotila JR (1990) Metabolism of leatherback turtles, gigantothermy, and thermoregulation of dinosaurs. Nature 344:858–860
- Parmesan C, Yohe G (2003) A globally coherent fingerprint of climate change impacts across natural systems. Nature 421:37–42
- Pavlov V V., Rashad AM (2012) A non-invasive dolphin telemetry tag: Computer design and numerical flow simulation. Mar Mammal Sci 28:E16–E27
- Phillips B, Chipperfield J, Kearney M (2008) The toad ahead: Challenges of modelling the range and spread of an invasive species. Wildl Res 35:222
- Pike D a. (2013) Climate influences the global distribution of sea turtle nesting. Glob Ecol Biogeogr 22:555–566

- Purcell JE, Uye S, Lo W (2007) Anthropogenic causes of jellyfish blooms and their direct consequences for humans: a review. Mar Ecol Prog Ser 350:153–174
- Saba V, Stock C, Spotila J (2012) Projected response of an endangered marine turtle population to climate change. Nat Clim Chang 2:814–820
- Schultz W, Webb P (2002) Power requirements of swimming: Do new methods resolve old questions? Integr Comp Biol 1025:1018–1025
- Skrovan RC, Williams TM, Berry PS, Moore PW, Davis RW (1999) The diving physiology of bottlenose dolphins (*Tursiops truncatus*). J Exp Biol 202:2749–2761
- Spotila JR, Dunham AE, Leslie AJ, Steyermark AC, Plotkin PT, Paladino F V. (1996) Worldwide population decline of *Dermochelys coriacea*: Are leatherback turtles going extinct? Chelonian Conserv Biol 2:209–222
- Tapilatu RF, Tiwari M (2007) Leatherback turtle, *Dermochelys coriacea*, hatching success at Jamursba-Medi and Wermon beaches in Papua, Indonesia. Chelonian Conserv Biol 6:150–158
- Tieleman B, Williams J, Buschur M, Brown CR (2003) Phenotypic variation of larks along an aridity gradient: are desert birds more flexible? Ecology 84:1800–1815
- Tobalske B, Peacock W, Dial K (1999) Kinematics of flap-bounding flight in the zebra finch over a wide range of speeds. J Exp Biol 202:1725–39
- Tomillo PS, Saba VS, Piedra R, Paladino F V, Spotila JR (2008) Effects of illegal harvest of eggs on the population decline of leatherback turtles in Las Baulas Marine National Park, Costa Rica. Conserv Biol 22:1216–24
- Usherwood JR (2003) The aerodynamics of avian take-off from direct pressure measurements in Canada geese (*Branta canadensis*). J Exp Biol 206:4051–4056
- Ward S, Rayner J, MOLler U, Jackson D, Nachtigall W, Speakman J (1999) Heat transfer from starlings sturnus vulgaris during flight. J Exp Biol 202:1589–602
- Weems R (1988) Paleocene turtles from the Aquia and Brightseat formations, with a discussion of their bearing on sea turtle evolution and phylogeny. Proc Biol Soc Washingt 101:109–145
- Witherington B, Hirama S, Mosier A (2011) Barriers to Sea Turtle Nesting on Florida (United States) Beaches: Linear Extent and Changes Following Storms. J Coast Res 27:450–458

8

Chapter 1: Using empirical and mechanistic models to assess global warming threats to

leatherback sea turtles

<u>Authors:</u> Peter N. Dudley and Warren P. Porter

Department of Zoology, University of Wisconsin-Madison

Abstract

Global warming may pose a greater risk to species with unique thermal requirements during

each life stage than species with similar thermal requirement throughout all life stages. The

risk to these certain species is higher because their unique thermal ranges may become

geographically or temporally discontiguous. Additionally, modeling global warming's effects on

these animals is challenging due to their multiple thermal requirements. We explore these

issues using leatherback sea turtles (Dermochelys coriacea) as a study species. The

gigantothermy of adult leatherbacks and their subterranean egg incubation means global

warming will differentially affect adults and eggs. To assess the unique thermal requirements in

each life stage we use two distinct modeling approaches. We use a mechanistic

biophysical/physiological model to assess threats to adult leatherbacks, and Bayesian

regression with a mechanistic microclimate model to assess threats to leatherback eggs. We

combined these models with a comprehensive literature search and a global climate model to

establish the future thermal threats to the egg and adult leatherback life stages at three major

rockeries (Gabon, French Guiana, and West Papua). We found that adult internesting and

nesting core temperatures will not rise above the critical thermal maximum; however, at two of

the three sites, adult core body temperatures will rise above the point where hatchlings experience uncoordinated movement. We also found that increased temperatures will greatly reduce success rates of egg clutches in West Papua and Gabon by the end of the 21st century.

Introduction

Global warming poses a special risk to organisms with unique thermal requirements in each life stage because these required thermal conditions may become geographically or temporally disconnected. Modeling each life stage of a species under projected future climates may reveal during which part of their life cycle a species is most at risk. Depending on data accessibility and understanding of ecological processes and physiological mechanisms, different model classes may be more appropriate for assessing climatic threat to a species in different life stages. This paper demonstrates the use of a mechanistic microclimate model combined with a biophysical/physiological model or an empirical model to assess global warming threats to adult leatherback sea turtles or their eggs, respectively.

Leatherback sea turtles (*Dermochelys coriacea* (Vandelli 1761)) are the last remaining member of the 90 million year old family Dermochelyidae (Weems 1988). Tragically, they are critically endangered (Martinez 2011). Fishing bycatch (Spotila et al. 1996, Eckert 1997, Lewison et al. 2004), egg poaching (Kaplan 2005, Tapilatu & Tiwari 2007, Tomillo et al. 2008), beach development (Chan et al. 2007, Hernandez et al. 2007, Mazaris et al. 2009, Witherington et al. 2011), and pollution (Barreiros & Barcelos 2001, Bugoni et al. 2001, Mrosovsky et al. 2009) caused the 1980 global nesting population of 115,000 to decline to between 26,200 and

42,900 by 1996 (Spotila et al. 1996). Continued global warming will likely put additional pressure on future leatherback populations.

Adult leatherbacks are especially vulnerable to global warming because they are gigantotherms. Gigantotherms are poikilotherms whose activity and large body size elevates their body temperature considerably above ambient (as much as 18°C for leatherbacks (Bostrom & Jones 2007)) (Paladino et al. 1990). This gigantothermy allows leatherbacks to forage in cold northern waters (e.g. offshore of Nova Scotia, Canada), but also means that they can only persist in waters which can adequately cool them. Global warming could also threaten leatherback hatchlings as their success (percent that hatch and escape the nest) may also be temperature dependent (Spotila 2004). Some studies found no relation between temperature and leatherback hatchling success (Wallace et al. 2012), but, like those of other reptiles, a leatherback embryo's growth and water uptake may be negatively correlated with temperature (Packard et al. 1987, Spotila & Zimmerman 1994, Lin et al. 2005). Thus, a large increase in global temperatures may make tropical waters inhospitably warm for adults and reduce hatchling success.

While two studies have used empirical models to predict leatherback populations and nesting sites under global warming conditions (Saba et al. 2012, Pike 2013), ours is the first study to use a mechanistic model to predict actual leatherback core temperatures under global warming conditions. To predict these temperatures we combined morphological, and behavioral data from the literature, a global climate model (GCM), and a novel transient and steady state biophysical/physiological model using an "effective insulating layer thickness" to calculate adult core body temperatures during nesting (while on land for oviposition) and

11

internesting (time in water between nestings). The literature and GCM data were also the

inputs for a meta-analysis using Bayesian regression to determine if hatchling success

negatively correlates with temperature. We then estimate the most credible future hatchling

success rates. With these methods, this paper attempted to answer the following questions.

First, how will temperature increases change adult core temperatures during nesting and

internesting at prominent leatherback nesting sites? Second, will core temperature changes

cause leatherback ranges to diverge from the equator? Third, how will temperature increases

affect hatchling success rates?

Our study only examines global warming's effects on leatherback adult core

temperatures and hatchling success. For an overview of global warming's many threats

(increased air and ocean temperature, sea level rise, skewed sex ratios, reduced hatchling

success, ocean acidification and changing large-scale ocean-atmosphere patterns) to all sea

turtle species the reader should consult the several comprehensive reviews (Poloczanska et al.

2009, Hawkes et al. 2009, Hamann et al. 2013). In addition there are many articles covering

proposed or implemented sea turtle management strategies under global warming (general

review (Fuentes et al. 2012), threat assessment (Garcon & Grech 2010, Donlan et al. 2010,

Fuentes & Cinner 2010, Fuentes et al. 2011), regional management units (Fuentes et al. 2013),

climate-smart practices (Hansen et al. 2010), and marine protected areas (Hooker et al. 2011)).

Materials and Methods

Literature search: Adult thermal effects

To aggregate current leatherback thermal and range data, we searched Web of Science using a combination of synonyms for leatherback, distribution, and thermal tolerance. Of the initial 131 results, we eliminated 97 articles based on title or abstract. Usable thermal range data was in 13 of the remaining articles. These 13 papers used one of three methods to measure ambient water temperatures around leatherbacks. Three studies matched fisherman and public leatherback sightings in their northern foraging waters (hence forth "foraging leatherbacks") with water temperature at the sighting location (McMahon & Hays 2006, James, Sherrill-Mix, et al. 2006, James et al. 2007). Two articles had trackers measuring water temperature on foraging leatherbacks and one had water temperatures from bycatch incidents (Goff & Lien 1988, James & Mrosovsky 2004, James, Davenport, et al. 2006). Nine articles had trackers on internesting leatherbacks (Southwood et al. 1999, 2005, James, Davenport, et al. 2006, Sherrill-Mix et al. 2007, Shillinger et al. 2008, Fossette et al. 2009, López-Mendilaharsu et al. 2009, Casey et al. 2010, Witt et al. 2011). We calculated a weighted average and weighted standard deviation for these three sets of temperature data. In addition to measuring ambient temperatures, three studies measured internal body temperatures with deep cloaca probes or ingested data loggers. The cloaca probe study was in foraging waters (James & Mrosovsky 2004) and the two data logger studies were during internesting (Southwood et al. 2005, Casey et al. 2010). We calculated a weighted average body temperature from the two internesting studies.

Wallace and Jones (2008) aggregated metabolic data from marine turtles. We pulled from these studies average leatherback metabolic rates for internesting (Wallace *et al.*

2005), crawling (Paladino *et al.* 1990, 1996), oviposition (Lutcavage et al. 1992, Paladino et al. 1996), and nest covering (Paladino *et al.* 1990).

Biophysical/Physiological model

The biophysical/physiological model had two stages, a steady state stage when the leatherback is in water and a transient stage when the leatherback is nesting (outlined in Fig. 1). Both stages used an ellipsoid (the 3D analogue of an ellipse) shape to approximate the leatherback. The ratios of the ellipsoid semi-principal axes corresponded to the ratio of leatherback body dimensions measured from images. We used nine leatherback images where the perspective allowed us to measure a ratio without distortions (Fig. 2) (Skerry 2009, Perrine 2010, National Park Service 2010, 2013, Goeorges 2011, Majza 2012, Bioexpedition.com 2013, Isley 2013, Project 2013). As leatherbacks are close to neutrally buoyant, we set the turtle tissue to the same density as seawater, and set the ellipsoid volume so its mass matched the leatherback's mass. We used two turtle sizes (curved carapace length (CCL) 125 and 172 cm, mass 197 and 593 kg) based on the size range James et al. (2007) documented. We divided the ellipsoid into two regions. The first was a core region with uniform temperature, and the second was an insulating layer.

The first stage (steady state internesting model) used the current average temperature difference we calculated above between internesting water and the leatherback core to calculate an "effective insulating layer thickness." "Effective insulating layer thickness" means a fat layer thickness that would result in the ellipsoid leatherback having the same temperature difference as real leatherbacks. Thus, this "effective insulating layer thickness" uses a single number to represent leatherback's total insulating capabilities, including flippers, soft head and

neck skin, and fat insulation around the body cavity. The effective insulating layer thickness is not meant to accurately predict the fat layer thickness in a leatherback, but rather to represent a leatherback's insulating capabilities. We set the size, ambient temperature and core temperature in our steady state model to the averages from the two studies reporting core and ambient temperatures. We then solved for an effective insulating layer thickness. We scaled this thickness to the two leatherback sizes in our model. McMahon and Hays (2006) showed leatherbacks behaviorally cool themselves during their internesting period. Thus, we assumed that this effective insulating layer thickness represented the minimum achievable physiological insulation of a leatherback.

In the second stage (transient nesting model), we used the same core volume and effective insulating layer as the steady state internesting model (Fig. 3). The transient nesting model divided the turtle's surface into two regions. One region was in contact with the ground and transferred heat by conduction. This region was either 40 or 50 percent of the leatherback's surface area and matched the portion of the leatherback's surface in contact with the ground during different nesting phases (i.e. crawling vs. laying). The other region transferred heat by both convection and thermal infrared long wavelength radiation. As most leatherbacks nest at night, we did not include solar heating. The model did include metabolic heat and respiratory evaporative heat loss. We calculated respiratory heat loss using the turtle's tidal volume and respiration rate from the literature. We assumed the lungs' interior surfaces were free water surfaces. The heterogeneous core body volume had the thermal characteristics of animal tissue. We assigned the insulating layer the thermal properties of blubber. We used the Nusselt-Reynolds relation coefficients of a sphere to set the convection

coefficient. The characteristic length of the ellipsoid was the cube root of the volume (Mitchell 1976). We calculated the sky temperature from the Swinbank relation (Swinbank 1963). Table 1 presents these and other model parameters.

To compare current and future leatherbacks we selected three locations with sizable leatherback nesting populations (Gabon, French Guiana, and West Papua). These three locations represent the three largest nesting populations in the East Atlantic, West Atlantic, and East Pacific. We used GCM data from the Geophysical Fluid Dynamics Laboratory - Earth Systems Model with generalized ocean layer dynamics (GFDL-ESM2G) (Dunne et al. 2012). We compared two emission scenarios. The first is Representative Concentration Pathway 8.5 (RCP8.5) (Riahi et al. 2007) and the second is RCP2.6 (Vuuren et al. 2007). RCP8.5 is the "business as usual" pathway while RCP2.6 is a mitigation scenario aimed at limiting the global increase in temperature to 2 °C. The scenarios result in a radiative forcing increase of 8.5 W/m² and 2.6 W/m² by 2100 (the standard end year for climate projections). In each of the three locations, we extracted monthly minimum, maximum, and mean air temperatures; water temperatures; relative humidities; and average wind speeds for the 2100 nesting period (Gabon (November - February), French Guiana (March - August), West Papua (May - September)). Local weather stations provided current temperature data; all other current climate data was the GCM simulation conditions in the year 2010.

As leatherbacks come ashore, their movement digs down through several centimeters of sand. Thus, to find the sand temperature the leatherback plastron is in contact with, we used Niche MapperTM's microclimate model (Porter et al. 1973, Porter & Mitchell 2006) to calculate the sand temperature 15 cm below the surface.

Table 2 presents the inputs for this Niche MapperTM simulation. The calculated results from Niche MapperTM were in good agreement (average difference 2.2%) with two studies which measured beach temperatures at leatherback nesting sites (Hilterman et al. 2003, Santidrián Tomillo et al. 2009).

Literature search: Incubation thermal effects

This Web of Science search combined terms for leatherbacks, eggs or hatchlings, and hatchling success. Removing studies based on title and abstract reduced the initial 80 articles to 32. Selecting only papers with in-ground or in-nest temperatures and which measured hatchling success reduced the number to four papers with a total of 530 nests (Tapilatu & Tiwari 2007, Houghton et al. 2007, Santidrián Tomillo et al. 2009, Patino-Martinez et al. 2012). Two of these studies used in-nest temperature measurements and two used probes at nest depths. Using the known metabolic heat which a set quantity of successful eggs produces we scaled the in-clutch temperatures to remove the metabolism-caused temperature increase (Patino-Martinez et al. 2012).

Bayesian Regression

In order to calculate the 2100 credible hatchling success rate distributions (i.e. those future values of success that are the most likely and therefore lay inside the 95% HDI (highest density interval)) we conducted a Bayesian regression on the hatchling success data. We weighted each data point by the number of nests it represented. The model (i.e. the likelihood function) was a logistic function (Equation 1) about which the data was normally distributed (Equation 2) (Fig. 4). This model had four parameters (the three coefficients that describe the

shape of the logistic function and the normal distribution precision (t) (inverse of variance)) and one variable (ground temperature).

$$y_i(T_i) = \beta_0 \left(1 - \frac{1}{\left(1 + e^{\left(-\beta_1(T_i - \beta_2) \right)} \right)} \right)$$
 (1)

$$z_i(y) = \sqrt{\frac{t}{2\pi}} e^{\frac{-t(y - y_i)^2}{2}}$$
 (2)

z_i: The probability of a data point occurring at y

y_i: The average of the success at a given temperature (T_i)

T_i: A set sand temperature at nest depth

t: The precision of the normal distribution

 β_0 : A scaling coefficient of the logistic equation

 β_1 : A shape coefficient of the logistic equation

 β_2 : A displacement coefficient of the logistic equation

All priors were noncommittal. The prior on β_0 was a uniform distribution from 0.001 to 1.0. The prior on β_1 was a uniform distribution from $1x10^{-6}$ to $1x10^6$. The prior on β_2 was a uniform distribution from 0 to 100. The precision prior was a gamma distribution with shape and scale parameter set to 0.001. There were three MCMC (Markov chain Monte Carlo) runs with 500 burn-in steps and 500 adaption steps. We saved a total of 100,000 non-thinned points from the chain.

In order to calculate future temperatures the nests will experience we again used the microclimate model in Niche MapperTM. We calculated the average belowground temperature at a depth of 0.5 m (near the depth of a typical leatherback nest (Chan & Liew 1995, Godfrey & Barreto 1996)) for both shaded and exposed nests during the nesting season plus 60 days (the incubation time).

Results

Adult thermal effects

For internesting and foraging adults the average water temperature was 26.4 ± 1.6 °C and 13 ± 4 °C, respectively, and the average foraging sighting temperature was 16 ± 2 °C (Fig. 5). We expected the sighting temperature to be warmer than the tracking temperature for any region because the tracking temperatures include colder waters that the leatherback encounters during dives. Combining this data with of RCP8.5 GCM data we find that by 2100, the North Atlantic 16 °C isotherm (the location with the most foraging leatherback sightings) will likely move approximately 3.5° north along the western Atlantic coast and 4.5° along the eastern Atlantic coast (Fig. 6).

The two studies that measured internesting external and internal body temperatures showed that leatherbacks maintain their body temperature 2.2 ± 1.1 °C above ambient. Inputting the internesting temperature difference into our biophysical/physiological model, we found that under RCP8.5 West Papua leatherbacks experienced the largest increase in internesting core temperatures at 3.4 °C. Gabon experienced the smallest increase between current and future internesting core temperatures with an increase of 1.8 °C. Under RCP2.6

there was a small decrease in core temperature between Gabon and West Papua leatherbacks and a slight increase in core temperature in French Guiana leatherbacks (Table 3).

The typical results from the transient model showed the core body temperature increased during all stages except oviposition (e.g. Fig 7.). During oviposition, a leatherback reduces its metabolic rate by an order of magnitude when compared to crawling and covering/digging (Lutcavage et al. 1990, Paladino et al. 1990, 1996). At the point of oviposition we calculated that the turtle had heated to between 1.4 to 3.1 °C above water temperature, which is in agreement with measurements made by Mrosovsky and Pritchard (1971) (2.3 to 3.0 °C no CCLs given). Comparing present conditions to 2100 conditions under RCP8.5, all leatherbacks experienced most of their increase in core body temperature while in the water. Almost all of the French Guiana leatherbacks' core temperature increase happened during the internesting period. West Papua leatherbacks experienced a substantial increase during nesting but still less than during internesting (Fig. 8). Under RCP8.5 the larger leatherback in West Papua had the highest core temperature (37.2 °C) while the smaller leatherback at the same location had the greatest increase in core temperature over present (4.6 °C) (Table 4).

None of the future internesting or nesting body temperatures were above the presumed leatherback critical thermal maximum (CTM) (40 °C) (Spotila et al. 1997). This result, however, is not a guarantee of persistence in these regions (see discussion).

Incubation thermal effects

The Bayesian regression achieved a good fit with a narrow 95 % HDI (Fig. 9). The future posterior distributions (Fig. 10 and 11) for projected belowground temperatures showed some consistent trends. Shaded nests always had higher credible seasonal average success values

than exposed nests. There was generally a small difference between present and RCP2.6 credible seasonal average success values. The exception to this finding is the exposed Gabon nests. For exposed nests under RCP8.5 in all three locations zero was a credible seasonal average success value. In general, nests in Gabon and West Papua are more at risk of having low credible seasonal average success values.

Discussion

Adult thermal effects

The adult leatherback biophysical/physiological models suggest it is possible but unlikely that thermal distress will make the equatorial region inaccessible. The maximum steady state core temperature was 36.0 °C in West Papua. This temperature was below the presumed CTM of 40 °C. This adult CTM value is, however, only an estimate and researchers have not explicitly measured it. Secondly, while optimum temperature does correlate with CTM, exceeding other lower temperature limits, such as pejus range (turning worse, progressively deleterious) or the critical thermal minimum, does have a negative effect on fitness (Huey *et al.* 2012). Therefore, results near the assumed CTM should raise concern. West Papua and Gabon under RCP8.5 were also of concern because temperatures were above the 33.6 °C threshold where hatchlings begin to experience uncoordinated movement (Drake & Spotila 2002). If adults do not have a higher thermal tolerance than hatchlings, they will likely not nest in these regions.

Overheating during nesting is a greater concern than overheating while internesting.

The increased metabolic heat as well as the reduced convective cooling puts leatherbacks at additional thermal risk. Our model under scenario RCP8.5 showed that large leatherbacks in

West Papua were within 2.8 °C of their presumed CTM and those in Gabon were within 4.6 °C. Under scenario RCP8.5, all leatherbacks in Gabon and West Papua were above 33.6 °C and leatherbacks in French Guiana were only slightly below 33.6 °C.

While these results were concerning they indicated that leatherbacks could possibly tolerate the projected warming even under "business as usual" scenarios. An important caveat is that the longer a leatherback remains on land the more its temperature rises. Thus in cases where nesting takes longer than our modeled 90 minutes, the leatherback will face an increased threat from rising global temperatures.

Adult leatherback thermal distress experiments are excessively difficult as well as unethical. Thus, the most appropriate tool for determining if leatherbacks will be in thermal distress may be advanced thermal models. Like Bostrom and Jones (2007) and Paladino et al. (1990), this paper used simple models to examine the relation between metabolic rate and temperature difference. Leatherbacks, however, have a much more complex shape than a cylinder or ellipsoid (i.e. lower volume to area ratio) and so have many more opportunities to dissipate heat. In addition, their ability to shed heat both through their soft skin and flippers (Greer et al. 1973, Spotila 2004) means they can likely maintain a lower thermal gradient than a basic model can calculate. This paper used the calculated effective insulating layer thickness to account for this complexity. Future models should attempt to incorporate the leatherback's complex morphology and physiology. In addition to advanced modeling, we suggest an increased focus on research of adult thermal tolerances through advanced trackers (measuring both acceleration and sub-carapace temperature) and increased efforts to sustain leatherbacks in captivity.

Incubation thermal effects

Our analysis showed that while a scenario like RCP2.6 is of minimal concern, emissions scenario RCP8.5 is a threat in all three regions but particularly West Papua. Our results for shaded nests showed there are possible refuges from this increased heat. While the shaded credible seasonal average success values decrease from present values, a zero success value was not credible. However, while vegetation may provide shade refuges, it also may pose risks. For example, if the hatchlings emerge in dense vegetation they are unable to visually orient themselves toward the ocean (Kamel & Mrosovsky 2004).

The excavation and frenzy period is another point where elevated temperature may have deleterious effects. Increased nest temperatures can elevate hatchling temperatures and change sand properties possibly forming a surface thermal barrier (J. Wyneken, pers. comm.). With a CTM of 40.2 °C and uncoordinated movement beginning at 33.6 °C it is unsafe for hatchlings to emerge from the nest if the sand surface temperature is over 36 °C (Drake & Spotila 2002). Under RCP8.5, exposed nests in West Papua on average will already be above the temperature that causes uncoordinated movement.

In addition to reduced hatchling success rates, skewed sex ratios are also a threat to leatherbacks as they are a temperature-dependant sex determination species. There are five studies in the literature that measured and report leatherback sex ratios under different temperatures. One study uses natural nests and records sand temperatures but does not report success (Godfrey & Barreto 1996). Thus, we cannot scale this data to correct for metabolic heating. Another study examined Malaysian clutches in incubators (Chan & Liew 1995). All their clutches were all one sex with 27.3 °C being the hottest all male clutch and 28.4

°C being the coolest all female clutch (which had a very small sample size (n=5)). Chevalier et al. (1999) conducted a maximum likelihood analysis with the data from the other three studies. For a Pacific population nesting in Costa Rica, 28.8 °C and 30.0 °C are the temperature cutoffs for five percent and 95 percent female hatchlings, respectively. For an Atlantic population nesting in French Guiana, 29.2 °C and 29.8 °C are the temperature cutoffs for five percent and 95 percent female hatchlings, respectively. For our simulations, all 2100 RCP8.5 exposed clutches were above 30.0 °C, along with West Papua shaded clutches, and 2100 RCP2.6 Gabon exposed clutches. The only clutch in between the two different 95 percent female cutoffs was 2100 Gabon RCP8.5 shaded. We reiterate that our temperatures were the ground temperature at the location of the clutch (i.e. no egg metabolic heating) and that the metabolic heat of the clutch raises the temperature approximately 0.7 °C (Patino-Martinez et al. 2012).

Despite the relative accessibility of nests compared to adults, questions remain about the aggregate effect of abiotic factors on the internal clutch temperature. Santidrián Tomillo et al. stastically examined the aggregate effect of precipitation and atmospheric temperature on hatchling success in northwest Costa Rica (2012). Although not directly comparable to our results, their projections show similar decreases in hatchling success under a global warming scenario analogue to RCP8.5. However, as most of these abiotic effects are understood in isolation (i.e. evaporative cooling, conduction, etc.) numerical models may be able to sum the effects of a suite of abiotic factors and estimate the clutch temperatures under differing conditions.

Conclusion

We demonstrated that the incubation phase in the leatherback life cycle is the most vulnerable to temperature increases. Since the internesting steady state core temperatures were below the CTM the adults will not definitively diverge from the equatorial region; however, temperatures high enough to possibly induce uncoordinated movement may force them to leave some regions. The transient model showed that nesting leatherback core temperatures will not rise above the CTM, but will come dangerously close.

Managers and conservationists should investigate the possibilities of constructing shade devices out of local, biodegradable materials that will not disorient hatchlings and deploying them over nests on beaches. Patino-Martinez et al. have already used shading techniques to incress the percentage of males and overall hatchling success (Patino-Martinez et al. 2012). Also managers may consider beginning public awareness campaigns in regions traditionally cooler than current nesting locations as leatherback nesting may shift to those regions in the future.

Acknowledgements

We would like to thank the three anonymous reviewers whose thoughtful critique of our manuscript greatly improved its quality. We would also like to thank Samantha Greene for writing and stylistic editing of this manuscript. An NSF EAGER grant number 1116343 to WPP provided one summer of support to PND. Any opinions, findings, and conclusions or recommendations expressed in this material are those of the author(s) and do not necessarily reflect the views of the National Science Foundation

Figures and Tables

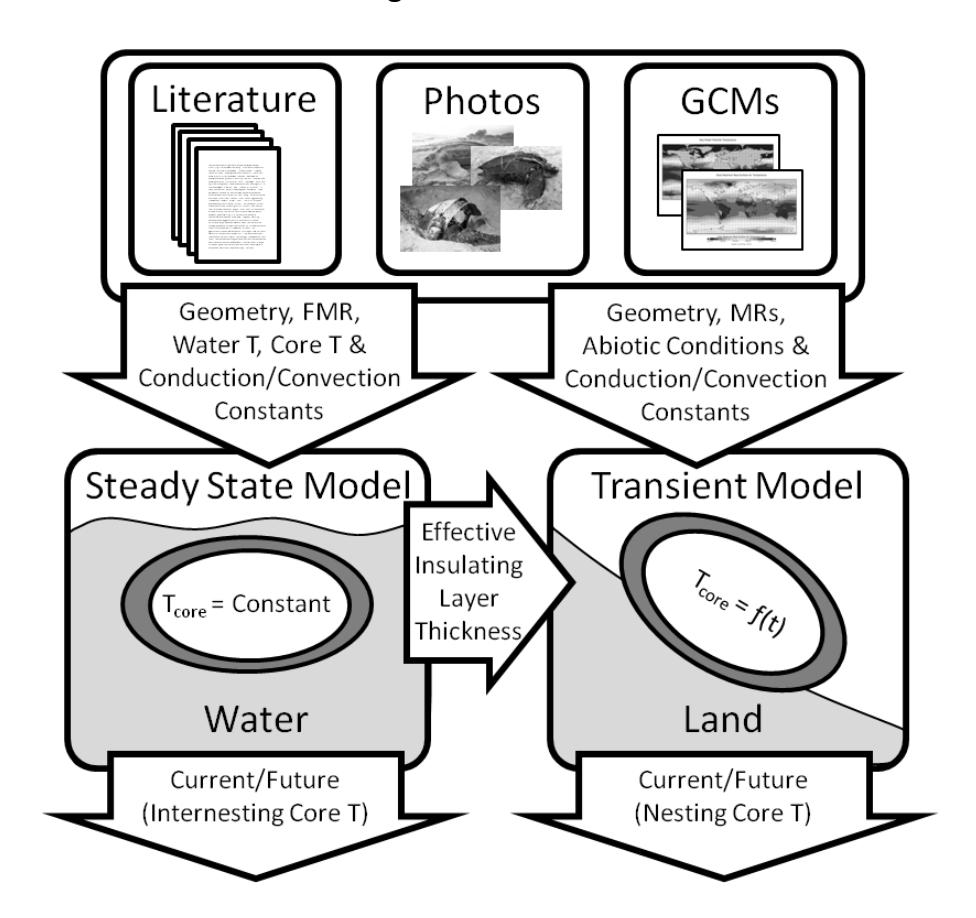


Fig. 1. A schematic diagram of the physiological model. A steady state model uses core temperatures, water temperatures, field metabolic rates (FMR), an ellipsoidal geometry, and conduction and convection coefficients to establish a minimum effective insulating layer thickness. The insulating layer thickness, the abiotic conditions, the same ellipsoidal geometry, the metabolic rates for different nesting phases (i.e. crawling, covering, laying, etc.), and the conduction and convection coefficients are the inputs for a transient, nesting leatherback model. We use both of these models to predict current and future core body temperatures during both terrestrial and marine parts of the nesting season.

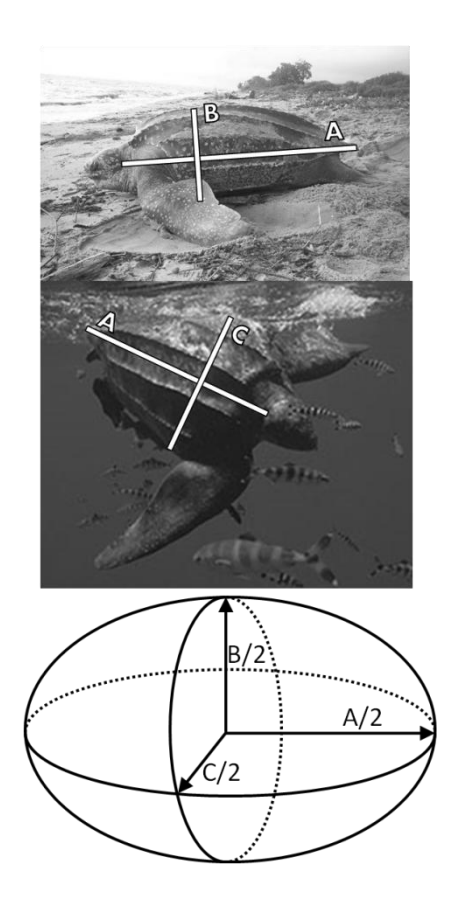


Fig. 2. We approximated the leatherback's body geometry as and ellipsoid. We based the ellipsoid axes ratios on ratios taken from nine leatherback pictures (two examples shown in figure). The leatherbacks weight sets the absolute size of the axes.

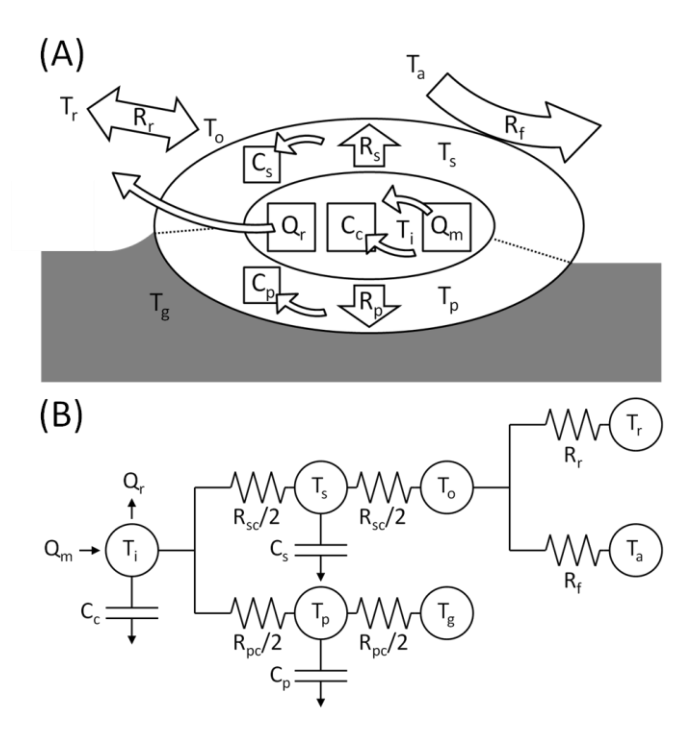


Fig. 3. (A) A representation of the four thermal regions (core, insulating layer, air and ground) that comprise the transient thermal model. (B) An equivalent circuit diagram for the nesting leatherback transient model. The symbols are as follows: Metabolic heat $(Q_m [W])$, respiratory heat loss $(Q_r [W])$, core body temperature $(T_i [^\circ C])$, core body heat capacitance $(C_c [J/K])$, shell thermal resistance $(R_s [K/W])$, plastron thermal resistance $(R_p [K/W])$, inner shell temperature $(T_s [^\circ C])$, inner plastron temperature $(T_p [^\circ C])$, shell heat capacitance $(C_s [J/K])$, plastron heat capacitance $(C_p [J/K])$, outer skin temperature $(T_o [^\circ C])$, ground temperature $(T_g [^\circ C])$, radiative resistance $(R_r [K/W])$, convective resistance $(R_f [K/W])$, sky radiative temperature $(T_r [^\circ C])$, and air temperature $(T_a [^\circ C])$. Since most leatherbacks nest at night, the model did not include solar radiation. The initial temperatures were the steady state temperatures from a swimming turtle.

Table 1. The additional data necessary for the steady state and/or transient model. This data was in addition to present and future climatic data for the three locations. Values with multiple citations indicate an average from several sources weighted by number of measurements.

Parameter	Value	Units	Reference
Mass	197.4 - 593.2	kg	James M., Mar Ecol Prog Ser, 337. 2007
			Same as 35 ppt 20 °C seawater.
		. , 3	Sharqawy M., Desalination and
Tissue density	1025	kg/m	Water Treatment, 2010
Length to width to height			l
ratio	1.000:0.830:0.425		Various images
Specific heat of tissue	3750	J/kg/K	Bostrom B., Comp Biochem Physiol A, 147:2. 2007
			Minard D., Physiological and Behavioral
Specific heat of blubber	1880	J/kg/K	Temperature Regulation. 1970
Crawl up time	180	S	Carr A., American Museum Noviates. 1959
Crawr up time	100		Carr A., American Museum
Dig time	1320	S	Noviates. 1959
			Carr A., American Museum
Lay time	900	S	Noviates. 1959
			Carr A., American Museum
Cover time	2700	S	Noviates. 1959
Crawl time	480	S	Carr A., American Museum Noviates. 1959
			Carr A., American Museum
Total time	5580	S	Noviates. 1959
			Paladino F., Chelonian Conserv Bi, 2:2. 1996
Metabolism crawling	1.045	W/kg	Paladino F., Nature, 344. 1990
Metabolism digging or			
covering	1.381	W/kg	Paladino F., Nature, 344. 1990
			Paladino F., Chelonian Conserv Bi,
			2:2. 1996
Metabolism laying	0.148	W/kg	Luctcavage M., Physiol Zool, 63:5. 1990
Metabolism swimming	0.395	W/kg	Wallace B., J Exp Zool, 208:20. 2005

Ventilation frequency active	0.083	1/s	Paladino F., Chelonian Conserv Bi, 2:2. 1996
Ventilation frequency laying	0.065	1/s	Paladino F., Chelonian Conserv Bi, 2:2. 1996
Tidal volume active	0.00412 - 0.01240	m ³	Paladino F., Chelonian Conserv Bi, 2:2. 1996
Tidal volume laying	0.00150 - 0.00450	3	Paladino F., Chelonian Conserv Bi, 2:2. 1996
Effective insulating layer thickness	0.0087 - 0.0127	m	First stage of model
Blubber Conductance	0.25	W/K/m	Bostrom B., PLoS ONE, 5:11. 2010
Swim speed	0.7	m/s	Eckert S., J Exp Biol, 205. 2002

Table 2. The inputs for the Niche MapperTM microclimate model.

Parameter	Value	Units
Surface roughness	0.0001	m
Soil thermal conductivity	3.0	W/m °C
Soil reflectivity	0.3	Fraction
Soil density	1922	kg/m³
Soil specific heat	1830	J/kg K
Soil IR emissivity	0.76	Fraction
Cloud cover	0.0	Fraction
Fraction shade	0-1	Fraction
Relative humadity	0.8	Fraction
Wind speed	1.0	m/s
Temperature	Varies	°C

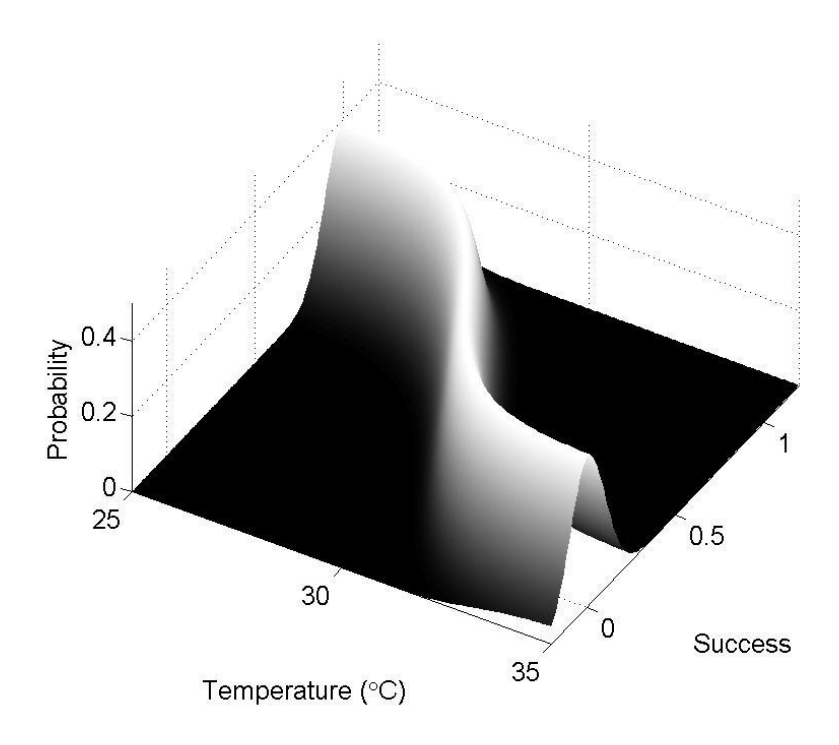


Fig. 4. A representation of the likelihood function used in the hatchling success vs. temperature Bayesian regression. The function is a logistic curve about which the data is normally distributed. The numbers are for demonstration and not actual data.

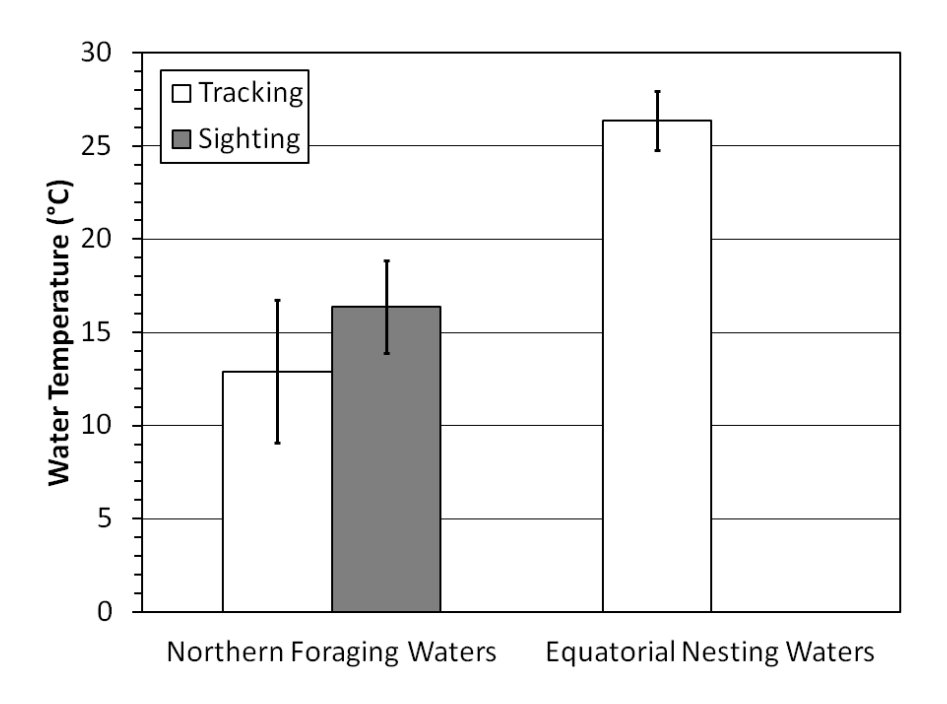


Fig. 5. The ambient water temperature leatherbacks experience while in their foraging (three articles for tracking and three for sighting) and nesting waters (nine articles). The white bars are from attached data loggers or direct water measurement during a leatherback encounter. The gray foraging bar represents average water temperature from public and fishermen sightings. We combined data for foraging with trackers (Goff & Lien 1988, James & Mrosovsky 2004, James, Davenport, et al. 2006), foraging sightings (McMahon & Hays 2006, James, Sherrill-Mix, et al. 2006, James et al. 2007), and internesting (Southwood et al. 1999, 2005, James, Davenport, et al. 2006, Sherrill-Mix et al. 2007, Shillinger et al. 2008, Fossette et al. 2009, López-Mendilaharsu et al. 2009, Casey et al. 2010, Witt et al. 2011) into averages weighted by number of turtles counted or tagged.

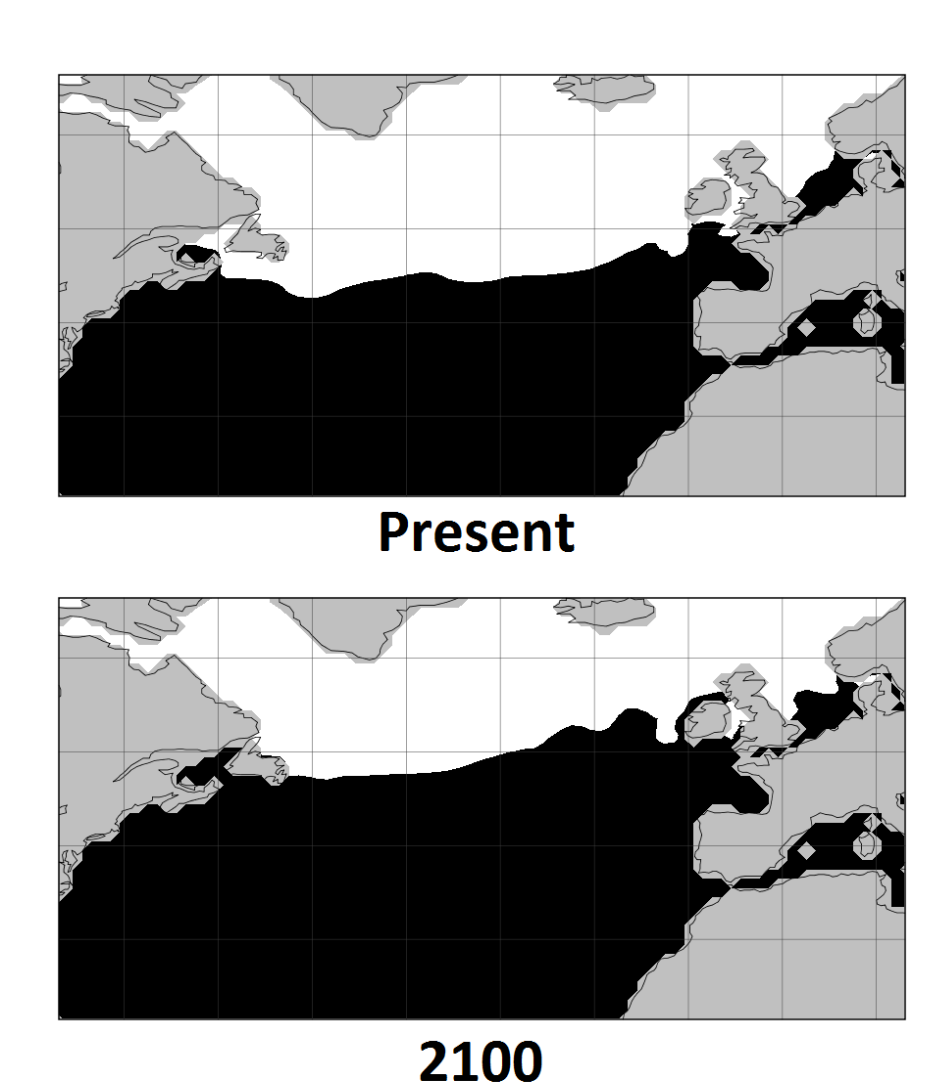


Fig. 6. The boundary between black and white is the 16 °C isotherm for the most active foraging month in the North Atlantic. A value of 16 °C is the most common water temperature for leatherback sightings in the North Atlantic. The line moves approximately 3.5° north along the western Atlantic coast and 4.5° along the eastern Atlantic coast.

Table 3. The current and future internesting core body temperature for two sizes based on curved carapace length (CCL) of leatherback sea turtles at three locations under two different emissions scenarios. RCP8.5 is the "business as usual" pathway while RCP2.6 is a mitigation scenario aimed at limiting the global increase in temperature to 2 °C.

Turtle		Core Temperature [°C]			
Location	CCL [cm]	Present	2100 RCP2.6	2100 RCP8.5	
Gabon	172	32.3	31.9	34.1	
Gabon	125	30.9	30.6	32.7	
West Papua	172	32.6	32.4	36.0	
West Papua	125	31.2	31.1	34.6	
French Guiana	172	29.0	29.9	32.0	
French Guiana	125	27.7	28.6	30.7	

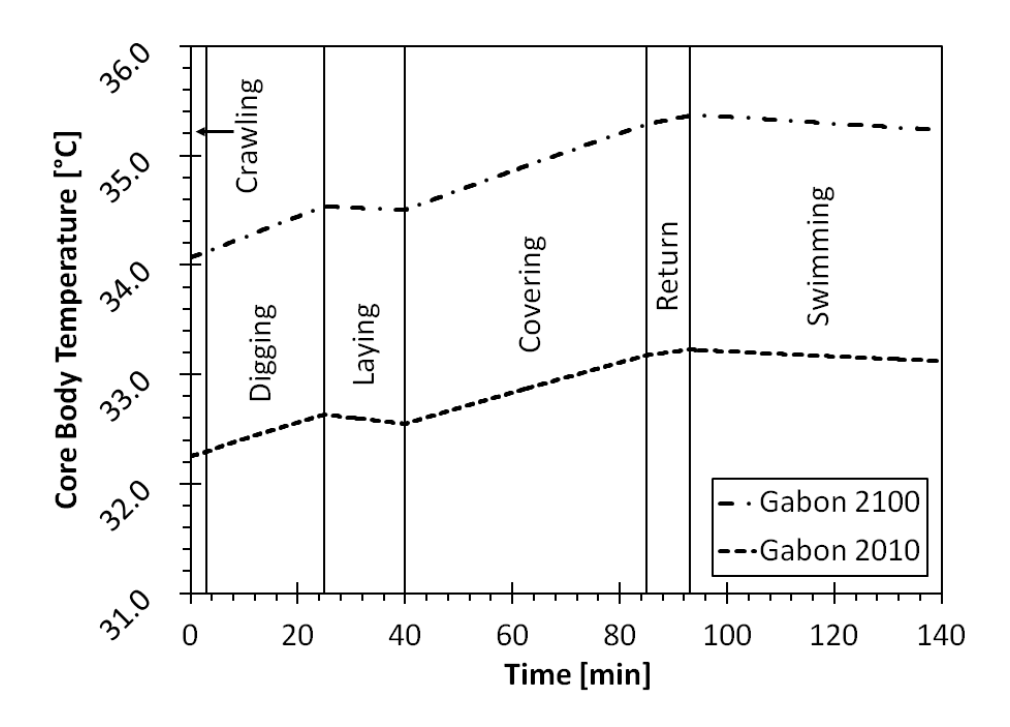


Fig. 7. An example of a core temperature profile for a 172 cm curved carapace length (CCL) Gabon leatherback under emission scenario RCP8.5. The vertical lines separate different phases of the nesting process. These functions are exponential despite looking linear. They appear linear owing to the large thermal inertia of the leatherback and the short time spent on land.

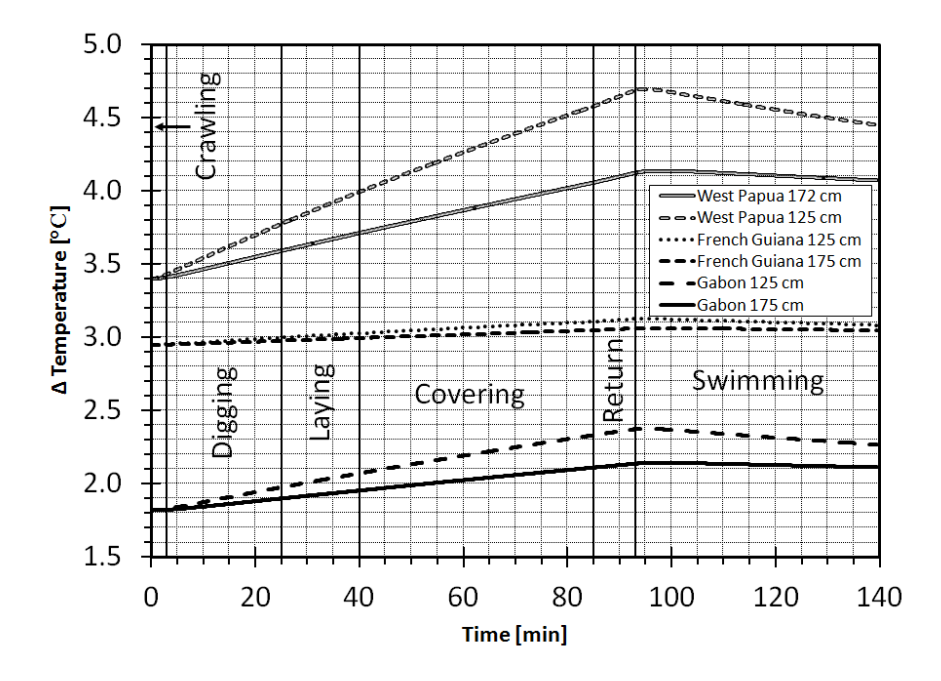


Fig. 8. The increase in leatherback body temperature during the nesting process between present and the emission scenario RCP8.5 for the year 2100. The vertical lines separate different phases of the nesting process.

Table 4. The maximum present nesting core body temperatures and 2100 nesting core body temperatures of two sizes (curved carapace length (CCL)) of leatherback sea turtles at three locations under two different emissions seniors.

Turtle		Max Core Temperature [°C]			
Location	CCL [cm]	Present	2100 RCP2.6	2100 RCP8.5	
Gabon	172	33.2	33.1	35.4	
Gabon	125	31.8	31.9	34.2	
West Papua	172	33.1	33.4	37.2	
West Papua	125	31.3	31.9	35.9	
French Guiana	172	30.4	31.2	33.5	
French Guiana	125	29.3	30.1	32.4	

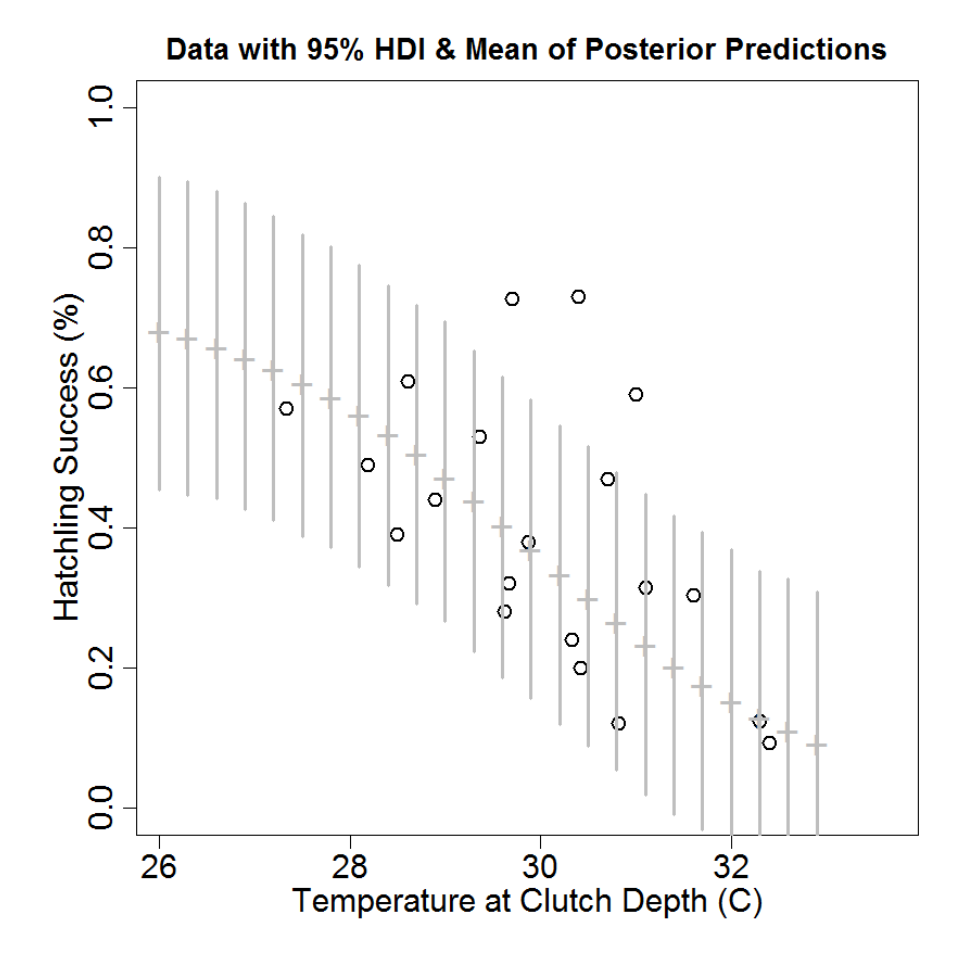


Fig. 9. A graph of the raw data from four studies (Tapilatu & Tiwari 2007, Houghton et al. 2007, Santidrián Tomillo et al. 2009, Patino-Martinez et al. 2012) with 95% HDIs (highest density interval) overlaid at several temperature values. The hash marks in the middle of the HDI vertical bars are the most credible success value for the given temperature. For each given temperature, 95% of the credibility lies within the vertical line. Data is weighted by number of nests, thus certain data points have more weight in the regression than others.

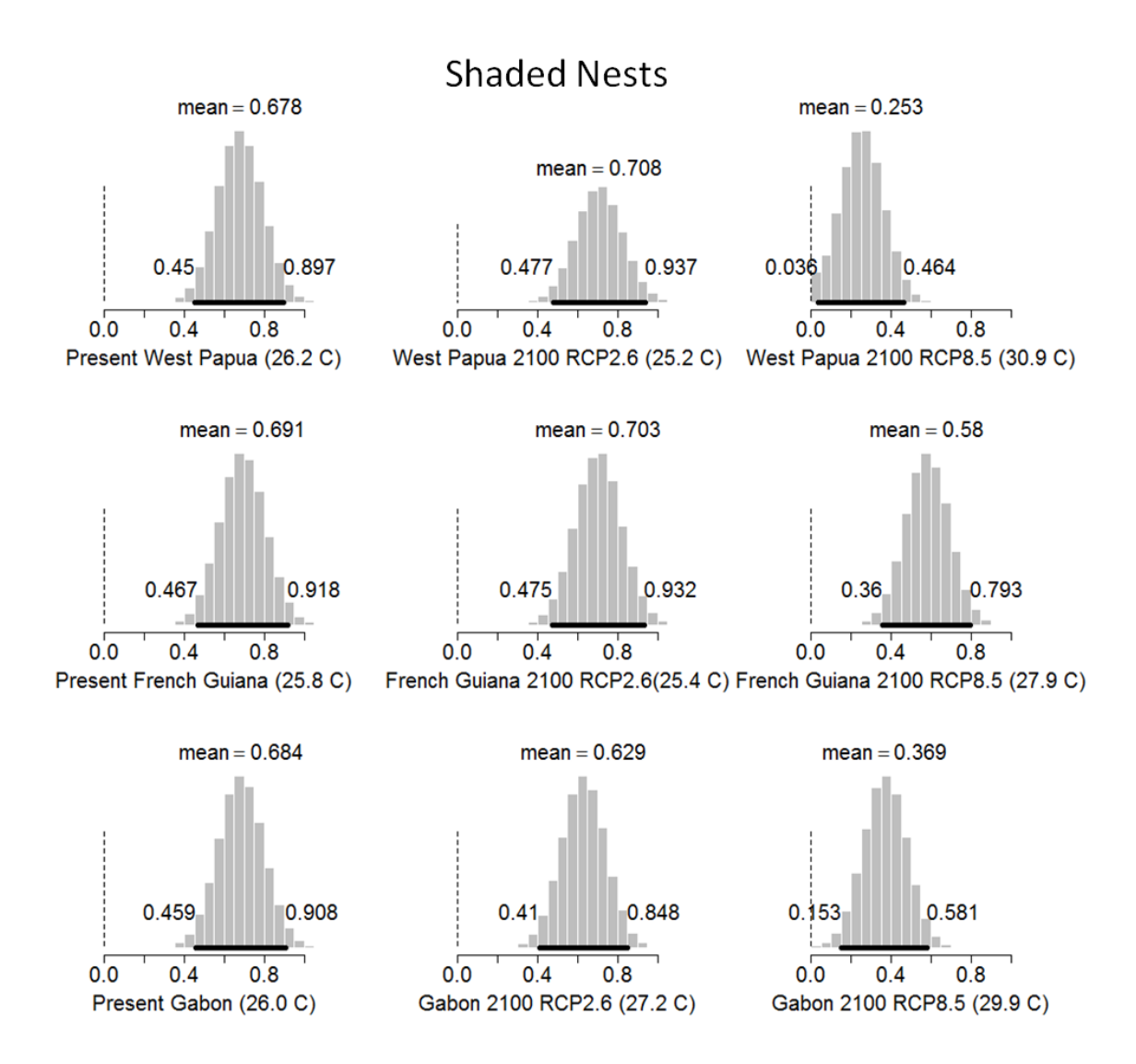


Fig. 10. The posterior distributions for the average temperature that shaded clutches will experience at present and in year 2100 under two different emission scenarios. The most credible values are the means of the distributions and the region above the black horizontal bar denoting the 95% HDI (highest density interval) contains 95% of the credible values.

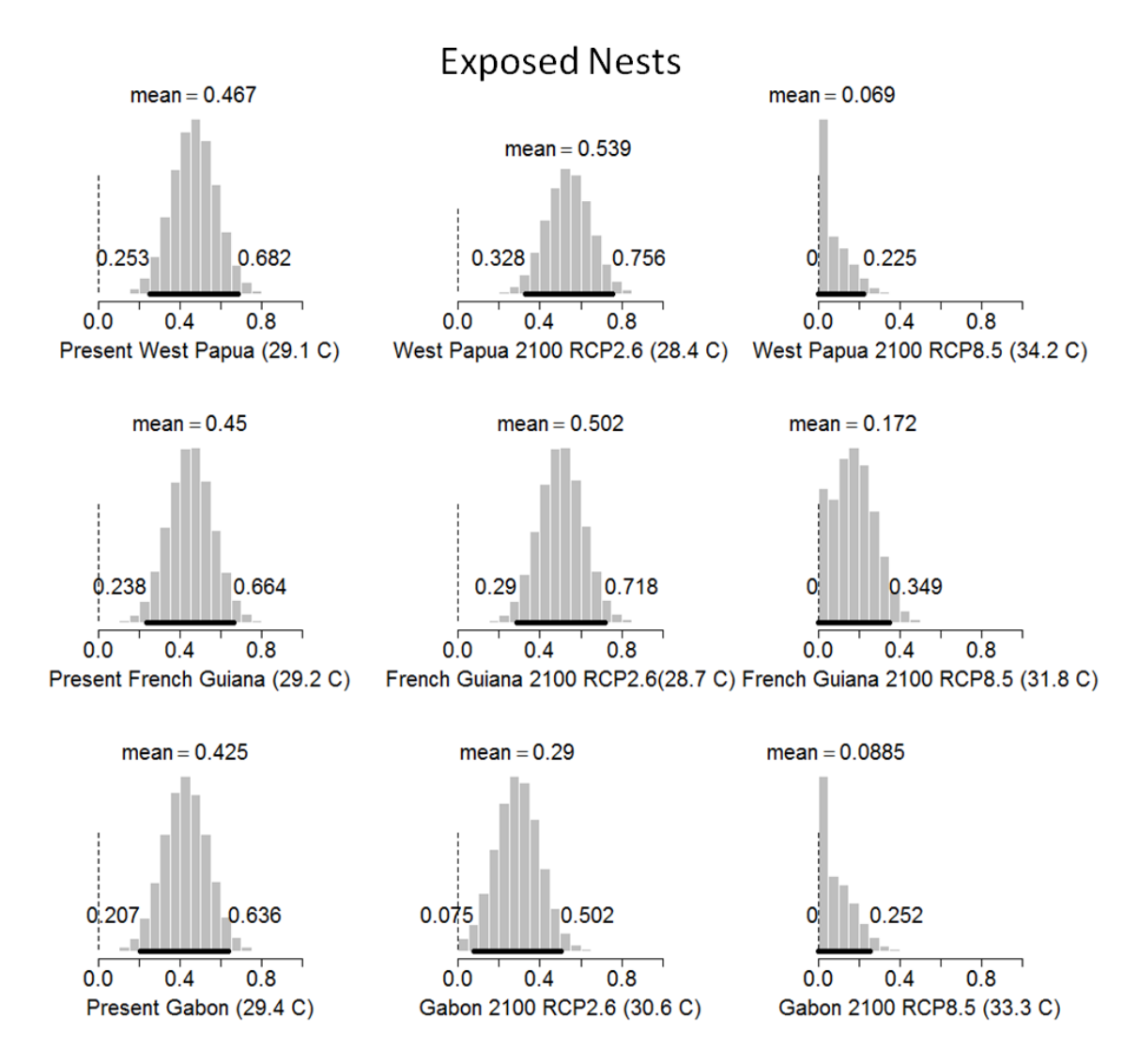


Fig. 11. The posterior distributions for the average temperature that exposed (i.e. not shaded) clutches will experience at present and in year 2100 under two different emission scenarios. The most credible values are the means of the distributions and the region above the black horizontal bar denoting the 95% HDI (highest density interval) contains 95% of the credible values.

References

- Barreiros JP, Barcelos J (2001) Plastic ingestion by a leatherback turtle (*Dermochelys coriacea*) from the Azores (NE Atlantic). Mar Pollut Bull 42:1196–1197
- Bioexpedition.com (2013) Leatherback Sea Turtle. http://bioexpedition.com/wp-content/uploads/2012/06/Leatherback 600.jpg (accessed 17 Jun 3013).
- Bostrom BL, Jones DR (2007) Exercise warms adult leatherback turtles. Comp Biochem Physiol Part A Mol Integr Physiol 147:323–31
- Bugoni L, Krause L, Petryà MV (2001) Marine debris and human impacts on sea turtles in Southern Brazil. Mar Pollut Bull 42:1330–1334
- Casey J, Garner J, Garner S, Williard AS (2010) Diel foraging behavior of gravid leatherback sea turtles in deep waters of the Caribbean Sea. J Exp Biol 213:3961–71
- Chan SKF, Cheng IJ, Zhou T, Wang HJ (2007) A comprehensive overview of the population and conservation status of sea turtles in China. Chelonian Conserv Biol 6:185–198
- Chan EH, Liew HC (1995) Incubation temperatures and sex-ratios in the Malaysian leatherback turtle *Dermochelys coriacea*. Biol Conserv 74:169–174
- Chevalier J, Godfrey MH, Girondot M (1999) Difference of temperature-dependent sex determination between French Guiana (Atlantic) and Playa Grande (Costa-Rica, Pacific) leatherbacks (Dermochelys). Ann des Sci Nat 20:147–152
- Donlan CJ, Wingfield DK, Crowder LB, Wilcox C (2010) Using expert opinion surveys to rank threats to endangered species: a case study with sea turtles. Conserv Biol 24:1586–95
- Drake DL, Spotila JR (2002) Thermal tolerances and the timing of sea turtle hatchling emergence. J Therm Biol 27:71–81
- Dunne JP, John JG, Adcroft AJ, Griffies SM, Hallberg RW, Shevliakova E, Stouffer RJ, Cooke W, Dunne K a., Harrison MJ, Krasting JP, Malyshev SL, Milly PCD, Phillipps PJ, Sentman LT, Samuels BL, Spelman MJ, Winton M, Wittenberg AT, Zadeh N (2012) GFDL's ESM2 Global Coupled Climate—Carbon Earth System Models. Part I: Physical formulation and baseline simulation characteristics. J Clim 25:6646—6665
- Eckert SA (1997) Distant fisheries implicated in the loss of the worlds largest leatherback nesting population. Mar Turt Newsl 78:2–7

- Fossette S, Girard C, Bastian T, Calmettes B, Ferraroli S, Vendeville P, Blanchard F, Georges J-Y (2009) Thermal and trophic habitats of the leatherback turtle during the nesting season in French Guiana. J Exp Mar Bio Ecol 378:8–14
- Fuentes MMPB, Cinner JE (2010) Using expert opinion to prioritize impacts of climate change on sea turtles' nesting grounds. J Environ Manage 91:2511–8
- Fuentes M, Fish M, Maynard J (2012) Management strategies to mitigate the impacts of climate change on sea turtle's terrestrial reproductive phase. Mitig Adapt Strateg Glob Chang
- Fuentes MMPB, Limpus CJ, Hamann M (2011) Vulnerability of sea turtle nesting grounds to climate change. Glob Chang Biol 17:140–153
- Fuentes MMPB, Pike D a, Dimatteo A, Wallace BP (2013) Resilience of marine turtle regional management units to climate change. Glob Chang Biol 19:1399–406
- Garcon J, Grech A (2010) Relative Exposure Index: an important factor in sea turtle nesting distribution. Aquat Conserv Mar Freshw Ecosyst 149:140–149
- Godfrey MH, Barreto R (1996) Estimating past and present sex ratios of turtles in Suriname. Can J Zool 74:267–277
- Goeorges J (2011) Atlantic Leatherback Strategy Retreat at St. Catherines Island. http://www.conserveturtles.org/images/seaturtles/leatherback-on-beach-Georges.jpg (accessed 17 Jun 3013).
- Goff GP, Lien J (1988) Atlantic leatherback turtles, *Dermochelys coriacea*, in cold water off Newfoundland and Labrador. Can Field-Naturalist 102:1–5
- Greer AE, Lazell JD, Wright RM (1973) Anatomical evidence for a counter-current heat exchanger in the leatherback turtle (*Dermochelys coriacea*). Nature 244:181
- Hamann M, Fuentes MMPB, Ban NC, Mocellin VJL (2013) Climate change and marien turtles. In: Sea Turtle Biology, Vol III. CRC Press, p 353–378
- Hansen L, Hoffman J, Drews C, Mielbrecht E (2010) Designing climate-smart conservation: guidance and case studies. Conserv Biol 24:63–9
- Hawkes L, Broderick A, Godfrey M, Godley B (2009) Climate change and marine turtles. Endanger Species Res 7:137–154
- Hernandez R, Buitrago J, Guada H, Hernandez-Hamon H, Llano M (2007) Nesting distribution and hatching success of the Leatherback, *Dermochelys coriacea*, in relation to human pressures at Playa Parguito, Margarita Island, Venezuela. Chelonian Conserv Biol 6:79–86

- Hilterman M, Goverse E, Godfrey M, Girondot M, Sakimin C (2003) Seasonal sand temperature profiles of four major leatherback nesting beaches in the Guyana Shield. In: 22nd Annual Symposium on Sea Turtle Biology and Conservation.p 189–190
- Hooker S, Cañadas a, Hyrenbach K, Corrigan C, Polovina J, Reeves R (2011) Making protected area networks effective for marine top predators. Endanger Species Res 13:203–218
- Houghton JDR, Myers AE, Lloyd C, King RS, Isaacs C, Hays GC (2007) Protracted rainfall decreases temperature within leatherback turtle (*Dermochelys coriacea*) clutches in Grenada, West Indies: Ecological implications for a species displaying temperature dependent sex determination. J Exp Mar Bio Ecol 345:71–77
- Huey RB, Kearney MR, Krockenberger A, Holtum J a M, Jess M, Williams SE (2012) Predicting organismal vulnerability to climate warming: roles of behaviour, physiology and adaptation. Philos Trans R Soc Lond B Biol Sci 367:1665–79
- Isley J (2013) Leatherback turtle (*Dermochelys coriacea*). http://cdn2.arkive.org/media/D1/D123BCA6-C8CB-4FCC-8AFA-F8341EFBC3F6/Presentation.Large/Dead-captured-leatherback-turtle-hanging-underfishing-boat.jpg (accessed 17 Jun 3013).
- James MC, Davenport J, Hays GC (2006) Expanded thermal niche for a diving vertebrate: A leatherback turtle diving into near-freezing water. J Exp Mar Bio Ecol 335:221–226
- James MC, Mrosovsky N (2004) Body temperatures of leatherback turtles (*Dermochelys coriacea*) in temperate waters off Nova Scotia, Canada. Can J Zool 1306:1302–1306
- James MC, Sherrill-Mix SA, Martin K, Myers RA (2006) Canadian waters provide critical foraging habitat for leatherback sea turtles. Biol Conserv 133:347–357
- James MC, Sherrill-Mix SA, Myers RA (2007) Population characteristics and seasonal migrations of leatherback sea turtles at high latitudes. Mar Ecol Prog Ser 337:245–254
- Kamel SJ, Mrosovsky N (2004) Nest site selection in leatherbacks, *Dermochelys coriacea*: individual patterns and their consequences. Anim Behav 68:357–366
- Kaplan IC (2005) A risk assessment for Pacific leatherback turtles (*Dermochelys coriacea*). Can J Fish Aquat 1719:1710–1719
- Lewison RL, Freeman SA, Crowder LB (2004) Quantifying the effects of fisheries on threatened species: the impact of pelagic longlines on loggerhead and leatherback sea turtles. Ecol Lett 7:221–231

- Lin Z-H, Ji X, Luo L-G, Ma X-M (2005) Incubation temperature affects hatching success, embryonic expenditure of energy and hatchling phenotypes of a prolonged egg-retaining snake, Deinagkistrodon acutus (Viperidae). J Therm Biol 30:289–297
- López-Mendilaharsu M, Rocha CFD, Miller P, Domingo A, Prosdocimi L (2009) Insights on leatherback turtle movements and high use areas in the Southwest Atlantic Ocean. J Exp Mar Bio Ecol 378:31–39
- Lutcavage ME, Bushnell PG, Jones DR (1990) Oxygen transport in the leatherback sea turtle Dermochelys coriacea. Physiol Zool 63:1012–1024
- Lutcavage ME, Bushnell PG, Jones DR (1992) Oxygen stores and aerobic metabolism in the leatherback sea turtle. Can J Zool 70:348–351
- Majza B (2012) Leatherback.

 http://intelligenttravel.nationalgeographic.com/files/2012/08/Leatherback_Bernard_Majz
 a 225326-950x626.jpg (accessed 17 Jun 3013).
- Martinez S (2011) Dermochelys coriacea. IUCN Red List Threat Species
- Mazaris AD, Matsinos G, Pantis JD (2009) Evaluating the impacts of coastal squeeze on sea turtle nesting. Ocean Coast Manag 52:139–145
- McMahon CR, Hays GC (2006) Thermal niche, large-scale movements and implications of climate change for a critically endangered marine vertebrate. Glob Chang Biol 12:1330–1338
- Mitchell J (1976) Heat transfer from spheres and other animal forms. Biophys J 16:561–569
- Mrosovsky N, Pritchard PCH (1971) Body temperatures of *Dermochelys coriacea* and other sea turtles. Copeia 4:624–631
- Mrosovsky N, Ryan GD, James MC (2009) Leatherback turtles: the menace of plastic. Mar Pollut Bull 58:287–9
- National Park Service (2013) Virgin Islands National Park: Photo Gallery, Sea Turtles. http://www.nps.gov/common/uploads/photogallery/akr/park/viis/2D4053B6-1DD8-B71C-07F4200E8812FB0D/2D4053B6-1DD8-B71C-07F4200E8812FB0D-large.jpg (accessed 17 Jun 3013).
- National Prak Service (2010) Leatherback Turtle (Dermochelys coriacea). http://www.nature.nps.gov/biology/migratoryspecies/images/exLeatherback.jpg (accessed 17 Jun 3013).

- Packard G, Packard M, Miller K, Boardman T (1987) Influence of moisture, temperature, and substrate on snapping turtle eggs and embryos. Ecology 68:983–993
- Paladino FV, O'Connor MP, Spotila JR (1990) Metabolism of leatherback turtles, gigantothermy, and thermoregulation of dinosaurs. Nature 344:858–860
- Paladino FV, Spotila JR, O'Connor MP, Gatten, Robert E. J (1996) Respiratory physiology of adult leatherback turtles (Dermochelys coriacea) while nesting on land. Chelonian Conserv Biol 2:223–229
- Patino-Martinez J, Marco A, Quiñones L, Hawkes L (2012) A potential tool to mitigate the impacts of climate change to the caribbean leatherback sea turtle. Glob Chang Biol 18:401–411
- Perrine D (2010) Conservation Coalitions Support Leatherback Critical Habitat. http://seaturtles.org/img/original/Doug%20Perrine%20Leatherback%201.jpg (accessed 17 Jun 2013).
- Pike D a. (2013) Climate influences the global distribution of sea turtle nesting. Glob Ecol Biogeogr 22:555–566
- Poloczanska ES, Limpus CJ, Hays GC (2009) Vulnerability of marine turtles to climate change. In: Advances in marine biology, VOL 56, 1st edn. Elsevier Ltd, p 151–211
- Porter WP, Mitchell JW (2006) Method and system for calculating the spatial-temporal effects of climate and other environmental conditions on animals.
- Porter W, Mitchell J, Beckman W, DeWitt CB (1973) Behavioral implications of mechanistic ecology. Thermal and behavioral modeling of desert ectotherms and their microenvironment. Oecologia 13:1–54
- Project STR (2013) Leatherback on International Climate Change Hit List. http://seaturtles.org/img/original/Doug%20Perrine%20Leatherback%202.jpg (accessed 17 Jun 3013).
- Riahi K, Grübler A, Nakicenovic N (2007) Scenarios of long-term socio-economic and environmental development under climate stabilization. Technol Forecast Soc Change 74:887–935
- Saba V, Stock C, Spotila J (2012) Projected response of an endangered marine turtle population to climate change. Nat Clim Chang 2:814–820

- Santidrián Tomillo P, Saba VS, Blanco GS, Stock C a, Paladino F V, Spotila JR (2012) Climate driven egg and hatchling mortality threatens survival of eastern Pacific leatherback turtles. PLoS One 7:e37602
- Santidrián Tomillo P, Suss JS, Wallace BP, Magrini KD, Blanco G, Paladino F V., Spotila JR (2009) Influence of emergence success on the annual reproductive output of leatherback turtles. Mar Biol 156:2021–2031
- Sherrill-Mix SA, James MC, Myers RA (2007) Migration cues and timing in leatherback sea turtles. Behav Ecol 19:231–236
- Shillinger GL, Palacios DM, Bailey H, Bograd SJ, Swithenbank AM, Gaspar P, Wallace BP, Spotila JR, Paladino F V, Piedra R, Eckert SA, Block BA (2008) Persistent leatherback turtle migrations present opportunities for conservation. PLoS Biol 6:e171
- Skerry B (2009) Ancient Mariner. http://s.ngm.com/2009/05/leatherbacks/img/leatherbacks-01-615.jpg (accessed 17 Jun 3013).
- Southwood A, Andrews R, Paladino F, Jones DR (1999) Body temperatures of leatherback sea turtles during the internesting interval. In: Proceedings of the Nineteenth Annual Symposium on Sea Turtle Conservation and Biology.p 117–119
- Southwood AL, Andrews RD, Paladino F V, Jones DR (2005) Effects of diving and swimming behavior on body temperatures of pacific leatherback turtles in tropical seas. Physiol Biochem Zool 78:285–297
- Spotila JR (2004)Sea Turtles: A Complete Guide to Their Biology, Behavior, and Conservation, 1st edn. The John Hopkins University Press, Baltimore, MD
- Spotila JR, Dunham AE, Leslie AJ, Steyermark AC, Plotkin PT, Paladino F V. (1996) Worldwide population decline of *Dermochelys coriacea*: Are leatherback turtles going extinct? Chelonian Conserv Biol 2:209–222
- Spotila JR, O'Connor MP, Paladino F V. (1997) Thermal Biology. In: Lutz PL, Musick JA (eds) The Biology of Sea Turtles. CRC Press, Boca Raton, p 297–314
- Spotila J, Zimmerman L (1994) Effects of incubation conditions on sex determination, hatching success, and growth of hatchling desert tortoises, Gopherus agassizii. Herpetol Monogr 8:103–116
- Swinbank WC (1963) Long-wave radiation from clear skies. Q J R Meteorol Soc 89:339–348

- Tapilatu RF, Tiwari M (2007) Leatherback turtle, *Dermochelys coriacea*, hatching success at Jamursba-Medi and Wermon beaches in Papua, Indonesia. Chelonian Conserv Biol 6:150–158
- Tomillo PS, Saba VS, Piedra R, Paladino F V, Spotila JR (2008) Effects of illegal harvest of eggs on the population decline of leatherback turtles in Las Baulas Marine National Park, Costa Rica. Conserv Biol 22:1216–24
- Vuuren DP, Elzen MGJ, Lucas PL, Eickhout B, Strengers BJ, Ruijven B, Wonink S, Houdt R (2007) Stabilizing greenhouse gas concentrations at low levels: an assessment of reduction strategies and costs. Clim Change 81:119–159
- Wallace BP, Jones TT (2008) What makes marine turtles go: A review of metabolic rates and their consequences. J Exp Mar Bio Ecol 356:8–24
- Wallace BP, Sotherland PR, Spotila JR, Reina RD, Franks BF, Paladino F V (2012) Biotic and abiotic factors affect the nest environment of embryonic leatherback turtles, *Dermochelys coriacea*. Physiol Biochem Zool 77:423–32
- Wallace BP, Williams CL, Paladino F V, Morreale SJ, Lindstrom TR, Spotila JR (2005)

 Bioenergetics and diving activity of internesting leatherback turtles *Dermochelys coriacea* at Parque Nacional Marino Las Baulas, Costa Rica. J Exp Biol 208:3873–84
- Weems R (1988) Paleocene turtles from the Aquia and Brightseat formations, with a discussion of their bearing on sea turtle evolution and phylogeny. Proc Biol Soc Washingt 101:109–145
- Witherington B, Hirama S, Mosier A (2011) Barriers to Sea Turtle Nesting on Florida (United States) Beaches: Linear Extent and Changes Following Storms. J Coast Res 27:450–458
- Witt MJ, Augowet Bonguno E, Broderick AC, Coyne MS, Formia A, Gibudi A, Mounguengui Mounguengui GA, Moussounda C, NSafou M, Nougessono S, Parnell RJ, Sounguet G-P, Verhage S, Godley BJ (2011) Tracking leatherback turtles from the world's largest rookery: assessing threats across the South Atlantic. Proc R Soc Biol Sci

Chapter 2: Consider a non-spherical elephant: Computational fluid dynamics simulations of

heat transfer coefficients and drag verified using wind tunnel experiments

Authors: Peter N. Dudley¹, Riccardo Bonazza², and Warren P. Porter¹

¹Department of Zoology, University of Wisconsin-Madison

²Engineering Physics, University of Wisconsin-Madison

Abstract

Animal momentum and heat transfer analysis has historically used direct animal measurements or approximations to calculate drag and heat transfer coefficients. Research can now use modern 3-D rendering and computational fluid dynamics software to simulate animal-fluid interactions. Key questions are the level of agreement between simulations and experiments and how superior they are to classical approximations. In this paper we compared experimental and simulated heat transfer and drag calculations on a scale model solid aluminum African elephant casting. We found good agreement between experimental and simulated data and large differences from classical approximations. We used the simulation results to calculate coefficients for heat transfer and drag of the elephant geometry.

Introduction

Traditionally, animal momentum and heat transfer analysis made approximations of animal geometries. The simplest of these approximations is a sphere. In this paper we merged modern 3-D digital art and techniques from heat transfer analysis. We compared momentum

and heat balance experiments on a solid metal elephant scale model to computational fluid dynamics (CFD) simulations and classical spherical calculations. As this class of CFD software is developed, tested and optimized for industrial applications, a key question is how closely do simulations and experiments agree when geometries are biological?

Researchers often require the heat transfer coefficient (h_c) to aid in calculating an animal's energy needs, mechanistically model an animal's distribution, or investigate basic physiological aspects of heat transfer (Porter & Budaraju 2000, Tieleman et al. 2003, Natori & Porter 2007). For aquatic and in-flight aerial species the above calculations also require drag (Bullen & McKenzie 2007). Traditional methods for finding these values fall into three categories. First, direct measurements made using live animals. This method involves training live animals to fly in wind tunnels or swim in flumes to measure drag force and thermal gradients. Tethers or pressure sensors measure the force (Usherwood 2003, Blake & Chan 2007) while temperature sensors measure thermal gradients (Tieleman et al. 2003, Marom et al. 2006). There are alternative, noncontact, direct measurement techniques such as visualizing particle flows around the animal and using image capture software to calculate force (Drucker and Lauder '99), using cameras to see reference point movements (Skrovan et al. '99; Tobalske, Peacock, and Dial '99) or using thermal cameras to measure temperature profiles (Ward et al. '99). Second, measurements made using dead animals or castings (Dear et al. '97). This method places a dead animal in a moving fluid or drags it through a still fluid to approximate drag (Stephenson et al. '89). Third, models requiring these coefficients will often reduce the animal to a basic shape (sphere or cylinder) (Porter, Munger, and Stewart '94) or a combination of basic shapes (Natori & Porter 2007).

The advantage of using live animals is that it preserves most of the complex, natural environment interactions between the animal and the fluid (air or water). The disadvantages are the handling time, logistics of conducting live animal studies, size limitations on specimens, and inability to separate local fluid interactions. Using dead animals or castings is a simpler experiment, but loses some of the movement causing the most complex fluid-animal interactions. Models using simple shape approximations are quick; however, they lose the complex interactions between the animal and the fluid.

To capture some of the complex fluid interactions lost in dead animal, casting, and modeled measurements, researchers are beginning to use CFD programs. These simulations sometimes use simplified geometries (Sachs 2007, Hazekamp et al. 2009) or model part of an animal (Pavlov et al. 2007, Weber et al. 2009). Some, however, model a complete animal (Pavlov & Rashad 2012). To date none of these CFD models simulate terrestrial species and none calculate heat transfer coefficients.

Here, we used a commercial CFD package (*ANSYS®*, *Release 14.0*) to calculate the heat transfer coefficient and drag for a scale model African elephant aluminum casting, verify the simulation with wind tunnel experiments, and compare our simulation results to the classical spherical approximation. This simulation method keeps much of the complex fluid interactions, has no size limitations, permits analysis of local contributions to drag and the heat transfer coefficient, does not require a casting, and allows rapid and flexible data collection. If shown accurate, this experimental method has the promise to save researchers a great deal of time and expense.

Materials and Methods

Wind tunnel drag

We constructed a solid aluminum elephant in a walking posture from a wax, scale model sculpture using the lost wax process (Porter et al. '73) (table 1 details casting physical parameters and other experimental parameters). We connected the elephant's posterior to a sting balance via a 0.27 m long, 0.5 cm diameter metal rod. We placed each of its feet on a ball bearing recessed in a machined cavity in a solid Plexiglas sheet. The Plexiglas sheet had a knife edge at the top of the front end. The feet were flush with the sheet surface but on a movable ball bearing in each of four channels (Fig. 1). We mounted the 4.8 cm thick Plexiglas sheet on four posts bolted to the floor of the wind tunnel. The recirculating wind tunnel had a 0.9 x 1.2 x 1.84 m working section (Fig. 1). We measured the drag for set headwind velocities of 5 m/s to 25 m/s in 5 m/s increments. The wind tunnel does not stabilize at the exact set velocities, thus actual recorded velocities are different for set velocities. We averaged the drag force over a 13 s run for each air speed with measurements taken every 0.125 s.

Wind tunnel heat transfer coefficient, h_c .

We fitted the same aluminum elephant model with four copper-constantan thermocouples on the belly, on the left mid lateral portion of the body, centered behind the left ear and centered on the back (Fig. 2). We used a high intensity heat lamp to heat the elephant to approximately 30 °C above air temperature. We turned off the lamp before sealing the wind tunnel and beginning the experiment. We waited for the wind tunnel flow to stabilize before taking measurements. We reheated the elephant before the third (15.2 m/s) run. Given these methods, the initial, elephant temperature was not constant across runs. We measured the

transient cooling for each run (Fig. 3). As the velocity of the wind increased, there was an increase in the ambient wind tunnel temperature likely owing to fan waste heat. We measured the temperature change over a 150 s run for each air speed with measurements taken every 0.125 s. Using Equation 1, we did a least squares fit using the casting temperature, initial and current air temperature at each time point to find the heat transfer coefficient at each wind speed (Wathen, Mitchell, and Porter '71).

$$ln\left(\frac{T_e - T_a}{T_i - T_a}\right) = -\frac{h_c A_s}{c_{pe} m_e} t \tag{1}$$

 T_e : Elephant casting temperature at any instant

T_i: Initial casting temperature

T_a: Air temperature

h_c: Heat transfer coefficient

A_s: Casting surface area

 c_p : Specific heat of the aluminum casting

m_e: Elephant casting mass

t: Time

Simulation

We used a NextEngine Multidrive 3-D laser scanner to scan the 3-D elephant model with millimeter precision to create a triangular mesh. We imported the 3-D mesh from the scanner into Rhinoceros v.4 software to convert the mesh to a non-uniform rational B-spline (NURBS) format. Computational fluid dynamics meshing requires this format. We imported the

3D NURBS image into ANSYS DesignModeler and enclosed it in a virtual box with a 0.5 meter buffer on each side except where the elephant's feet touched the floor. We imported the box into ANSYS Meshing and meshed the fluid zone with approximately equal parts 4-node tetrahedral and 6-node wedge elements and a few 5-node pyramid elements. We used a 1 cm, 16 layer inflation boundary around the elephant (Fig. 4). The mesh consisted of approximately 1,260,000 elements. We ran simulations for drag and heat transfer with both a headwind and a crosswind from the left at each wind tunnel speed (previous experiments show heat transfer's low sensitivity to wind direction (Wu & Gebremedhin 2001) and we wanted to verify this result). This combination gave us a total of 20 simulations. For each simulation we set the inlet velocity to the velocity measured in that wind tunnel run, the outlet to zero pressure and the other four boundaries to walls. We set the inlet flow to low turbulence (1%). We set physical conditions (i.e., air temperature, air dynamic viscosity, air density, air thermal conductivity, air specific heat and casting temperature) to match the values from each wind tunnel experiment. These values changed because of the increasing waste heat from the fans. We ran the steady state simulations in ANSYS Fluent using the $k-\omega$ shear stress transport (SST) and energy transfer model. We calculated drag and the heat transfer coefficient in ANSYS CFD Post.

Results

Figure 5 shows a contour map of the pressure for the fifth, (25.1 m/s) headwind, drag simulation. The largest contribution to the drag was from the front face owing to pressure

54

drag. There were low pressure sections on the side of the legs and around the edges of the

ears.

Figure 6 shows the simulated, experimental, and sphere drag force vs. air speed. The

headwind simulation and experimental data were in good agreement, both sphere sets had

much lower values, and the crosswind drag was the highest. The largest difference was during

the second run (10.1 m/s) while the smallest difference was during the final run (25.1 m/s). As

we were attempting to determine the predictive power of this method without feedback from

experimental data, we made no attempt to fine tune constants (viscosity or density of air) in

this simulation to better match the data. Using Equation 2 with A defined as the projected

frontal area, the drag coefficients for a headwind and crosswind calculated from the simulation

were 0.73 ± 0.02 and 0.80 ± 0.04 respectively. These drag coefficients mean that, depending on

its angle to the wind, an elephant would have between 34 - 74% more drag than the spherical

approximation would assume. For $3 \times 10^4 \le \text{Re} \le 1.8 \times 10^5$, the drag coefficient for a sphere is

0.469 ± 0.003 (Haider & Levenspiel 1989).

$$C_D = \frac{F}{\frac{1}{2}A_{f/s}U^2\rho_a} \tag{2}$$

*C*_D: Drag coefficient

F: Drag force

 $A_{f/s}$: Projected frontal or side area

U: Air speed

 ρ_a (rho): Air density

Figure 7 shows a contour map of the aluminum elephant heat flux for the fifth, (24.9 m/s), headwind, heat transfer run. The highest heat transfer was in the trunk and tusk tips, followed by the legs and ear edges. Figure 8 shows the same run with streamlines on the ears and left foreleg as well as a turbulence field. The figure shows the high velocity around the ear tips and the turbulence in the low heat transfer regions behind the ears and legs. The streamlines show that there was air flow off the chest which passed behind the ear. Figure 9 shows the experimental and simulated data for the heat transfer coefficient. There was good agreement at three velocities but the experimental data was lower than the calculations for the third (15.2 m/s) and final (24.9 m/s) runs. In these the sphere matched better. This simulation data allowed us to calculate the regression coefficients, a and a, in the heat transfer coefficient equation (Equation 3). For the headwind a was 0.723 a 0.004 and a was 0.101 a 0.005, while for the crosswind a was 0.71 a 0.03 and a was 0.11 a 0.04. For a sphere a is 0.6 and a is 0.37 (Mcadams 1954). As expected, these coefficients and figure 9 show little difference between crosswind and headwind heat transfer coefficients.

$$h_c = \frac{k_a}{L} a \left(\frac{\rho_a L U}{\mu_a}\right)^b \tag{3}$$

h_c: Heat transfer coefficient

 k_a : Thermal conductivity of the air

L: Characteristic length (cube root of volume)

 ρ_a (rho): Air density

U: Air speed

 μ_a (mu): Dynamic viscosity of the air

The Nusselt-Reynolds correlation makes the heat transfer coefficient equation more compact, $Nu = aRe^b$, where $Nu = h_cL/k$ (Bird et al. 2002).

Figure 10 shows the percentage difference between the heat transfer coefficient for a 3.5 m tall elephant and a sphere of equivalent volume. At wind speeds as low as 2 m/s the sphere was already off by 15%. Towards higher wind speeds which elephants may experience (Garstang et al. 1995), the difference reached 33%.

Discussion

With a few exceptions, we had good agreement between experiment and simulation. At low air speed, the experimental drag force did not follow the expected curve. Reduced precision of the sting balance at low forces may have caused this difference. There was the possibility that a transition to turbulence reduces the drag between the first (5.2 m/s) and second (10.1 m/s) runs. While the Reynolds numbers for the first and second runs were in the range of turbulent transitions (Re = 100000 (Kreith 1968)), the simulation was accounting for turbulence and should capture any transitions, therefore we think a transition is unlikely. In the higher numbers we could possibly achieve better agreement with slight changes to either the air density or viscosity; however, we did not attempt these changes as our goal is to test the predictive power of the simulation without reference to a model.

The heat transfer coefficient was in good agreement with the experimental data. The model's low initial temperature at the third (15.2 m/s) and final (24.9 m/s) air speed (Fig. 2) may have caused the low heat transfer coefficient. We also think that these experimental

values are incorrect as they were lower than a sphere of the same volume. This lower value was unreasonable given the more elaborate surface of the elephant. At temperatures that close to ambient, the model may have not had a high enough thermal gradient for an accurate heat transfer coefficient measurement. Nevertheless, the trend between experimental and simulated data is consistent.

We need to improve the simulation in several ways to successfully model an actual animal. First, and most easily, the simulation will need a surface roughness parameter input to Fluent. This parameter allows Fluent to account for the additional turbulence effects from surface roughness. Roughness data is accessible on preserved animal skins. Second, we will need to divide the animal model into different thermal conductivity regions. The need for this division is evident from the large heat loss from the elephant tusk, where an actual elephant tusk will have much less heat transfer. Conversely, elephants can control the perfused blood to their pinna resulting in higher or lower heat transfer coefficients than the animal body (Wright '84; Williams '90). The final and most difficult addition to the simulation is movement.

Considering the elephant, Fluent could simulate the additional fluid movement from thermoregulatory ear flapping which can substantially increase heat loss (Phillips and Heath '92). The ability to incorporate movement could also allow calculations on thrust and lift from aquatic and flying animals.

Researchers need biophysical parameters to compose models of animals in their environment. Given these parameters and the abiotic conditions of a habitat, researchers can construct models to predicted animal persistence, behavior, fitness, etc. These models are important guides for conservation (Porter et al. 2006, Kearney et al. 2008) as well as agriculture

practices (Parsons & Armstrong 2001, Souto et al. 2011). This paper's initial verification of Fluent's ability to correctly simulate complicated biological geometries is a first step towards using the thermal and momentum capabilities of ANSYS Fluent (or equivalent software) to model actual animals. Researchers could use these models to extract important physical coefficients without the need for live specimens. This method promises to save researchers time and expense as well as serve as a highly adaptable tool to calculate many biophysical parameters of organisms.

Acknowledgments

We would like to thank Pobtsuas Xiong in the University of Wisconsin Digital Media

Center for help in scanning the casting. This work was supported by NSF grant IOS-1116343 to

WPP and by a Dept. of Zoology summer research support grant to PND.

Table 1. The parameters used in the simulations. We set the parameters to match those experienced in the wind tunnel experiments. The ranges are for parameters which changed from run to run owing to the waste heat from the wind tunnel fan.

	Parameter	Symbol	Value	Units
Elephant Casting	Mass	$m_{ m e}$	3.5	kg
	Frontal Area	A_{f}	0.0147	m ²
	Side Area	A_{s}	0.0326	m²
	Characteristic Length	L	0.111	m
	Density	$ ho_{e}$	2560	kg/m³
	Specific Heat	c _{pe}	902	J/kg/K
	Thermal conductivity	k _e	202.4	W/m/K
Air	Density	$ ho_{a}$	1.137 - 1.161	kg/m³
	Specific Heat	c _{pa}	1007.8 - 1008.0	J/kg/K
	Thermal Conductivity	k _a	0.02583 - 0.02591	W/m/K
	Dynamic viscosity	μ_{a}	1.821 x 10 ⁵ - 1.835 x 10 ⁵	kg/m/s

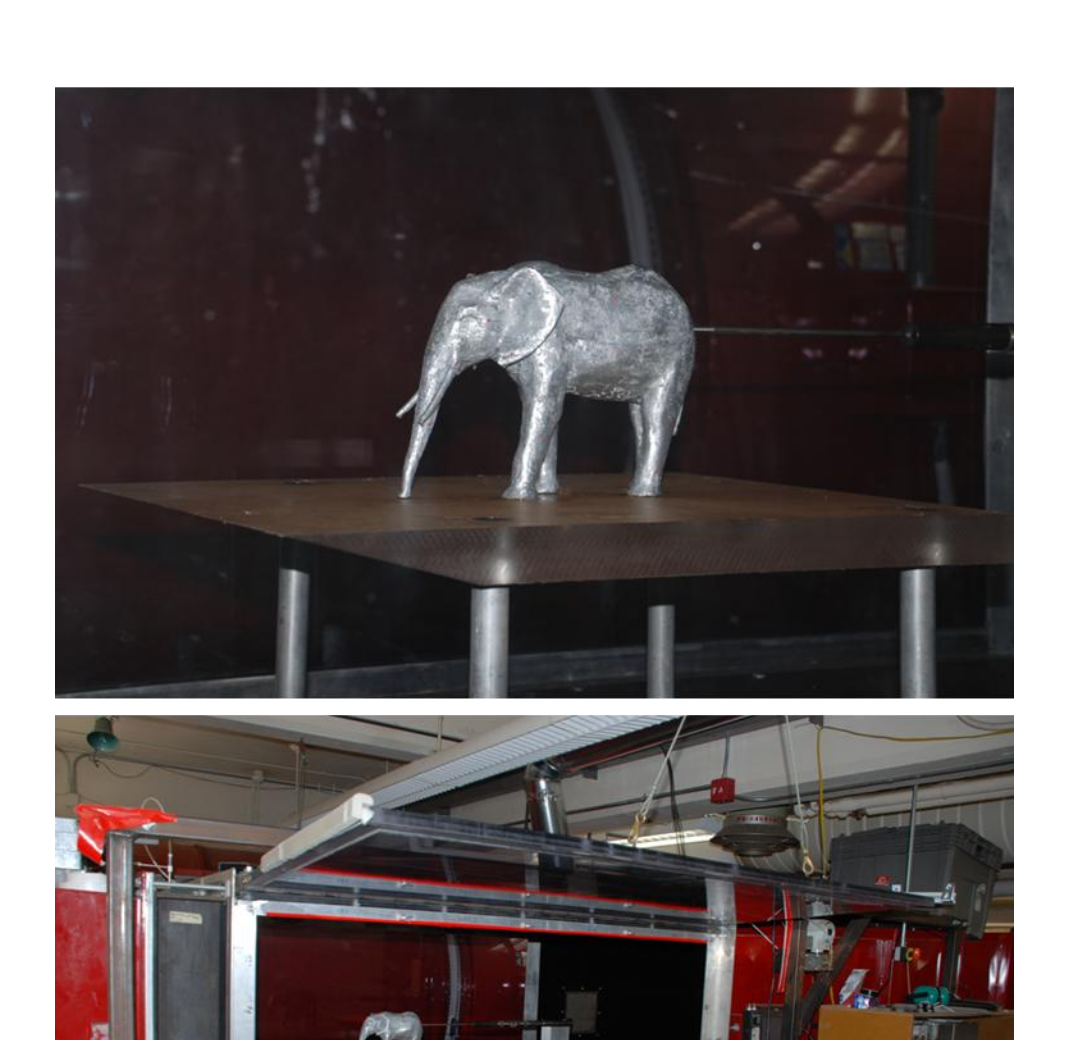


Fig.1. (Top) The solid aluminum elephant casting connected to a sting balance and placed on four ball bearings in recessed cavities in a solid Plexiglas sheet with a knife edge front end. (Bottom) The 4.8 cm thick Plexiglas sheet mounted on four posts bolted to the floor of the recirculating wind tunnel with a $0.9 \times 1.2 \times 1.84$ m working section.

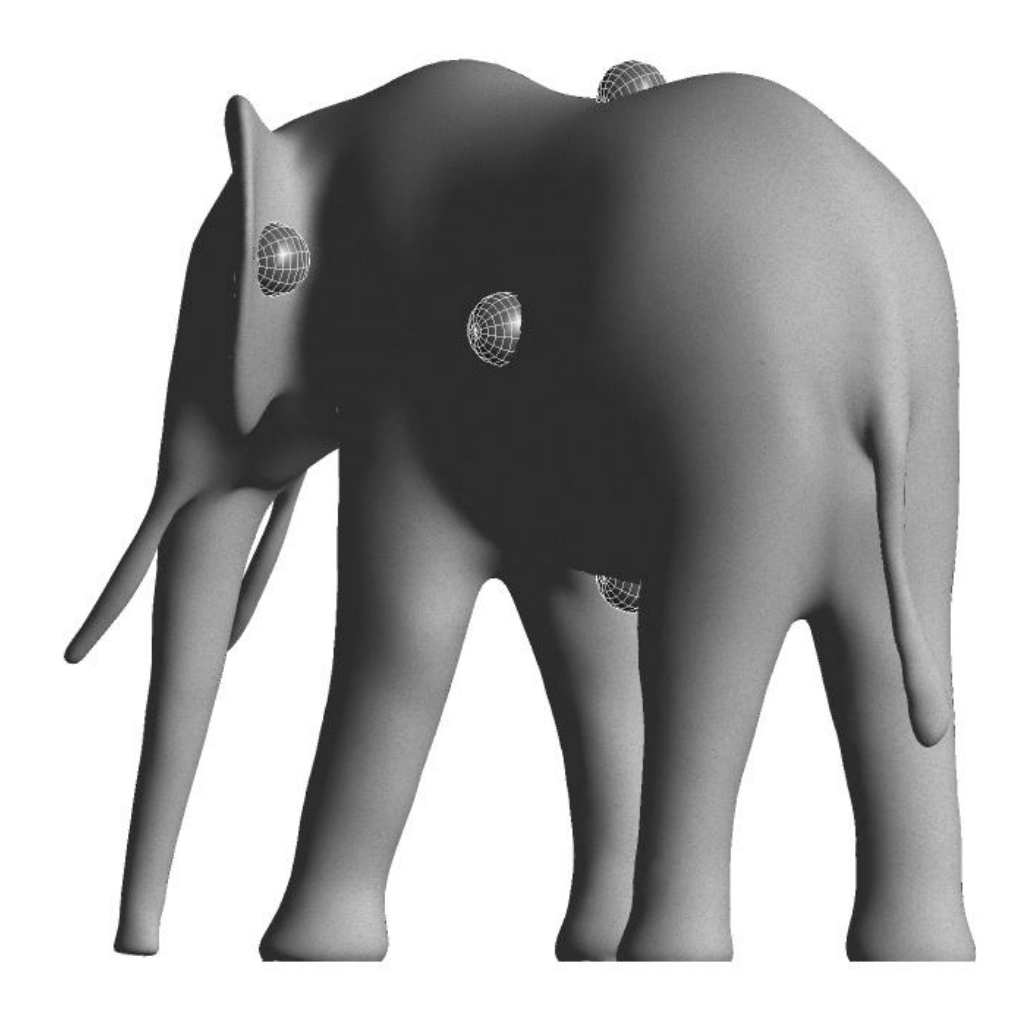


Fig.2. The location of the four thermocouples on the elephant. The thermocouples are represented by spheres for purposes of this figure. We placed the thermocouples on the belly, left mid lateral portion of the body, center back of the left ear and center back.

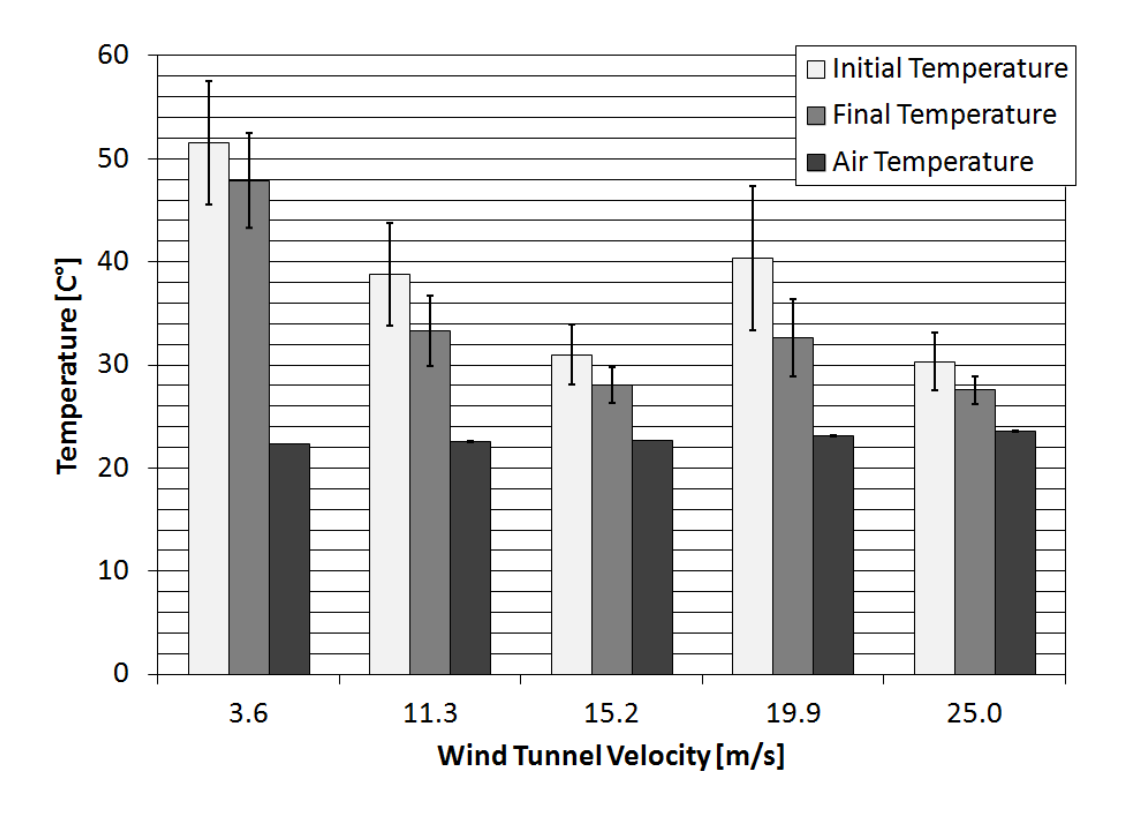


Fig. 3. The initial elephant, final elephant, and ambient air temperature for the five wind tunnel runs. The slight increase in ambient air temperature was likely due to waste heat from the wind tunnel fan. This temperature increase as well as other air properties (density, viscosity, thermal conductivity, and specific heat) were all matched between each simulation and experimental run. We used a heat lamp to heat the casting while the wind tunnel was shut down. We turned off the heat lamp before sealing the wind tunnel. We heated the model before the 3.6 m/s run and again after the 15.2 m/s run. Four thermocouples on the model measured the temperature and the graph presents the averages of these measurements with standard deviations. The low temperature difference between the elephant and ambient air may have affected the accuracy of the heat transfer coefficient calculation from the 15.2 m/s and 24.9 m/s runs.

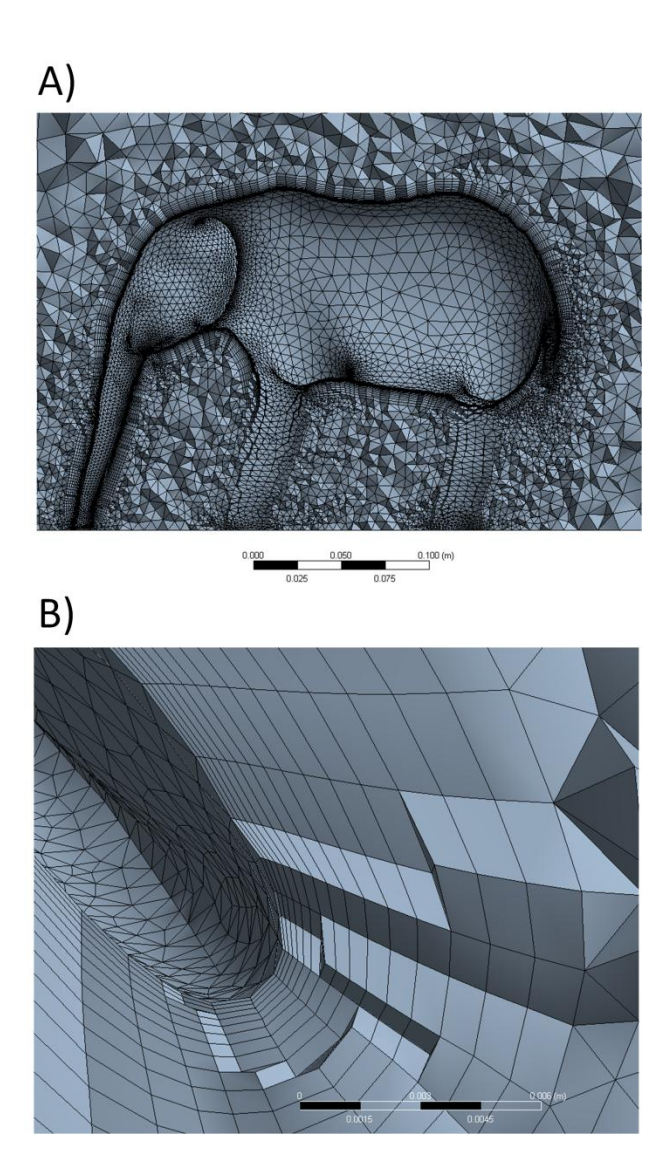


Fig.4. (A) The meshing of the fluid space around the elephant. Meshing was approximately equal parts 4-node tetrahedral and 6-node wedge elements with a few 5-node pyramid elements with an inflation layer in the boundary region around the elephant. (B) The mesh size was sensitive to curvature to achieve a high quality mesh around regions such as the elephant's ear. This figure shows a close up of the inflation layer near the elephants ear. The inflation region had 16 layers and a maximum height of 1 cm.

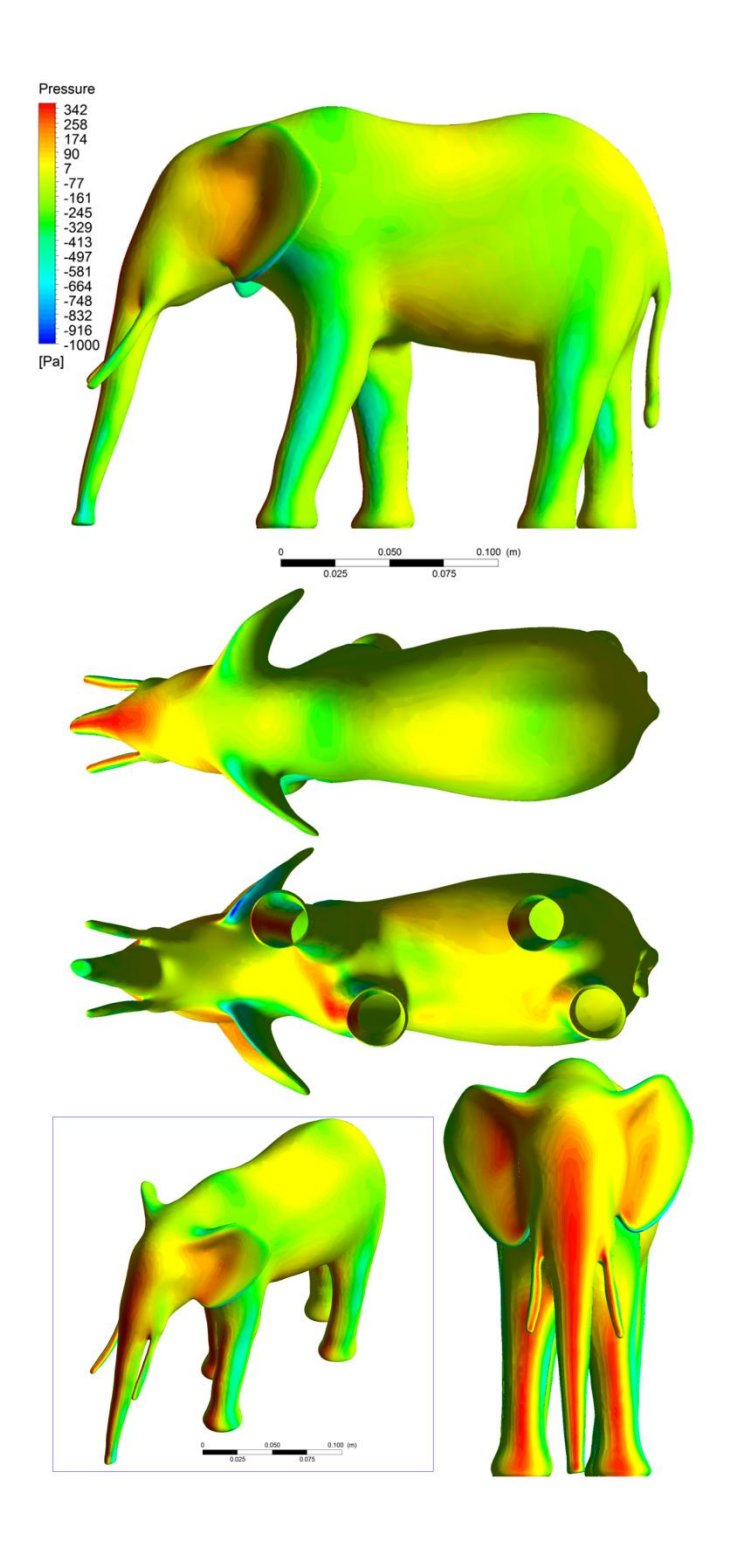


Fig.5. A contour map of the pressure on the elephant in a 25.1 m/s headwind. There was high pressure on the front face and a region of low pressure behind the ears. Both scale bars are 0.10 m long.

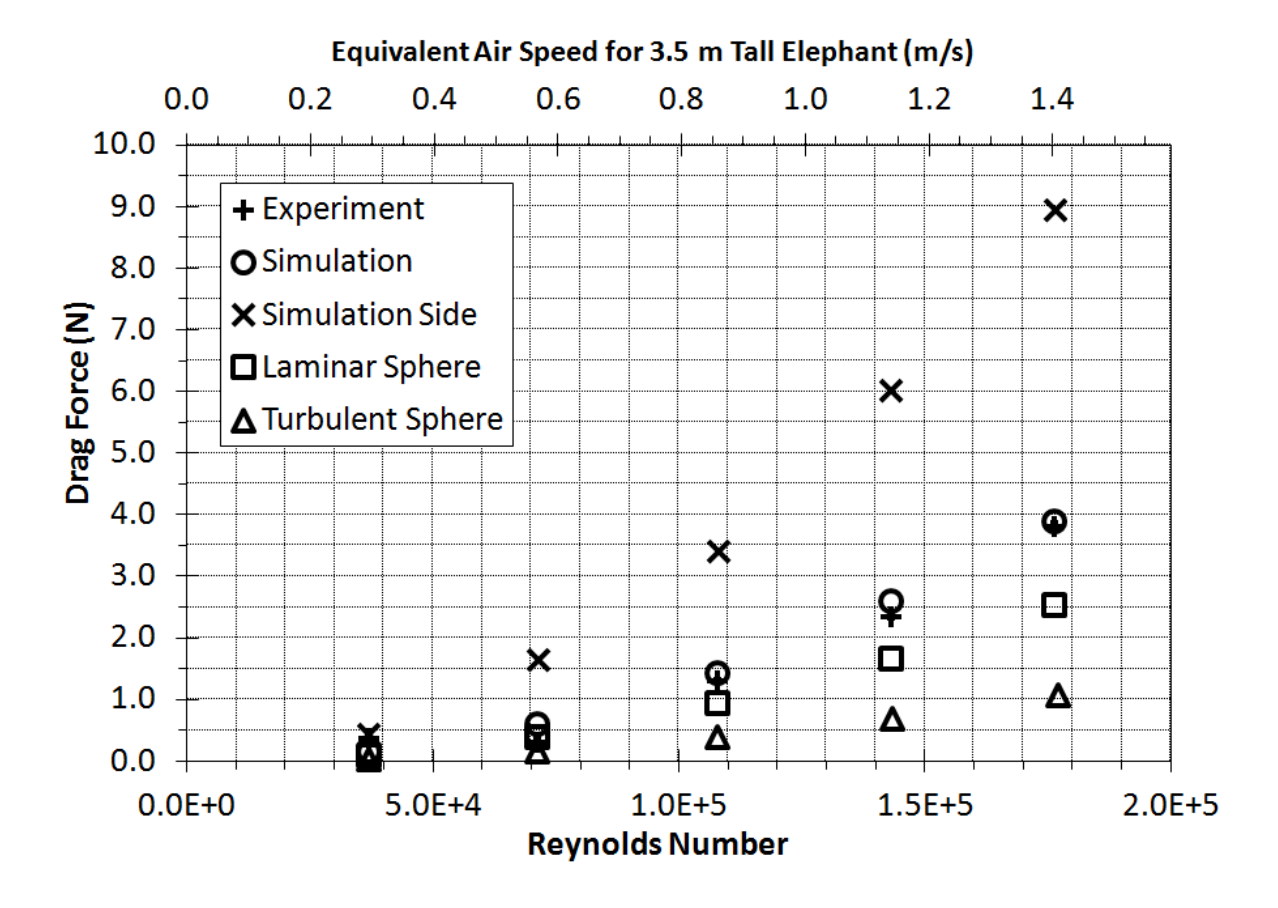


Fig.6. Experimental vs. simulated drag data. Poor agreement at the lower speeds was likely due to low precision of the sting balance at low loads. The drag coefficient from the simulated data was 0.73 ± 0.02 for a headwind and 0.80 ± 0.04 for a cross wind. We used the front and side projected area in the headwind and crosswind calculations respectively.

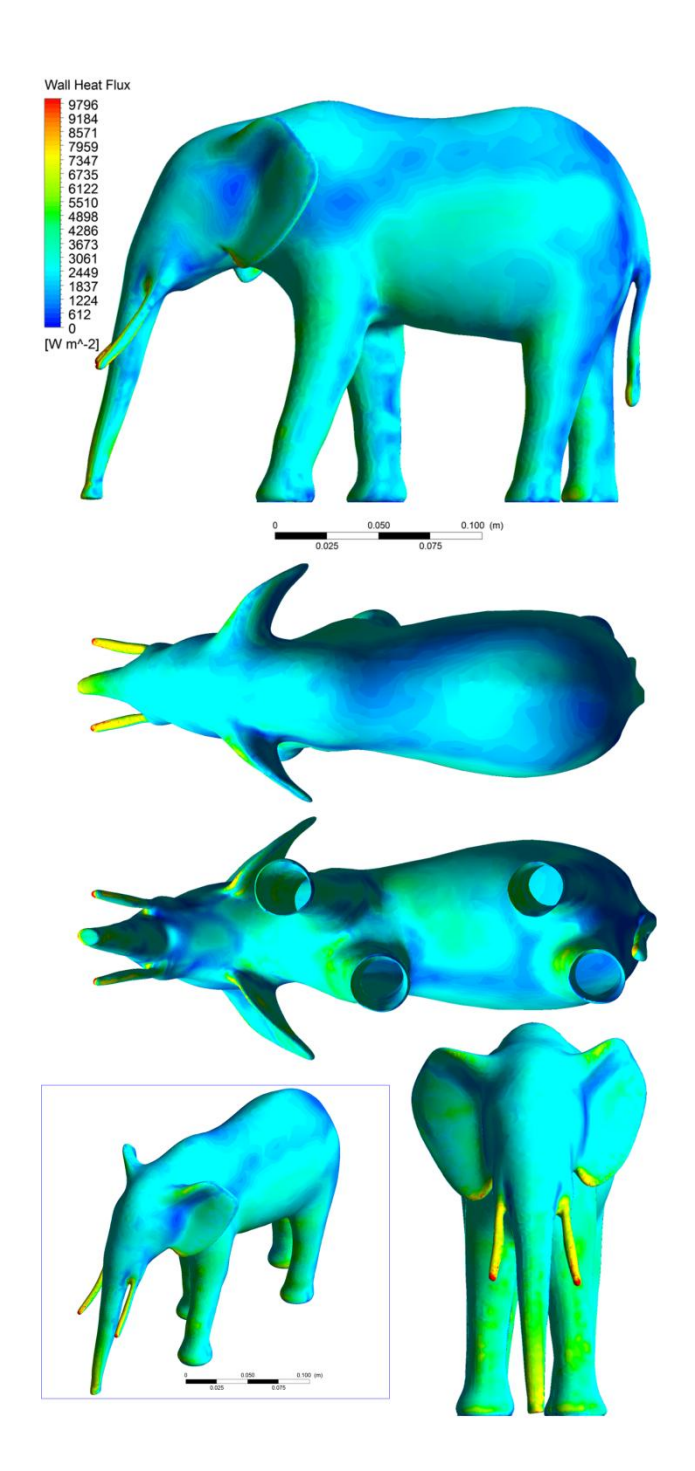


Fig.7. A contour map of the heat flux for an elephant in a 24.9 m/s headwind. The regions of highest heat transfer were the trunk and tips of the tusks followed by the legs and ear tips. Future simulations will isolate low or highly conductive regions to more accurately model the animal. Both scale bars are 0.1 m.

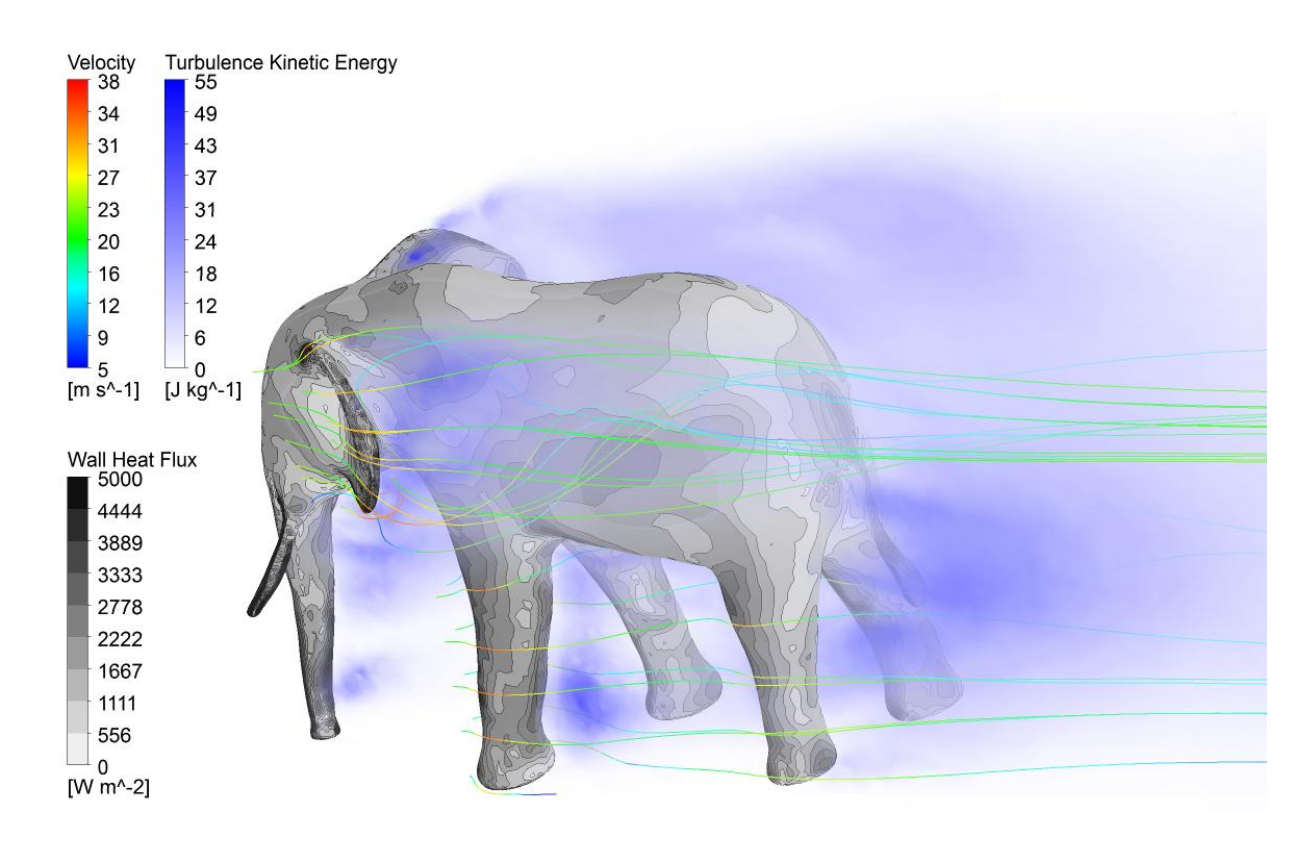


Fig.8. A contour map of the heat flux for an elephant in a 24.9 m/s headwind with streamlines around the ears and left foreleg. Regions of higher turbulence were in blue. There were regions of higher turbulence behind the legs and ears where there is low heat transfer.

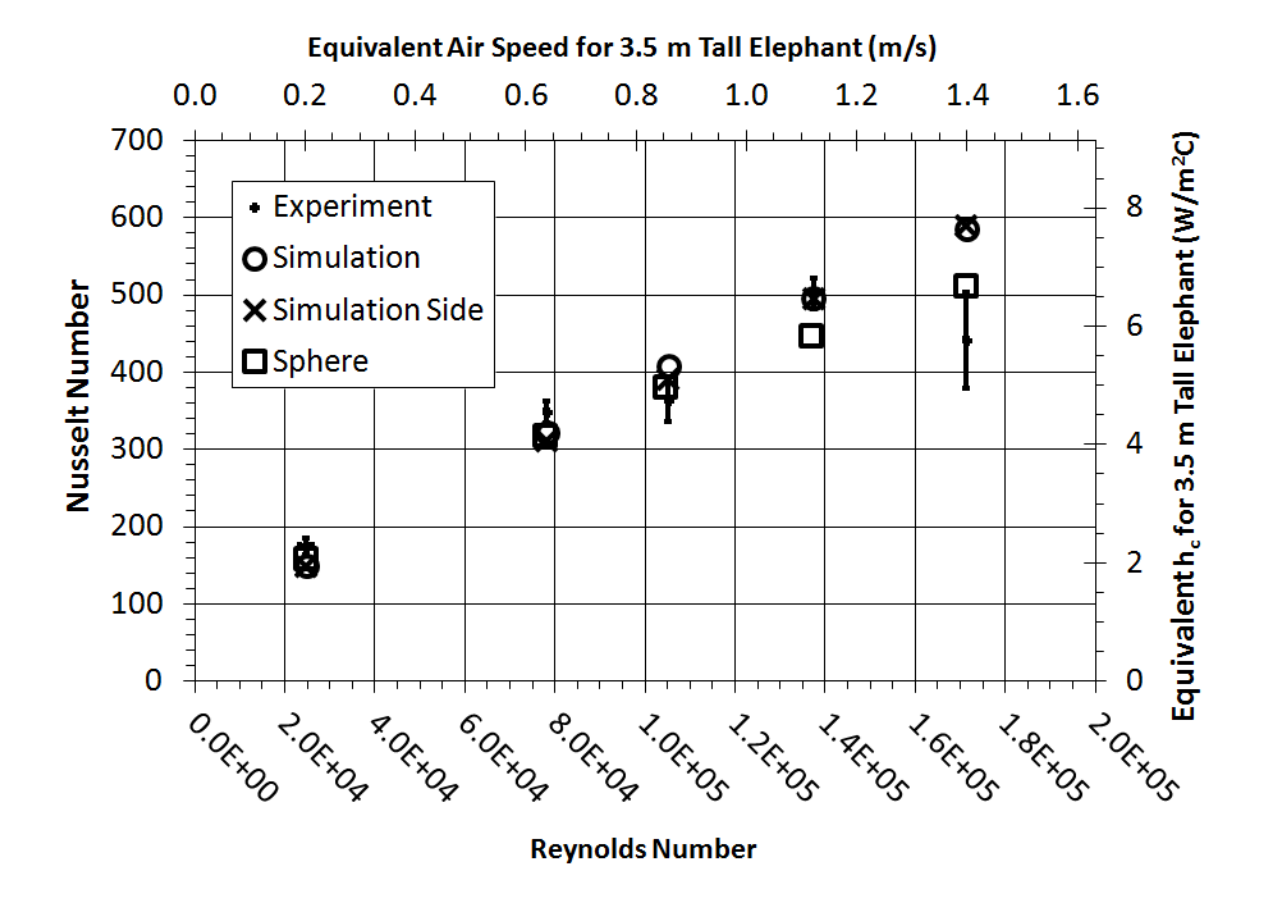


Fig.9. The experimental vs. simulated heat transfer coefficient, h_c , data. There was good agreement for three values when there was a high temperature difference between the model and the ambient temperature (Fig. 3), but when the elephant was cooler there was not as good agreement. The heat transfer coefficient regression coefficients (Equation 3) from the simulated data were $b = 0.705 \pm 0.013$ and $a = 0.118 \pm 0.018$ for a head wind and $b = 0.71 \pm 0.03$ and $a = 0.11 \pm 0.04$ for a crosswind.

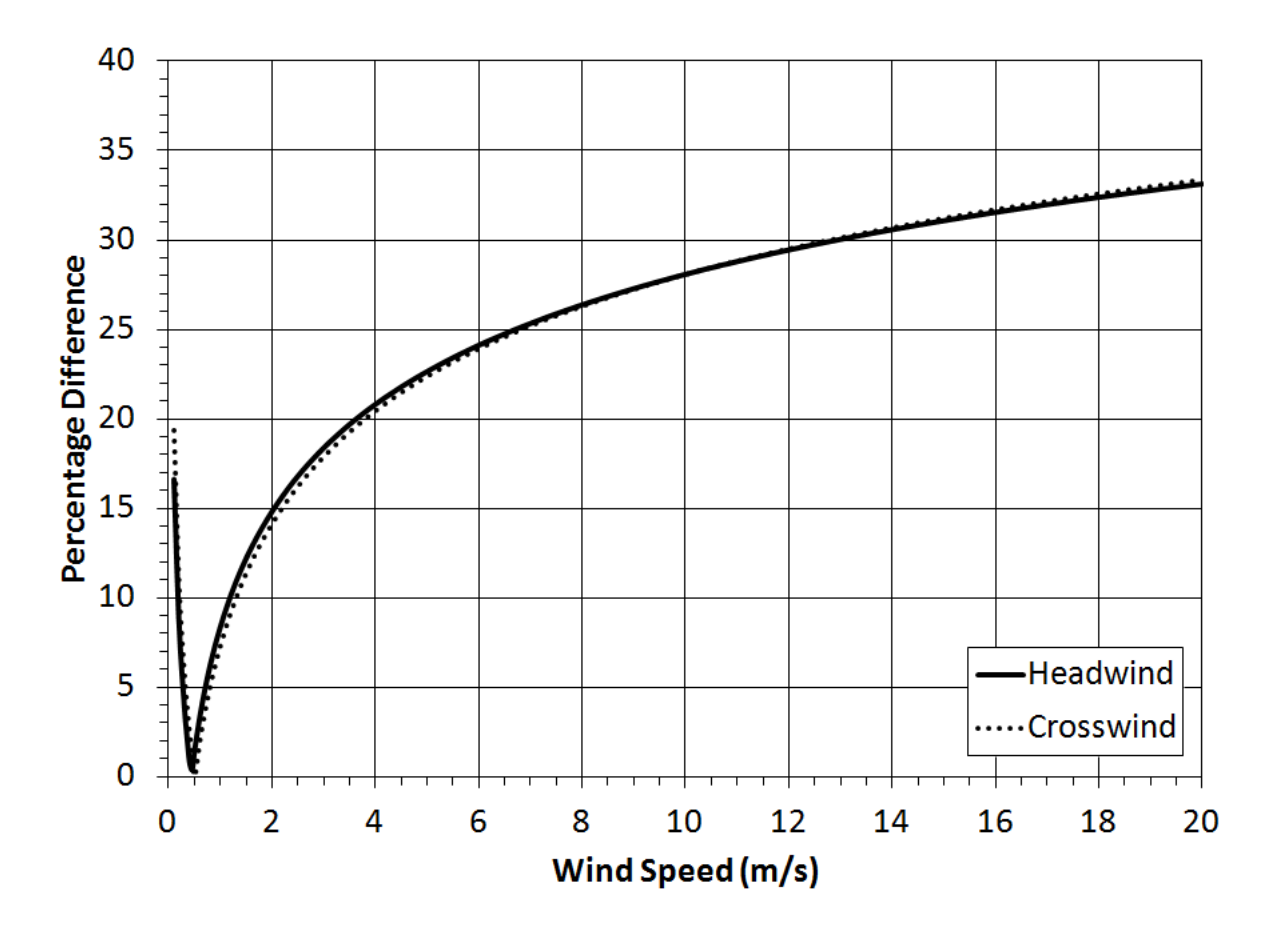


Fig.10. The percentage difference between the heat transfer coefficient for a 3.5 m tall elephant and a sphere of equivalent volume. At wind speeds less than 2 m/s the sphere was off by as much as 15%. Towards higher wind speeds elephants may experience, the difference reached 33%. This graph is the absolute percentage difference, thus below 0.5 m/s the sphere cools faster than the elephant, while the elephant cools faster at all wind speeds above 0.5 m/s.

References

- Bird RB, Stewart WE, Lightfoot EN (2002)Transport Phenomena, 2nd edn. Wiley and Sons, New York
- Blake RW, Chan KHS (2007) Swimming in the upside down catfish *Synodontis nigriventris*: it matters which way is up. J Exp Biol 210:2979–89
- Bullen RD, McKenzie NL (2007) Bat wing airfoil and planform structures relating to aerodynamic cleanliness. Aust J Zool 55:237
- Dear R de, Arens E, Hui Z, Oguro M (1997) Convective and radiative heat transfer coefficients for individual human body segments. Int J Biometeorol 40:141–156
- Drucker E, Lauder G (1999) Locomotor forces on a swimming fish: Three-dimensional vortex wake dynamics quantified using digital particle image velocimetry. J Exp Biol 202:2393–2412
- Garstang M, Larom D, Raspet R, M L (1995) Atmospheric controls on elephant communication. J Exp ... 198:939–51
- Haider A, Levenspiel O (1989) Drag coefficient and terminal velocity of spherical and nonspherical particles. Powder Technol 58:63–70
- Hazekamp A a. H, Mayer R, Osinga N (2009) Flow simulation along a seal: the impact of an external device. Eur J Wildl Res 56:131–140
- Kearney M, Phillips B, Tracy C, Christian K (2008) Modelling species distributions without using species distributions: The cane toad in Australia under current and future climates. Ecography (Cop):1–12
- Kreith F (1968)Principles of Heat Transfer (EF Obert, Ed.), 2nd edn. International Textbook Company, Scranton, Pennsylvania
- Marom S, Korine C, Wojciechowski MS, Tracy CR, Pinshow B (2006) Energy metabolism and evaporative water loss in the European free-tailed bat and Hemprich's long-eared bat (*Microchiroptera*): species sympatric in the Negev Desert. Physiol Biochem Zool 79:944–56
- Mcadams W (1954)Heat Transmission, 3rd edn. McGraw Hill, New York
- Natori Y, Porter WP (2007) Model of Japanese serow (Capricornis crispus) energetics predicts distribution on Honshu, Japan. Ecol Appl 17:1441–59

- Parsons D, Armstrong A (2001) Integrated models of livestock systems for climate change studies. 1. Grazing systems. Glob Chang Biol 7:93–112
- Pavlov V V., Rashad AM (2012) A non-invasive dolphin telemetry tag: Computer design and numerical flow simulation. Mar Mammal Sci 28:E16–E27
- Pavlov V V., Wilson RP, Lucke K (2007) A new approach to tag design in dolphin telemetry: Computer simulations to minimise deleterious effects. Deep Sea Res Part II Top Stud Oceanogr 54:404–414
- Phillips PK, Heath JE (1992) Heat exchange by the pinna of the African elephant (Loxodonta africana). Comp Biochem Physiol Part A Mol Integr Physiol 101:693–9
- Porter W, Budaraju S (2000) Calculating climate effects on birds and mammals: impacts on biodiversity, conservation, population parameters, and global community structure. Am Zool 40:597–630
- Porter W, Mitchell J, Beckman W, DeWitt CB (1973) Behavioral implications of mechanistic ecology. Thermal and behavioral modeling of desert ectotherms and their microenvironment. Oecologia 13:1–54
- Porter W, Munger J, Stewart W (1994) Endotherm energetics: From a scalable individual-based model to ecological applications. Aust J Zool 42:125–162
- Porter WP, Vakharia N, Klousie WD, Duffy D (2006) Po'ouli landscape bioinformatics models predict energetics, behavior, diets, and distribution on Maui. Integr Comp Biol 46:1143–1158
- Sachs G (2007) Tail effects on yaw stability in birds. J Theor Biol 249:464–72
- Skrovan RC, Williams TM, Berry PS, Moore PW, Davis RW (1999) The diving physiology of bottlenose dolphins (*Tursiops truncatus*). J Exp Biol 202:2749–2761
- Souto LF, Meneses JF, Bruce JM (2011) Prediction of the energy balance and milk production of grazing cows in the Azores for autumn and spring calving. Biosyst Eng 110:57–65
- Stephenson R, Loworn J, Heieis M, Jones DR, Blake RW (1989) A hydromechanical estimate of the power requirements of diving and surface swimming in lesser scaup (Aythya affinis). J Exp Biol 147:507–519
- Tieleman B, Williams J, Buschur M, Brown CR (2003) Phenotypic variation of larks along an aridity gradient: are desert birds more flexible? Ecology 84:1800–1815

- Tobalske B, Peacock W, Dial K (1999) Kinematics of flap-bounding flight in the zebra finch over a wide range of speeds. J Exp Biol 202:1725–39
- Usherwood JR (2003) The aerodynamics of avian take-off from direct pressure measurements in Canada geese (*Branta canadensis*). J Exp Biol 206:4051–4056
- Ward S, Rayner J, MOLler U, Jackson D, Nachtigall W, Speakman J (1999) Heat transfer from starlings sturnus vulgaris during flight. J Exp Biol 202:1589–602
- Wathen P, Mitchell JW, Porter WP (1971) Theoretical and experimental studies of energy exchange from jackrabbit ears and cylindrically shaped appendages. Biophys J 11:1030–1047
- Weber PW, Howle LE, Murray MM, Fish FE (2009) Lift and drag performance of odontocete cetacean flippers. J Exp Biol 212:2149–58
- Williams TM (1990) Heat transfer in elephants: thermal partitioning based on skin temperature profiles. J Zool 222:235–245
- Wright PG (1984) Why do elephants flap their ears? South African J Zool 19:266–269
- Wu B, Gebremedhin K (2001) Numerical simulation of flow field around a cow using 3-D bodyfitted coordinate system. J Therm Biol 26:563–573

<u>Chapter 3:</u> Leatherbacks in silico: Modeling the core temperature of a sea turtle using computational fluid dynamics

<u>Authors:</u> Peter N. Dudley¹, Riccardo Bonazza¹, T. Todd Jones², Jeanette Wyneken³, and Warren
P. Porter¹

¹University of Wisconsin—Madison

²NOAA Fisheries

³Florida Atlantic University

Abstract

As global temperatures increase throughout the coming decades, species ranges will shift. New combinations of abiotic conditions will make predicting these range shifts difficult. Biophysical mechanistic niche modeling places bounds on an animal's niche through analyzing the animals physical interactions with the environment. Biophysical mechanistic niche modeling is flexible enough to accommodate these new combinations of abiotic conditions. However, this approach is difficult to implement for aquatic species because of complex interactions between thrust, metabolic rate and heat transfer. We use modern computational fluid dynamic techniques to overcome these difficulties. We model the complex 3D motion of a swimming neonate and juvenile leatherback sea turtle to find power and heat transfer rates during the stroke. We combine the results from these simulations and a numerical model to accurately predict the core temperature of a swimming leatherback. These results are the first steps in

developing a highly accurate mechanistic niche model, which can assists paleontologist in in understanding biogeographic shifts as well as aid contemporary species managers about potential range shifts over the coming decades.

Introduction

Ecological niche modeling analyses a set of environmental conditions in a location to deterring likelihood or possibility of a species persistence. It is an important tool to answer the fundamental question of where a species can exist. Throughout the next century, climate change will likely shift many species' ranges (Parmesan & Yohe 2003). In addition to causing these range shifts, climate change makes predicting species future ranges difficult because it introduces regionally novel sets of abiotic conditions. With these novel circumstances, forming an empirical niche map (based on species presence/absence data and a statistical model) requires complex statistical methods and may still be inappropriate or inaccurate (Dormann 2007, Phillips et al. 2008). Under climate change conditions, a more appropriate niche mapping approach may be mapping the fundamental niche (Hutchinson 1957) using a biophysical mechanistic niche model. A biophysical model permits any combination of abiotic conditions, novel or otherwise, provided the model can accurately represent how they affect the organism (Kearney & Porter 2009).

While the biophysical niche model approach is successful with terrestrial animals (Kearney et al. 2008, Porter & Kearney 2009), it is more difficult to implement with aquatic organisms. The main reason for this difficulty is the strong links among heat transfer, metabolic rate and aquatic motion (Boisclair & Tang 1993), and the difficulty in measuring each of these.

First, while it is possible to measure metabolic rate for some aquatic animals (smaller tractable species), it is difficult or impossible to measure it for others (large species that do poorly in captivity). Second, the complex interaction between thrust and drag on a deforming body makes it difficult to quantify a moving animal's useful work (Schultz & Webb 2002). Finally, determining how rapidly a self-propelling, aquatic organism loses metabolic waste heat further complicates making a biophysical niche map.

Many methods attempt to address some of these difficulties. Trained live animals can fly/swim in a wind tunnel/flume or while tethered. The animals may wear pressure sensors (Usherwood 2003, Blake & Chan 2007) or temperature sensors (Tieleman et al. 2003, Marom et al. 2006). There are also non-contact methods such as filming particle flow around an animal and calculating force with software (Drucker & Lauder 1999), using cameras to measure reference point movement (Skrovan et al. 1999, Tobalske et al. 1999), or using thermal cameras to measure temperature profiles (not possible for aquatic animals) (Ward et al. 1999). In addition to logistical and ethical consideration of live animal trials, all these methods have limited resolution and cannot decouple thrust and drag.

Modern computational fluid dynamics (CFD) can address many live animal experiments' shortfalls while giving biophysical niche models necessary information to make accurate predictions. CFD is now capable of simulating drag (Pavlov & Rashad 2012) or heat transfer (Dudley et al. 2013) of static animals and even thrust and power of undulating swimmers (Liu et al. 1997). Here we use a novel CFD technique to not only measure the power and heat flux of the 3D complex motion of a leatherback sea turtle (*Dermochelys coriacea*), but also to model internal heat transfer accounting for complex physiological issues such as an insulating layer's

varying thickness, vasoconstriction and dilation, and counter current heat exchangers. We compare our results to tethered swimming neonate and juvenile turtles. Further, we show that, by using only an allometric equation for resting metabolic rate (RMR) and the turtle's flipper beat frequency, our methods can accurately predict the animal's core temperatures. To our knowledge, this work is the first use of a 3D dynamic CFD simulation to accurately predict the internal environment of an animal.

Methods

Neonate Experiments

Florida Atlantic University's Institutional Animal Care and Use Committee, Protocol A10-18 approved work with live neonate turtles, which occurred under Florida marine turtle permit 073 to Jeanette Wyneken. For animal collection and captive care, please see Miller et al. 2009 and Jones et al. 2011 (Miller et al. 2009, Jones et al. 2011).

To measure thrust of the swimming neonates, we attached turtles (n=11) by tether to a Futek® load cell (FUTEK Advanced Sensor Technology, INC. Irvine, CA USA, LSB200 JR S-Beam load cell, range 0-10 g, 5 pt. calibration with resolution 0.03% of total range). The turtles swam freely in a 35 cm X 35 cm X 35 cm (h, w, d) tank for 40 to 60 minutes with force recorded at 2.85 Hz. The tether ran through an eyelet just above the water surface (4cm) and attached to the force balance above the tank. The tether and eyelet had the dual purpose of allowing the turtles to swim or dive in any direction without hitting the tank walls and bottom while also directing thrust in line with the compression/tension of the load cell. We recorded the turtles' flipper motion using a high-speed camera (420 frames per second). The turtles' changes in

swimming direction through the trials allowed us to capture stroke video from lateral, posterior and anterior angles.

Neonate Simulations

Using commercial 3D rendering software (ZBrush[™]) we drew an anatomically realistic leatherback neonate in non-uniform rational basis splines (NURBS) format (Fig. 1). The neonate had a curved carapace length (CCL) of 7 cm and would weigh approximately 60 g (morphology and summary data is in Table 1). We imported this NURBS model into ANSYS DesignModeler (ANSYS®, Release 14.0) and enclosed one side of the model in a half cylinder, with the plane dividing the cylinder in half also dividing the turtle along the sagittal plane. This half cylinder is the fluid region surrounding the turtle. Enclosing only half the turtle and using a symmetry boundary condition on the plane bisecting the turtle increases computational efficiency. The enclosing half cylinder had front, side and back buffers of 0.2 m, 0.4 m and 0.5 m respectively (Fig. 2). The half cylinder's total volume (total fluid domain) was 0.3 m³. We imported this cylinder into ANSYS Meshing and meshed the entire fluid domain with 138,000 tetrahedral elements (Fig. 3). We then imported this mesh into the CFD program ANSYS Fluent.

We analyzed frames from the high-speed video using ImageJ version 1.46r analysis software to measure the flipper motion. We wrote a supplemental program, which describes the turtles' swimming motion we observed in the video. The flipper had four zones. The 14% of the flipper closest to the shoulder was the transition zone from no motion to steady roll (flipper moving dorsally to ventrally) and yaw (flipper moving posteriorly to anteriorly). The next 22% of the flipper was the transition zone from steady roll and yaw to steady roll, yaw, and pitch (flipper twisting). The next 21% of the flipper was a zone of constant roll, yaw, and pitch.

The last 43% of the flipper was the transition zone from steady roll, yaw, and pitch to roll, yaw, pitch, and bend (flexing of the flipper in the roll plane). The stroke had four phases. There was a down stroke (0.384 s), a turn at the bottom (0.199 s), an up stroke (0.497 s), and a turn at the top (0.163 s). To prevent discontinuities in the model's motion, each phase used 10% of its time to transition from the last phase. Figure 4 shows the yaw, pitch, and roll rates of the stroke.

The simulation used the k- ω shear stress transport (SST) viscosity model with a zero pressure inlet and outlet at the front and back of the turtle's half cylinder enclosure (i.e. no flow velocity as the turtle in the experiment was tethered). The plane of the half cylinder, which divided the turtle along the sagittal plane, had a symmetry boundary condition that reduced computation time by using only the left half of the 3D symmetrical image. We set the time step to 0.001 s and ran the simulation for 1442 time steps (one full period). We calculated the turtle's average thrust by numerically integrating over each mesh node the instantaneous thrust in the swimming direction (Eq. 1) every 0.01 s and averaging those data over the entire run. We compared it with the experimental neonate force data.

$$F_z = \int (P_z + \tau_z) dA_f + \int (P_z + \tau_z) dA_b \tag{1}$$

F_z: Instantaneous force in the swimming direction

P_z: Pressure component in the swimming direction

 τ_z : Shear stress component in the swimming direction

A_f: Flipper area

A_b: Body area

Literature Data

To assess the ability of our method to model heat production and flux, we conducted four simulations to model turtles from Bostrom et al. (2010). They used a swallowed thermometer pill to measure the core temperature of tethered swimming leatherbacks while counting flipper stroke frequency and measuring ambient water temperature.

Juvenile Swimming Simulations

We drew an anatomically realistic juvenile leatherback in NURBS format using commercial 3D design software (MoI) (Fig. 5). The juvenile had a curved carapace length (CCL) of 72 cm and would weigh approximately 37 kg. We imported this NURBS model into ANSYS DesignModeler and enclosed one side of the model in a half cylinder. The cylinder had front, side and back buffers of 1.9 m, 1.9 m and 3.8 m respectively (Fig. 6). The half cylinder's total volume was 60.3 m³. We imported this cylinder into ANSYS Meshing and meshed the entire fluid domain with 195,000 tetrahedral elements (Fig. 7). We then imported this mesh in to ANSYS Fluent.

We used the same supplemental program to describe the juvenile turtle's swimming motion that we used for the neonate turtle. We analyzed frames from publicly available video of leatherbacks freely swimming with ImageJ to measure the flipper motion. The flipper had the same four zones as the neonate. Again, the stroke had four phases. There was a down stroke (32.3% of stroke period), a turn at the bottom and at the top of the stroke (17.0% of stroke period for each), and an up stroke (33.7% of stroke period). To prevent discontinuities in the motion, we programmed smooth transitions into the top and bottom phase. To correctly

position the flipper, there was also a 0.5 s setup time. We used four of the flipper stroke frequencies from Bostrom et al. (6, 19, 25, and 29 beats per minute) (2010). Figure 8 shows the yaw, pitch, and roll rates of the stroke.

The simulation used the k- ω SST model with a zero pressure inlet and outlet at the front and back of the turtle's half cylinder enclosure (i.e. no flow velocity as the turtle in the experiment was tethered). The plane dividing the turtle had a symmetry boundary condition. We set the time step to 0.001 s and ran the simulation for one full period plus setup time. In all analyses, we removed the initial 500 set-up steps. We calculated average thrust (Eq. 1), power (Eq. 2), and flipper and body heat transfer coefficients (Eq 3.) by instantaneous numerical integration over each mesh node every 0.01 seconds and averaging those data over the run. To translate total work the turtle does on the water into expended energy, we used the aerobic efficiency of tortoise muscle (35% (Woledge 1968)).

$$W = \int ((P_z + \tau_z) \cdot v_z) + ((P_x + \tau_x) \cdot v_x) + ((P_y + \tau_y) \cdot v_y) dA_f$$
 (2)

W: The power the flipper puts into the water

 $P_{z,x,y}$: The z, x, or y pressure component

 $\tau_{z,x,y}$: The z, x, or y shear stress component

 $v_{z,x,y}$: The z, x, or y flipper velocity component

A_f: Flipper area

81

$$h = \frac{\int_{\overline{(T-T_{\infty})}}^{\Phi_{\mathbf{q}}} dA}{A} \tag{3}$$

h: Heat transfer coefficient

Φ_q: Heat flux

T: Wall temperature

T_∞: Free stream temperature

A: Area

Juvenile Internal Conduction Simulations

Using literature information on insulating layer thickness, we drew an anatomically realistic core region of the adult leatherback in NURBS format (Goff & Stenson 1988, Davenport et al. 1990, 2009, Chang et al. 2003). We also included a countercurrent heat exchanger region in the flipper (Fig. 9) (Greer et al. 1973). We set the insulating region density to that of blubber (980 kg/m³) (Parry 1949). We set the density of the core region to make the overall turtle neutrally buoyant (1035 kg/m³). This density is a reasonable number for a region comprised of bone, muscle, and organ tissue. We set the insulating region's thermal conductivity to that of blubber (0.280 W/m/K) (Kvadsheim et al. 1996) and the countercurrent heat exchanger region's thermal conductivity to that of dead tissue (0.531 W/m/K) (no blood flow) (Cheng & Plewes 2002). We described the core region's thermal conductivity as a temperature dependent function going from 0.531 W/m/K at 17 °C, to 0.622 W/m/K (conductivity of live muscle (Cheng & Plewes 2002)) at 28 °C, and to 50 W/m/K (a very high value to prevent the buildup of hot spots and unrealistic thermal gradients) at 47 °C. The actual value of the thermal conductivity at 47 °C had very little effect on the core temperature (a quadrupling of the thermal

conductivity results in an increase of less than 4% in the core temperature). This temperature dependence allows the model to simulate vasoconstriction and vasodilation given cold or hot temperatures. We set the insulating region's heat capacity to 2.94×10^3 J/kg/K based on an average of lipid heat capacities (Cedeno et al. 2000) weighted by the lipid content of blubber (Davenport et al. 1990) and water's heat capacity weighted by the water content of blubber (33%) (Bagge et al. 2012). We set the heat capacity of the core region to that of live tissue (4.18 $\times 10^3$ J/kg K) (Cheng & Plewes 2002). We used an allometric relation from Wallace & Jones (Eq. 4) to estimate the resting metabolic rate (RMR) for the juvenile turtle (Wallace & Jones 2008). We scaled the RMR with core temperature based on a Boltzmann factor relation for reptiles

(Eq. 5) (Gillooly et al. 2001). We set the external flipper boundary and body boundary heat

transfer coefficients to those obtained from the swimming simulation. We ran the internal

simulations in ANSYS Fluent using its built in solid heat transfer capabilities.

$$M(T = 30^{\circ}\text{C}) = 0.768m^{-0.169}$$
 (4)

M(T=30°C): Metabolic rate at 30°C (W/kg)

m: mass (kg)

$$M \sim e^{-E/kT} \tag{5}$$

M: Metabolic rate

E: Average activation energy (0.76 eV)

K: Boltzmann's constant (8.617 x 10⁻⁵ eV/K)

T: Temperature

Core temperature of the simulated turtle varied based on region. From the simulations we extracted the core region's minimum, maximum, and average temperatures. We also extracted temperatures for which 87.5%, 75%, 25% and 12.5% of the turtle's core volume was beneath (in other words, the temperatures bounding the 50th and 75th percentiles). We compared these temperatures to the measured internal temperatures for the live turtle in Bostrom, Jones, Hastings, & Jones (Bostrom et al. 2010).

Results

Neonate

The neonate thrust profile shows positive and steadily rising thrust during the up and down phases of the stroke with initial pulses of negative thrust during the top and bottom phases (Fig. 10). Figure 11 shows the pressure profile during the stroke. Our simulated average force was within a quarter of the standard deviation with the experimental force measurements (Fig. 12).

Juvenile

The juvenile thrust has a similar profile to the neonate thrust (Fig. 13). There is a gradual rise in positive force during the up and down phases and a sharp decrease in positive force, going shortly negative, during the top and bottom phases. The power profile shows a reasonable output with areas of positive thrust showing high power output (Fig. 14). As would be expected, the higher the stroke frequency, the higher the force and power output. Figure 15

shows the pressure profile during the stroke. In cooler waters, the metabolic cost of flipper movement (work energy) is responsible for a substantial portion of the total metabolic rate. In the warmest water, the work energy contributes little to the metabolic rate (Fig. 16).

As predicted, the swimming juvenile heat transfer coefficients are much higher for the flippers than the body (Fig. 17). The body heat transfer coefficient stays relatively constant over the stroke while the flipper's varies with phase. Figure 18 shows the higher heat flux on the flipper than the body.

The internal conduction model shows high heat flux in the channels of the shell, high heat flux around the neck and shoulders, moderate heat flux on the upper flipper, and low heat flux on the flipper tips (Fig. 19). The internal temperature profile shows the center of the core region was the hottest and that the temperature decreased outward with a particularly rapid decrease towards the plastron (Fig. 20).

Our simulated data are in good agreement with the internal temperatures of the real juvenile turtle (Bostrom et al. 2010). Temperatures for the three highest stroke frequencies are within the temperature range containing 75% of the turtle's core volume. The 29 BPM turtle's core temperature is slightly outside maximum simulated core temperature (Fig. 21).

Discussion

The agreement between the average simulated neonate thrust and the average experimental neonate thrust gives us confidence that our methods can accurately model the dynamics of a sea turtle stroke. While the simulation is not an exact representation of the live turtle experiment, the differences are minimal. The main difference between our simulation

and a live turtle is that we did not model the small translocations of the turtle's body during the stroke cycle. The agreement between our juvenile temperature simulations and the live juvenile temperature records (Bostrom et al. 2010) gives us confidence that we can accurately model the internal environment of a turtle, particularly in warmer waters. Warmer conditions will be most important when considering climate change's effects on leatherback's tropical and subtropical range. The temperatures from Bostrom, Jones, Hastings, & Jones contain more variation than the single reported number represents (Bostrom et al. 2010). Examples of variation are two runs with the same water temperature and flipper stroke frequency, which had a 0.2 °C difference in core temperature, and there was a case where a higher stroke frequency at the same water temperature resulted in a lower core temperature. The complex nature of this system means that anomalies like these are all but inevitable, yet we are still able to model this system accurately at temperatures important for implementing this method into a mechanistic niche model.

As mentioned in the introduction, this method and results have important applications in conservation. With these methods, we will be able to construct a highly accurate mechanistic niche map of leatherback sea turtles and could potentially expand this capability to other marine organisms. These maps will show managers the potential shifts in the ranges under climate change conditions. Such information allows planning for future species disappearances or appearances regionally based on abiotic conditions. As we integrate these methods into mechanistic niche mapping, other research groups should consider adopting more realistic animal geometries when considering animal-fluid interactions (Dudley et al. 2013).

In addition to conservation, these methods and results have important applications in the fields of physiology, biomechanics, fluid dynamics and engineering. There is much research going into the biomechanics of animal flight and swimming (Weber et al. 2009). Our method of 3D, full motion animal CFD provides a novel robust tool to clarify many difficult problems. In addition to animals that propel themselves through fluid, there is much research needed on animals that actively cool themselves by manipulating the fluid around them (Wright 1984). While CFD is used in understanding animal motion, currently, the only 3D, full animal motion CFD we were able to find was a 3D model with 2D motion (Liu et al. 1997). The Liu et al. simulation also used proprietary software (as opposed to our commercially available software) and did not simulate heat transfer (1997). There is also active research and development on submersibles and drones that mimic animal propulsion (sea turtle example: Low, Zhou, Ong, & Yu, 2007). Our methods could help reduce costs and expedite development of these technologies, which themselves could have important conservation applications.

Acknowledgements

We would like to thank Dr. Chin Wu from the University of Wisconsin-Madison for use of a high-speed camera. We thank Brittany Imlach for logistical support of the live neonate force trials.

Funding for the live neonate force trials was provided by NOAA Fisheries (Pacific Islands

Fisheries Science Center) and the Joint Institute for Marine and Atmospheric Research.

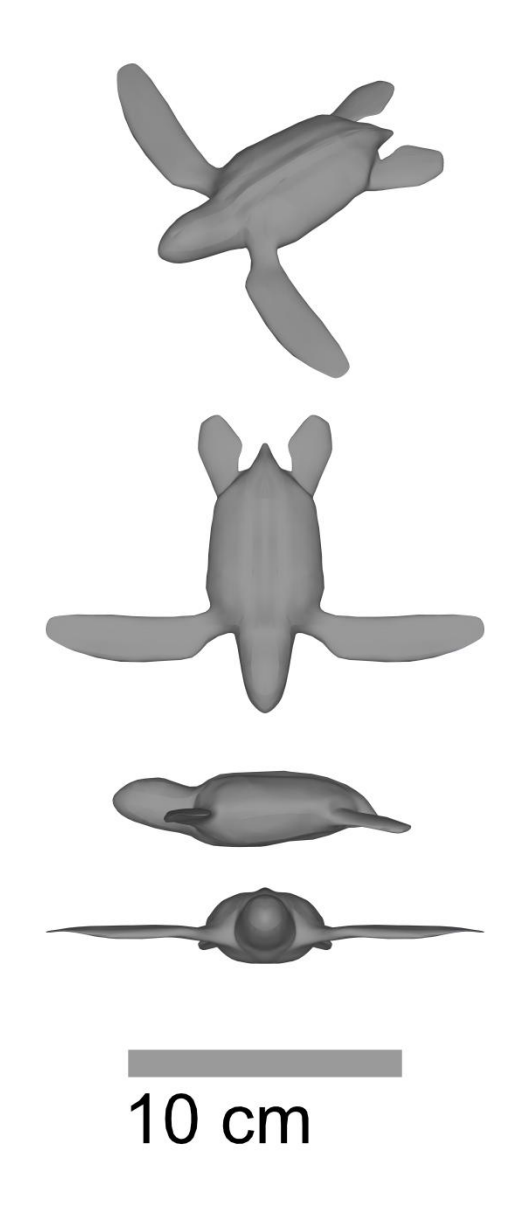


Figure 1. A 3D drawing of a neonate leatherback turtle

Table 1. A summary table of turtle morphologies and average run outputs. HTC is the heat transfer coefficient, and BPM is beats per minute.

Turtle/Run	Surface Area (m²)	Volume (m³)	Mass (kg)	Average Thrust (N)	Flipper HTC (W/K m²)	Body HTC (W/K m ²)	
Neonate	0.014	5.80x10 ⁻⁵	0.06	4.88x10 ⁻³	NA	NA	NA
6 BPM	0.89	0.036	36.9	0.060	464	260	0.043
19 BPM	0.89	0.036	36.9	0.832	775	303	0.371
25 BPM	0.89	0.036	36.9	1.540	952	305	0.904
29 BPM	0.89	0.036	36.9	2.070	1019	311	1.418

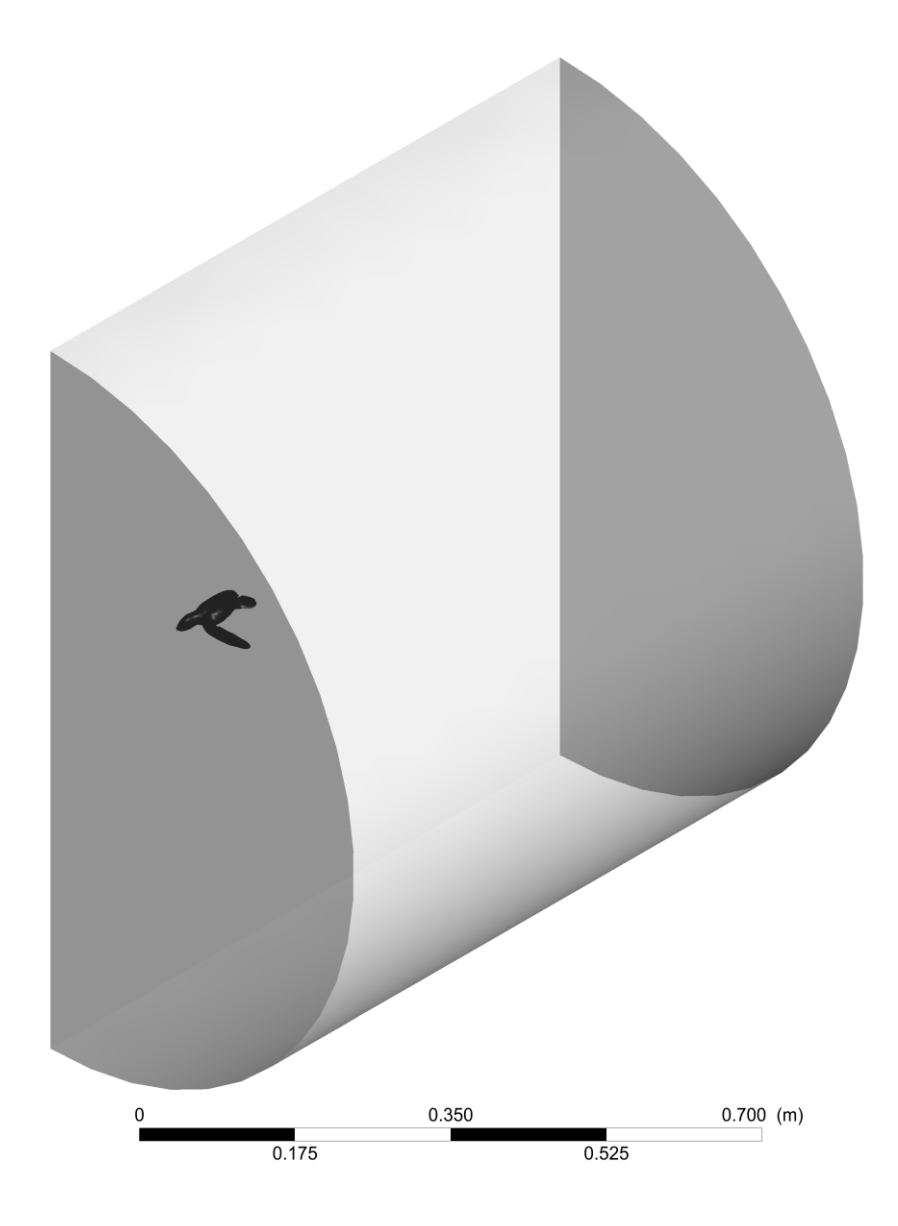


Figure 2. The fluid volume that surrounds the moving, neonate turtle. The plane that divides the turtle had a symmetry boundary condition. This allows for reduction by half the computational fluid dynamics resource requirements.

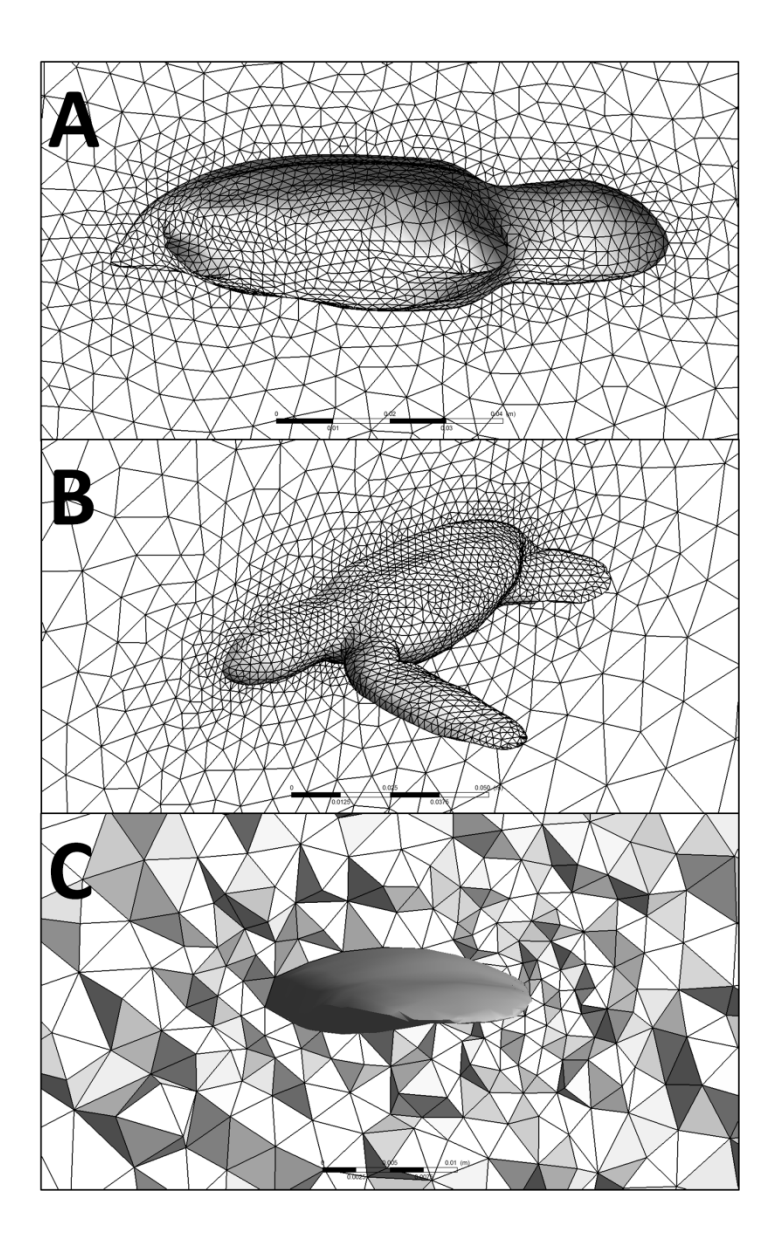


Figure 3. The mesh around the neonate model. A) The mesh seen from outside looking at the symmetry plane. B) The mesh as seen from inside the fluid volume looking towards the symmetry plane. C) The mesh on a plane bisecting the flipper at its midpoint.

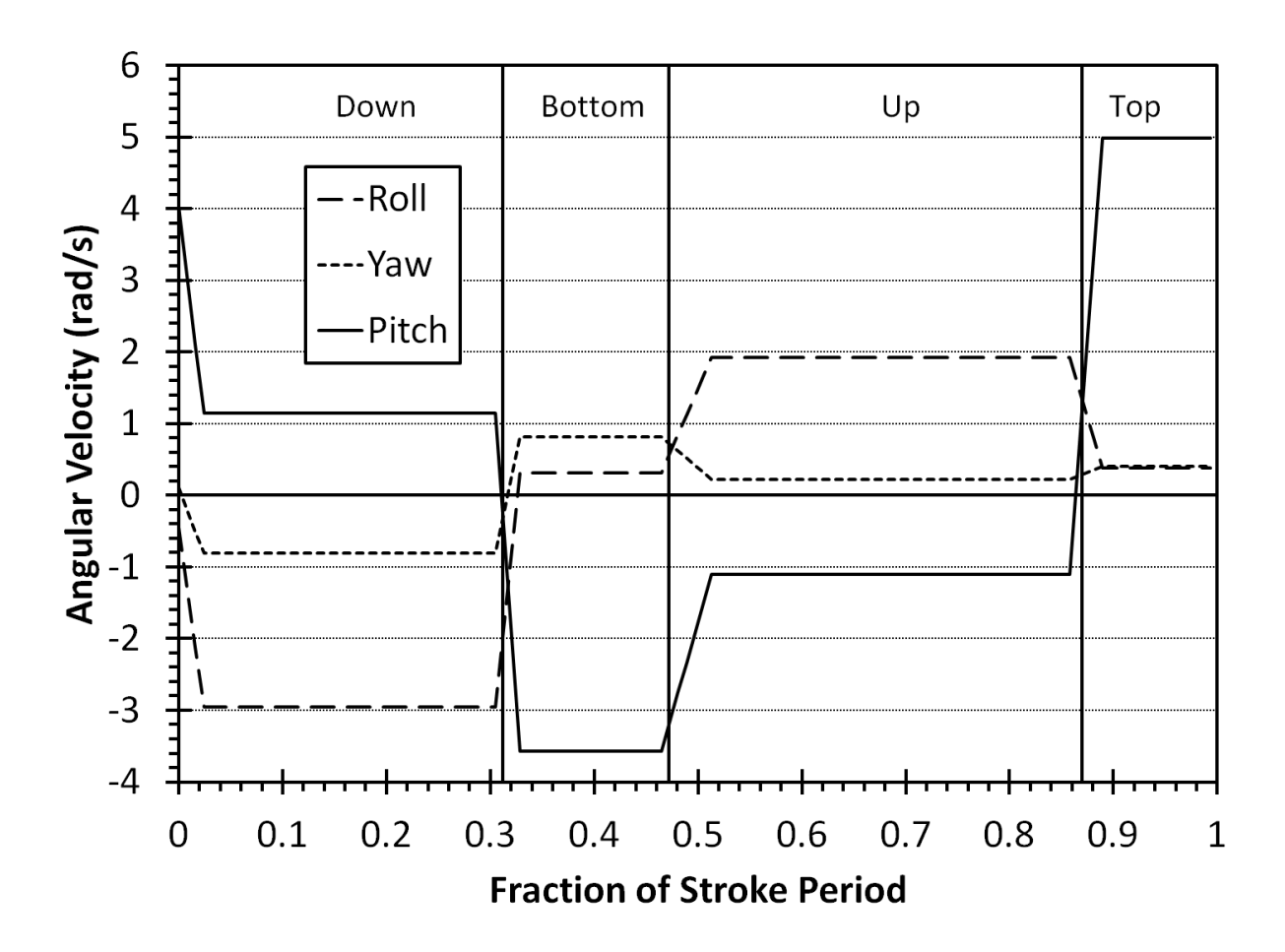


Figure 4. The angular velocities of the neonate flipper in the three movement planes as a function of the stroke percentage completed.

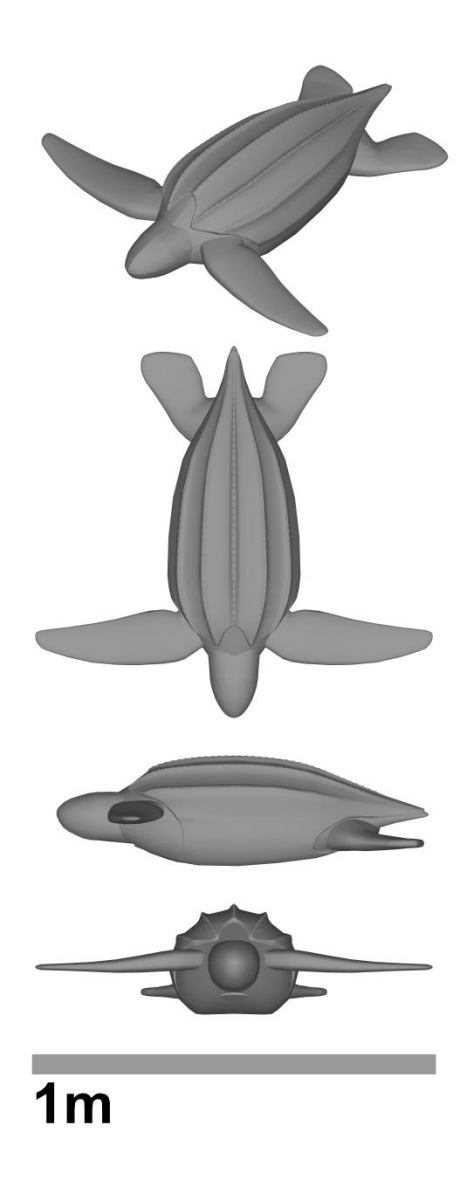


Figure 5. A 3D drawing of a juvenile leatherback turtle.

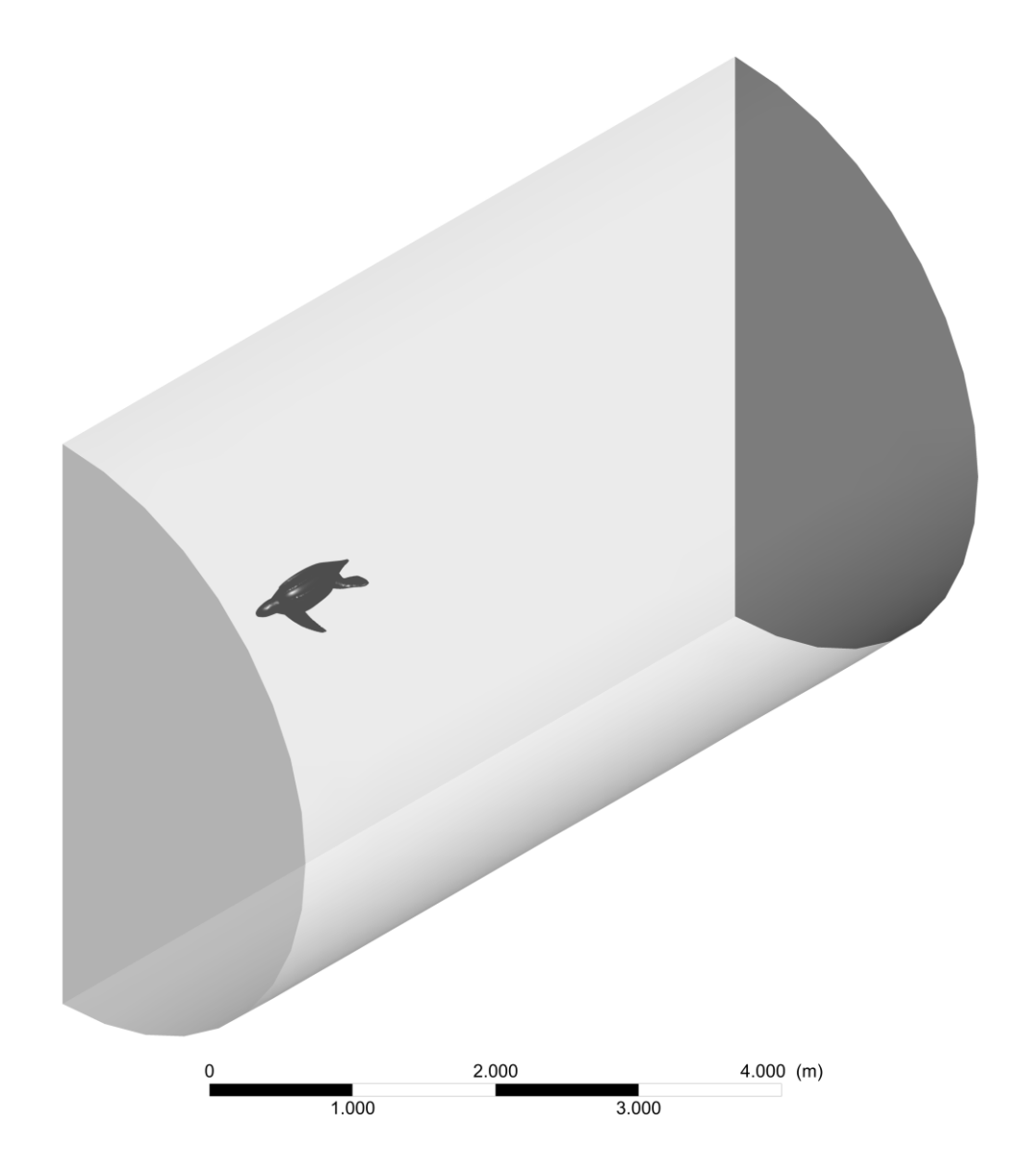


Figure 6. The fluid volume that surrounds the moving, juvenile turtle. The plane that divides the turtle had a symmetry boundary condition.

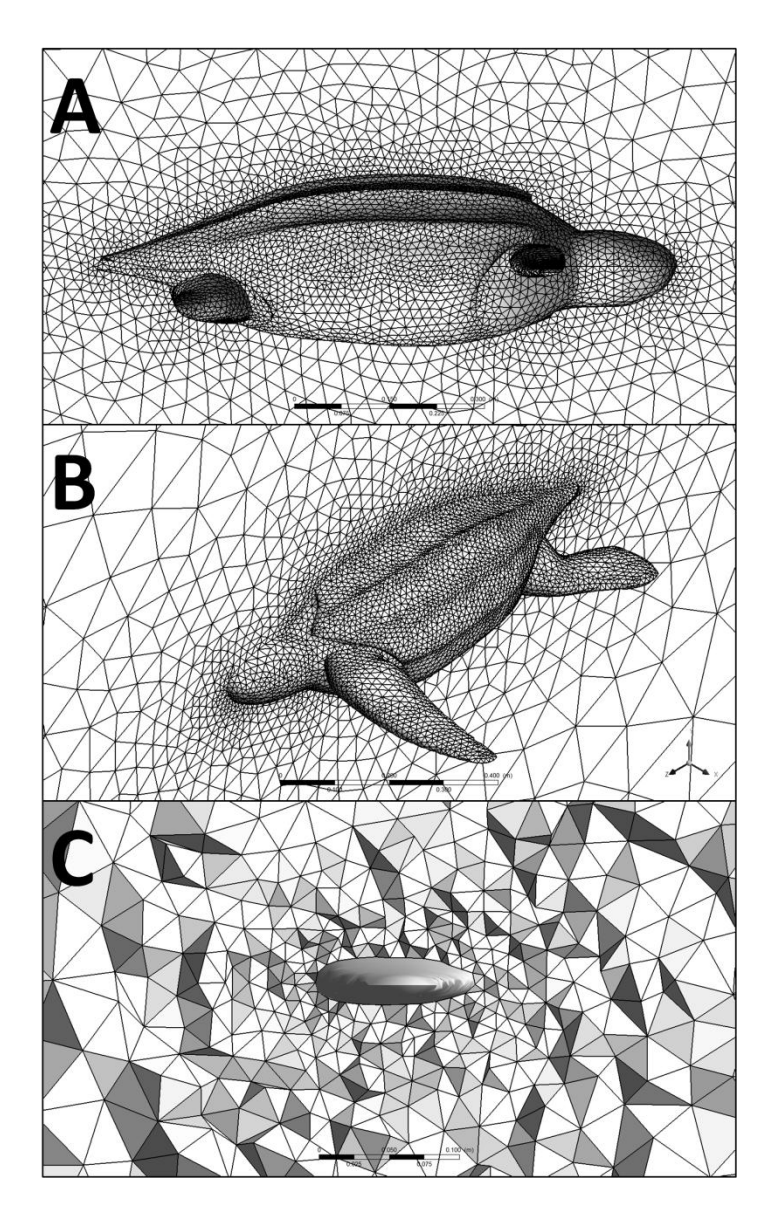


Figure 7. The mesh around the Juvenile model. A) The mesh seen from outside looking at the symmetry plane. B) The mesh as seen from inside the fluid volume looking towards the symmetry plane. C) The mesh on a plane bisecting the flipper at its midpoint.

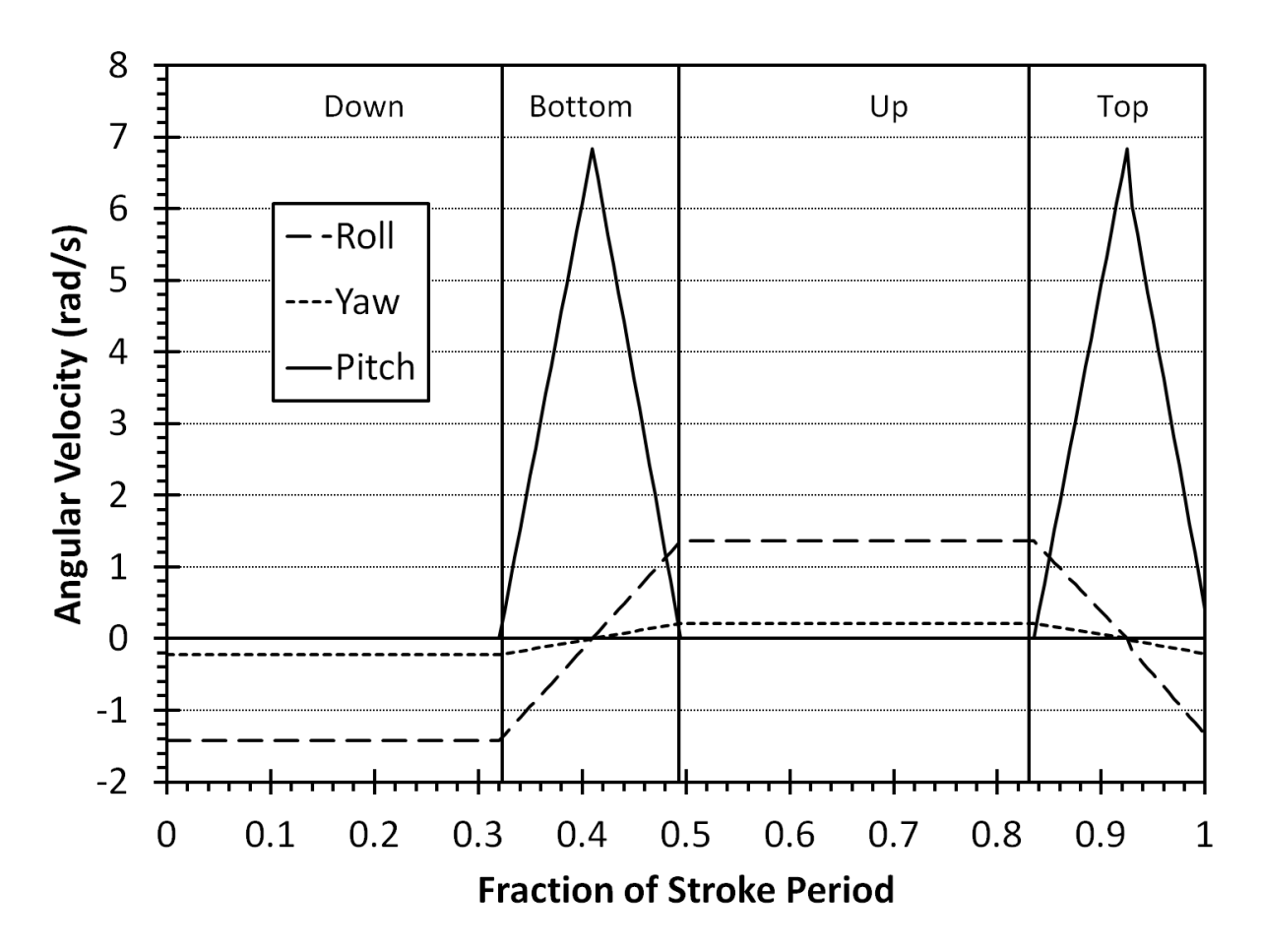


Figure 8. The angular velocities of the juvenile flipper at 29 beats per minute in the three movement planes as a function of the stroke percentage completed.

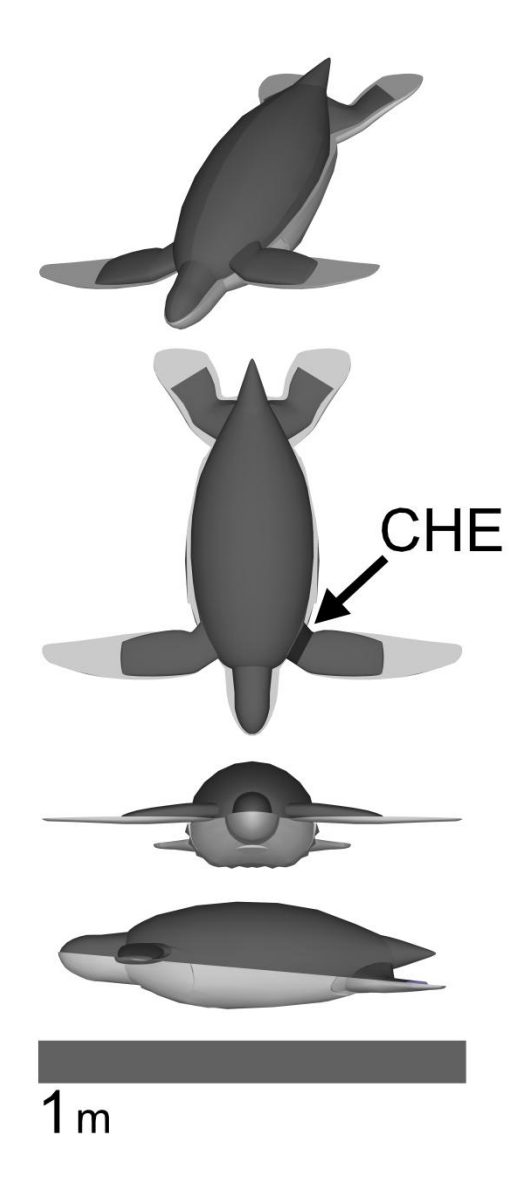


Figure 9. A 3D drawing of a juvenile leatherback turtle with the top of the insulating shell virtually cut away. The figure shows the core zone in dark gray. The countercurrent heat exchanges (CHE) is highlighted on only one side in black.

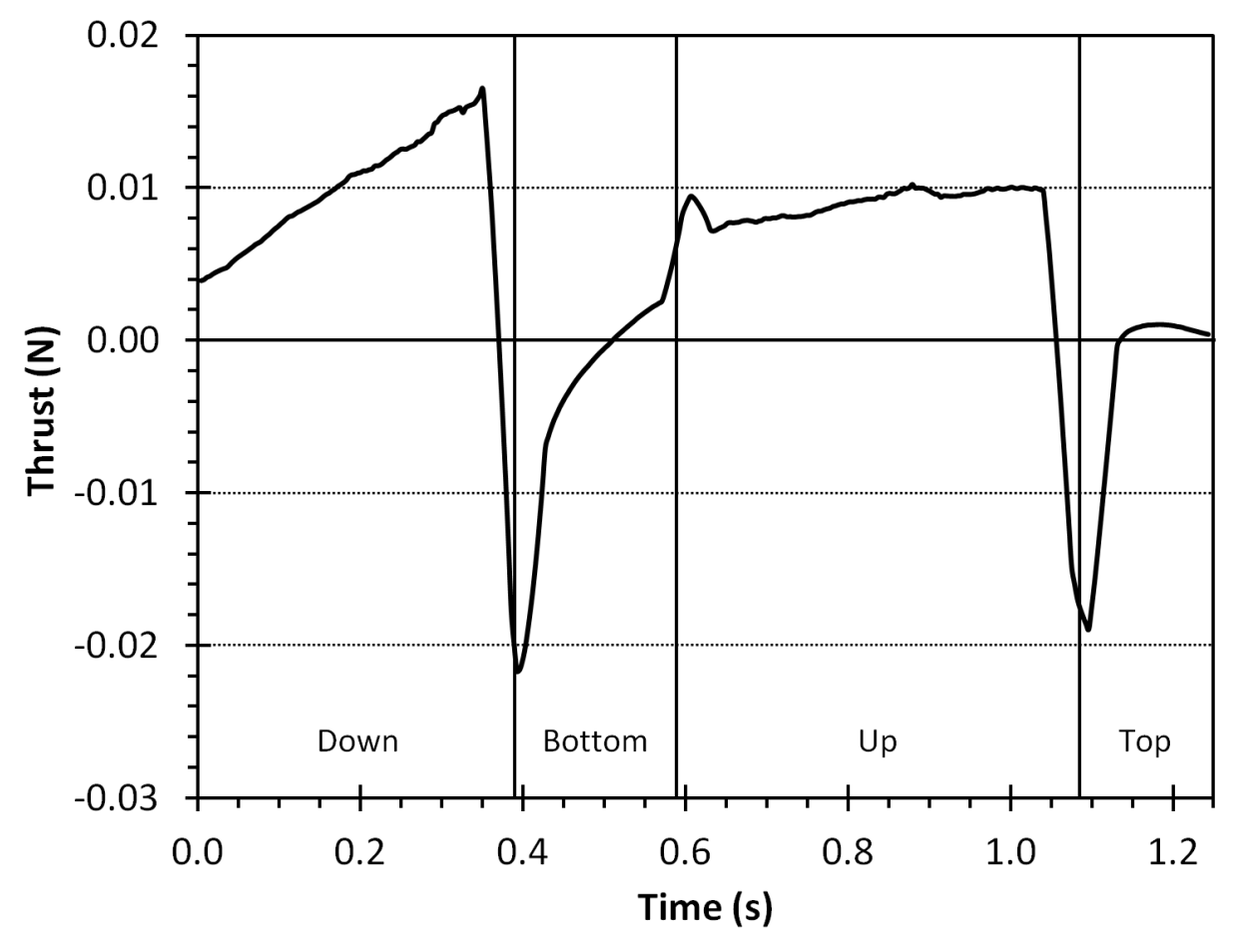


Figure 10. The thrust produced by our simulated neonate turtle as it goes through one stroke period. The vertical black lines demark the four different stroke phases (down, bottom, up, and top).

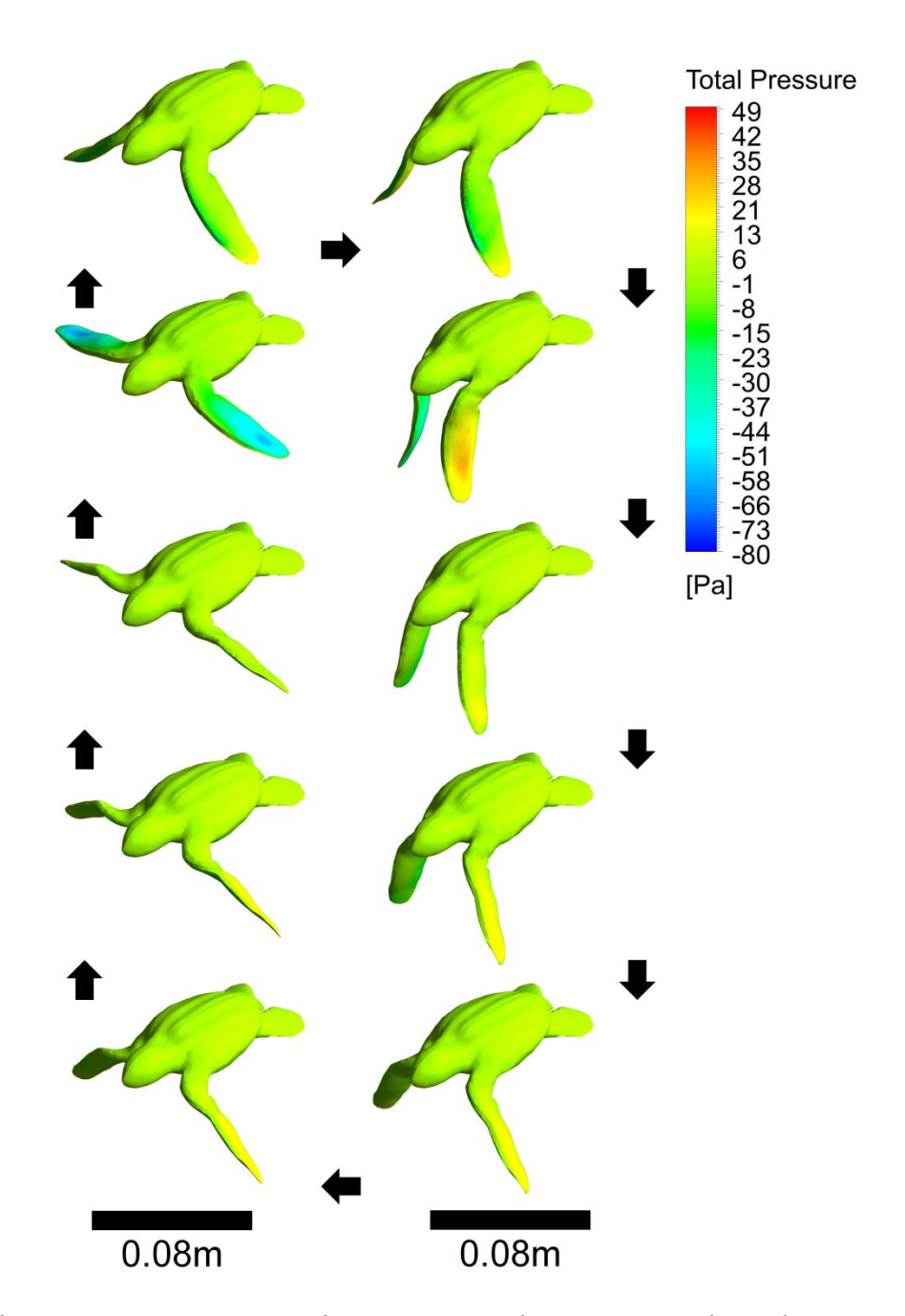


Figure 11. The pressure contours on the neonate turtle as it moves through one stroke period. Black arrows indicate the direction of the image sequence. This is an orthographic projection. The middle image in the left column represents one of the high negative thrust points recorded at the start of the bottom phase.

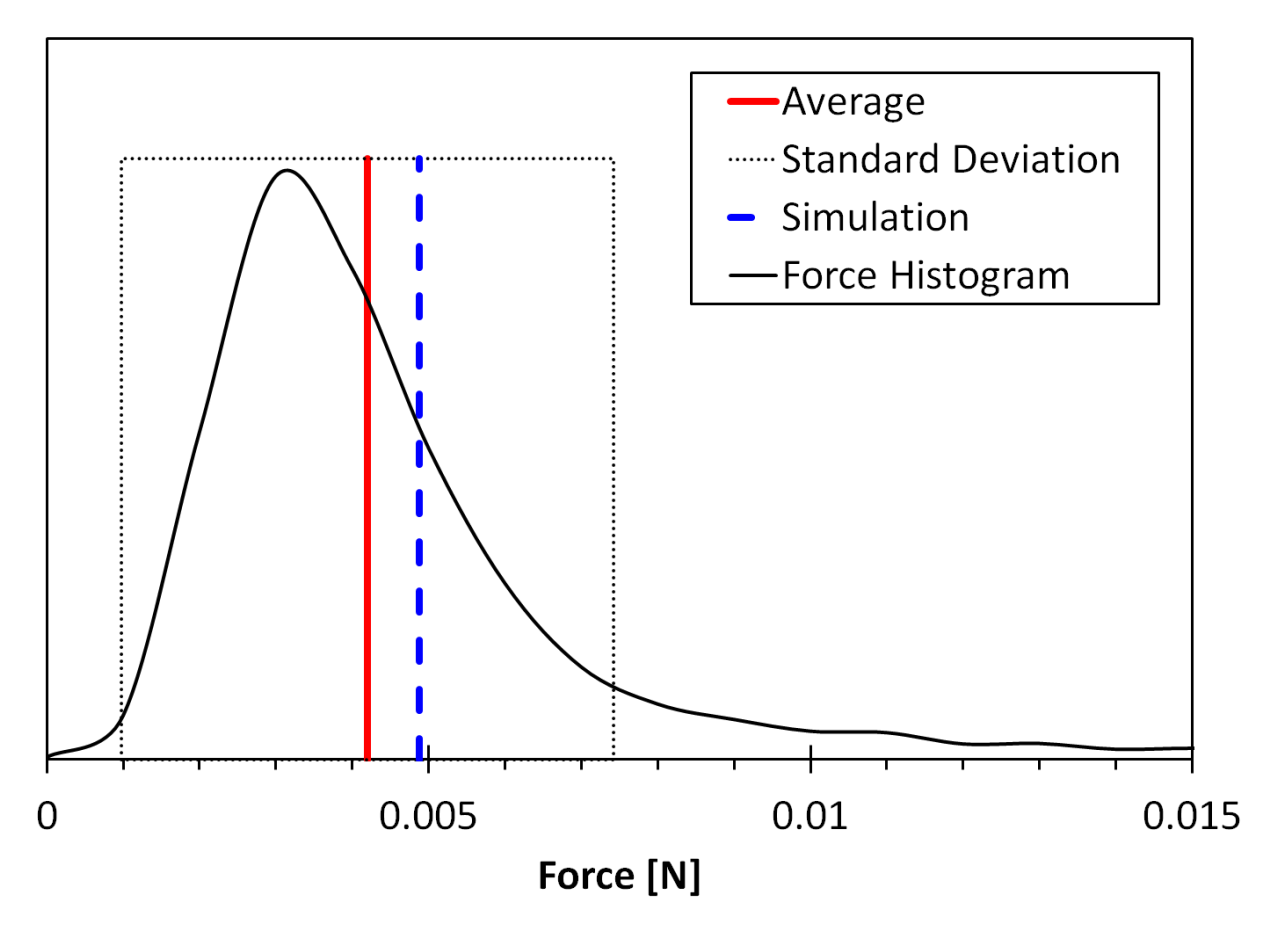


Figure 12. A comparison between measured and simulated neonate thrust. The width of the dotted box represents the experimental data's standard deviation. Force histogram displays the distribution of force measurements recorded during the experiment.

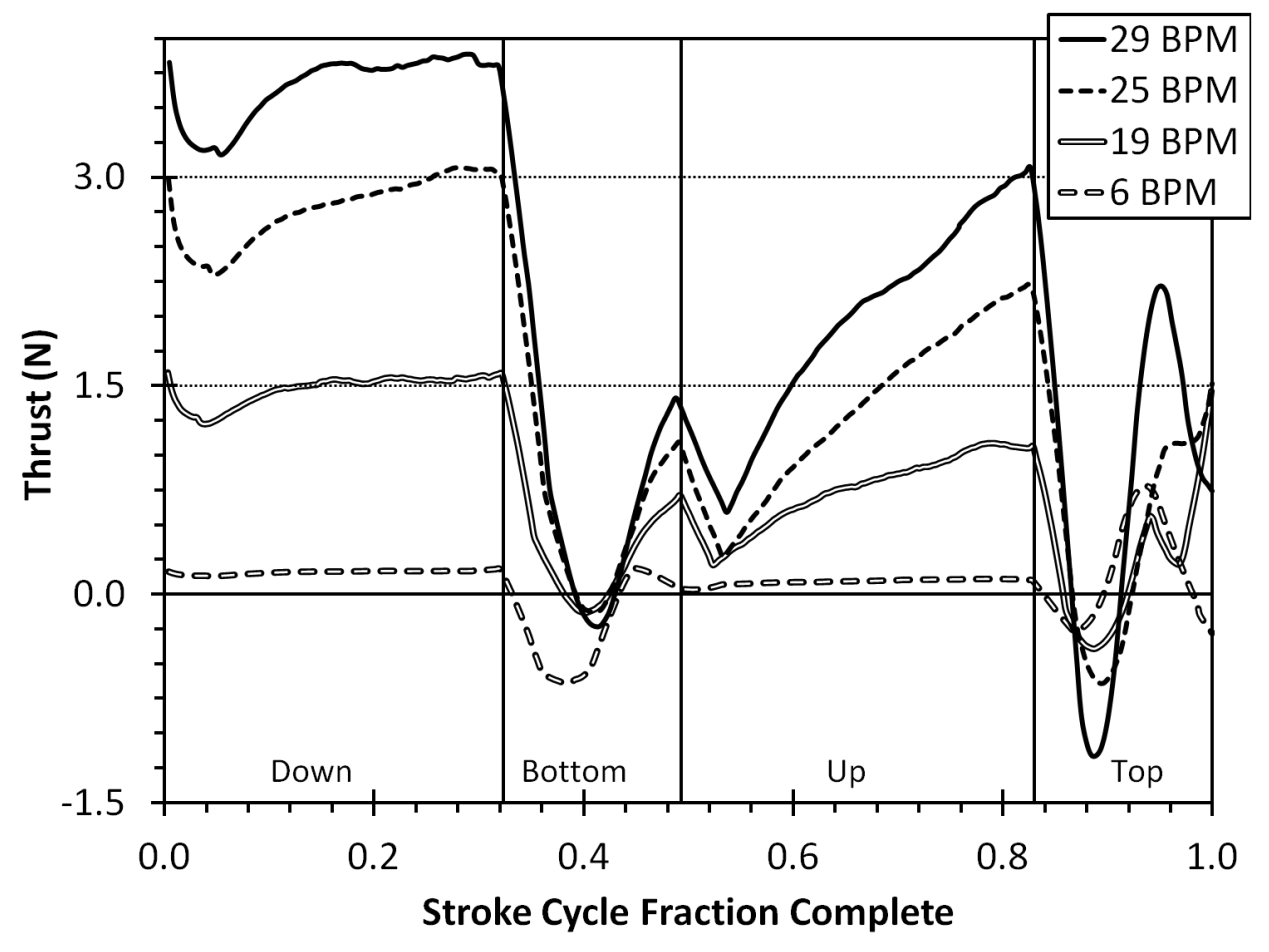


Figure 13. The thrust produced by our simulated juvenile turtles as they go through one stroke period. The vertical black lines demark the four different stroke phases (down, bottom, up, and top). Since each swimming frequency (beats per minute (BPM)) has its own period, the x-axis is percent of stroke completed.

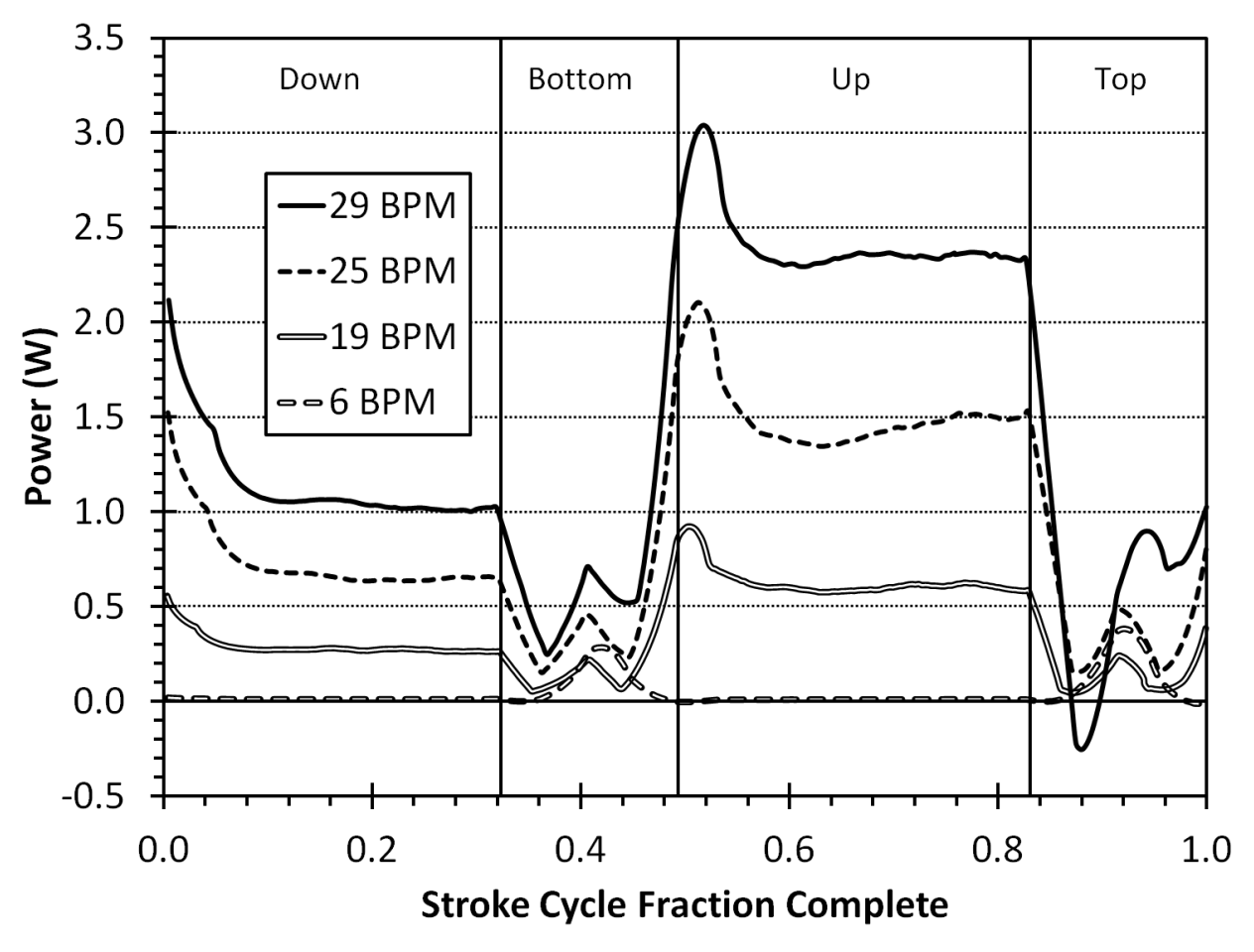


Figure 14. The power produced by our simulated juvenile turtles as they go through one stroke period. The vertical black lines demark the four different stroke phases (down, bottom, up, and top). Since each swimming frequency (beats per minute (BPM)) has its own period, the x-axis is percent of stroke completed.

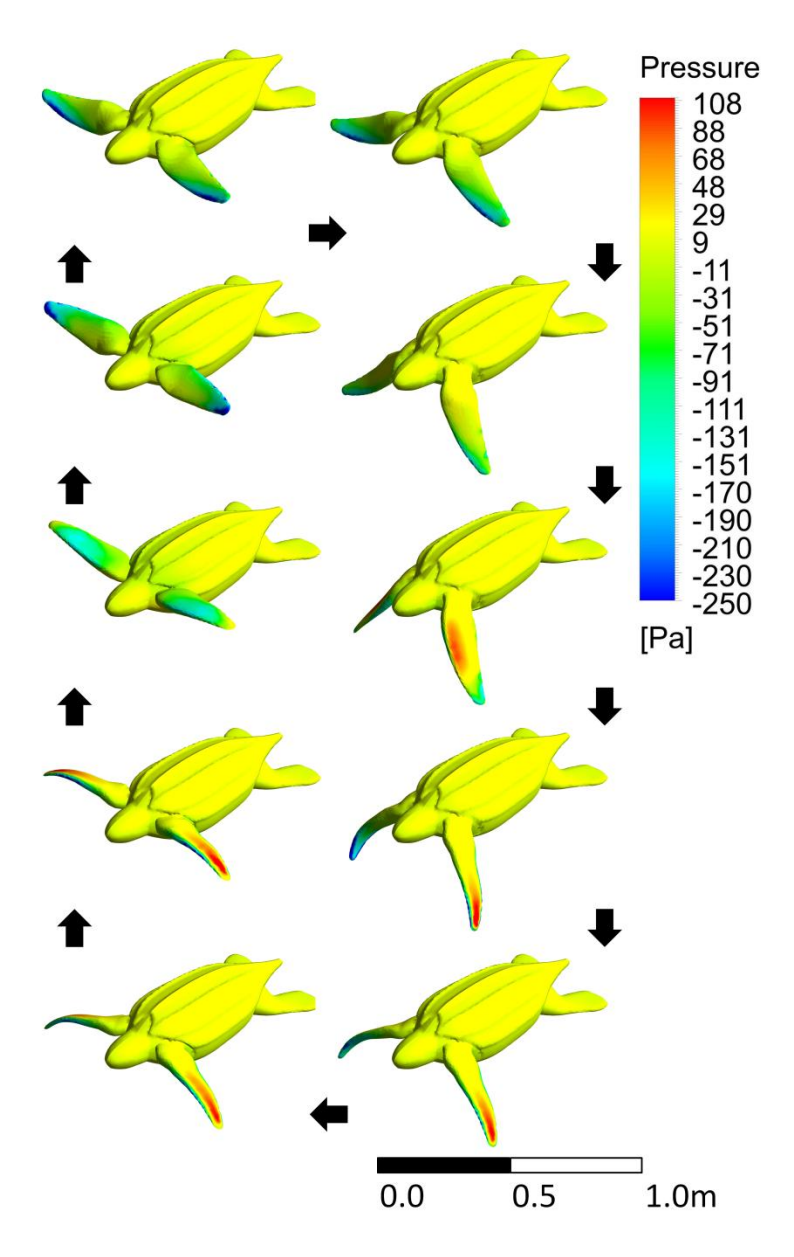


Figure 15. The pressure contours on the juvenile turtle as it moves through one stroke period. Black arrows indicate the direction of the image sequence. This is an orthographic projection. The third image in the left column represents one of the high negative thrust points recorded at the middle of the bottom phase.

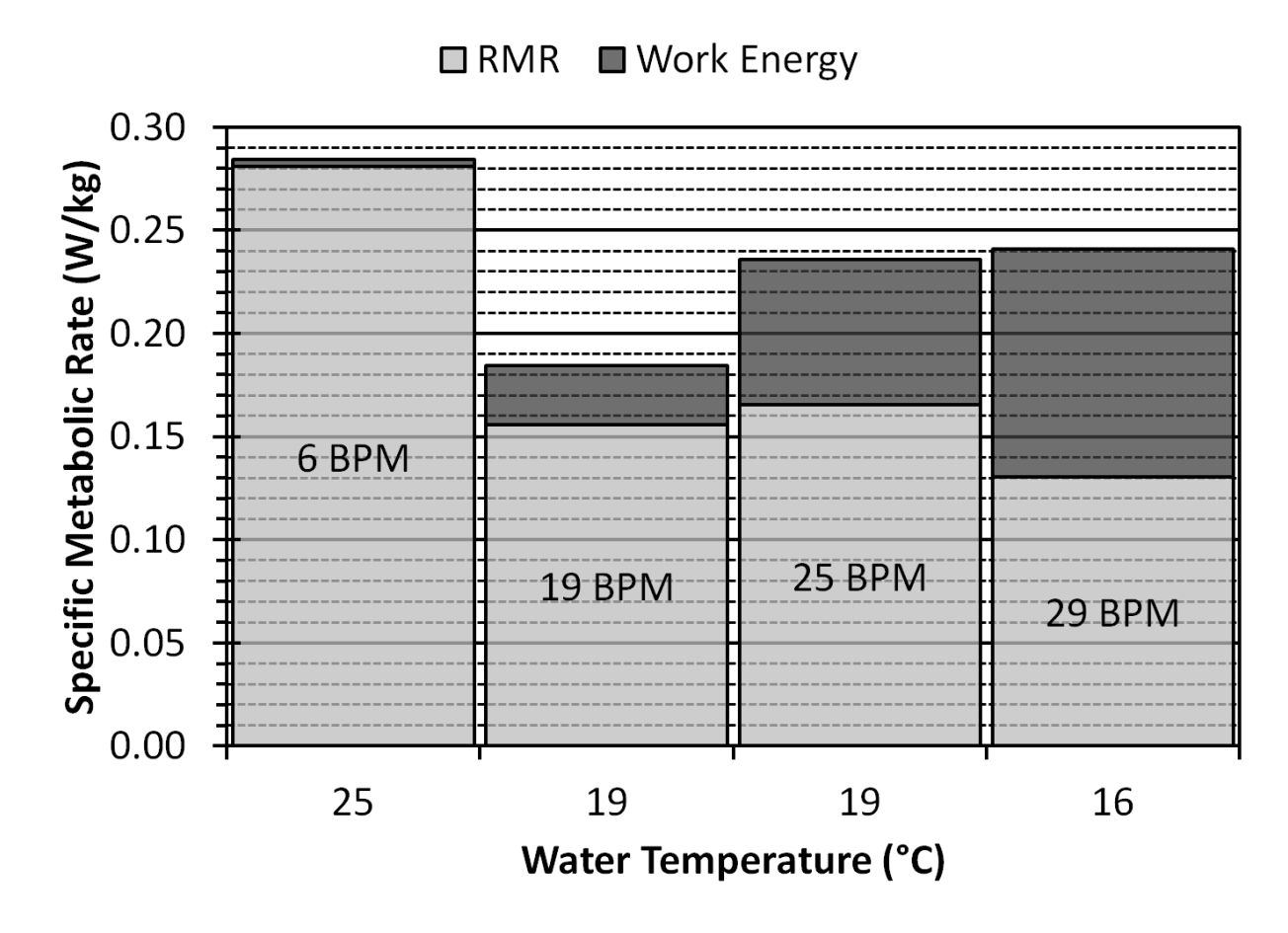


Figure 16. The proportion of specific metabolic rate owing to resting metabolic rate (RMR) and the metabolic cost of flipper movement (Work Energy). Each bar corresponds to a specific ambient water temperature (x-axis) and a specific flipper stroke frequency in beats per minute (BPM) (on bar labels).

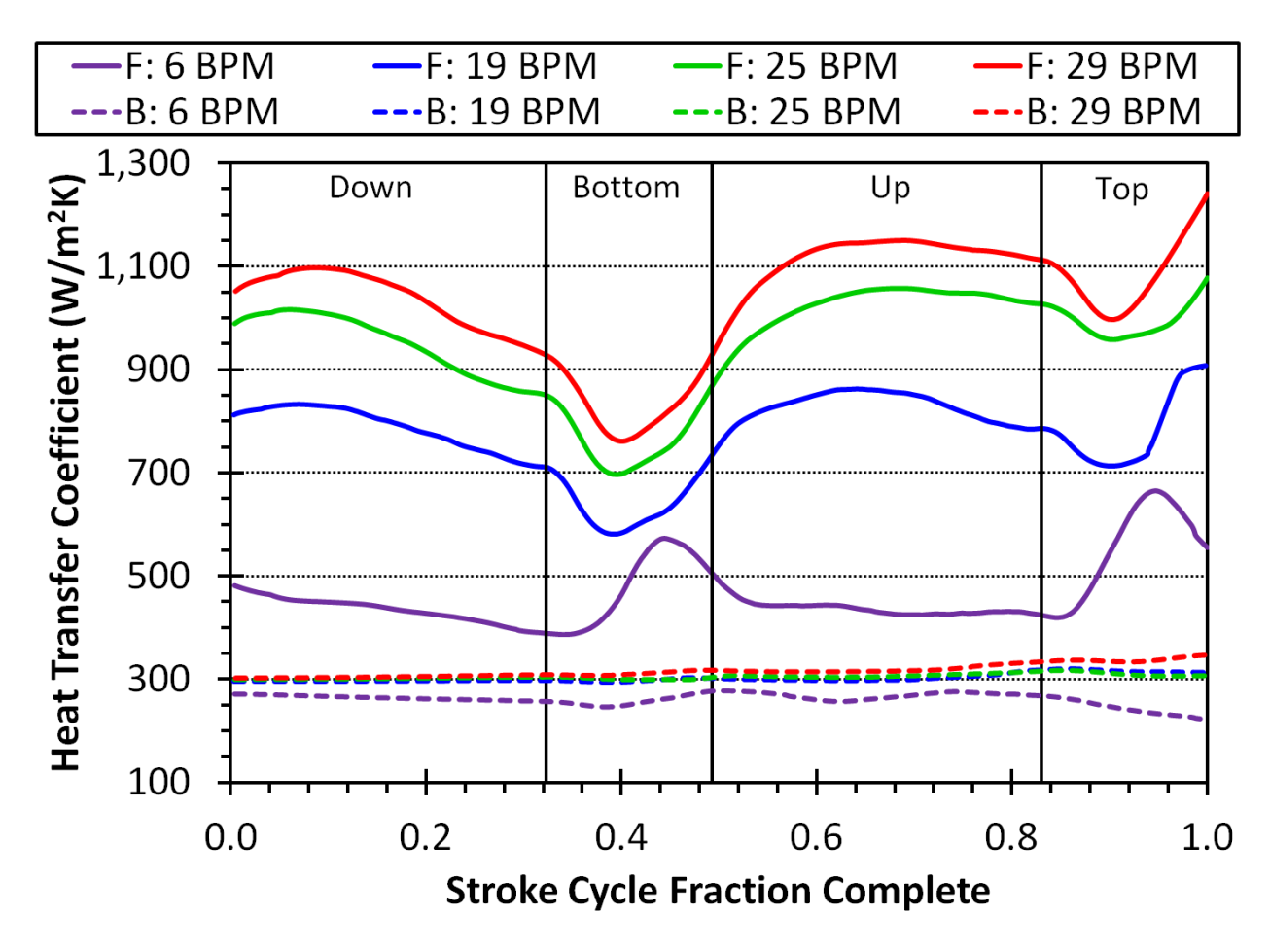


Figure 17. The heat transfer coefficients of our simulated juvenile turtles they go through one stroke period. B and F stand for the heat transfer coefficient on the body and flipper, respectively. The vertical black lines demark the four different stroke phases (down, bottom, up, and top). Since each swimming frequency has its own period, the x-axis is percent of stroke completed.

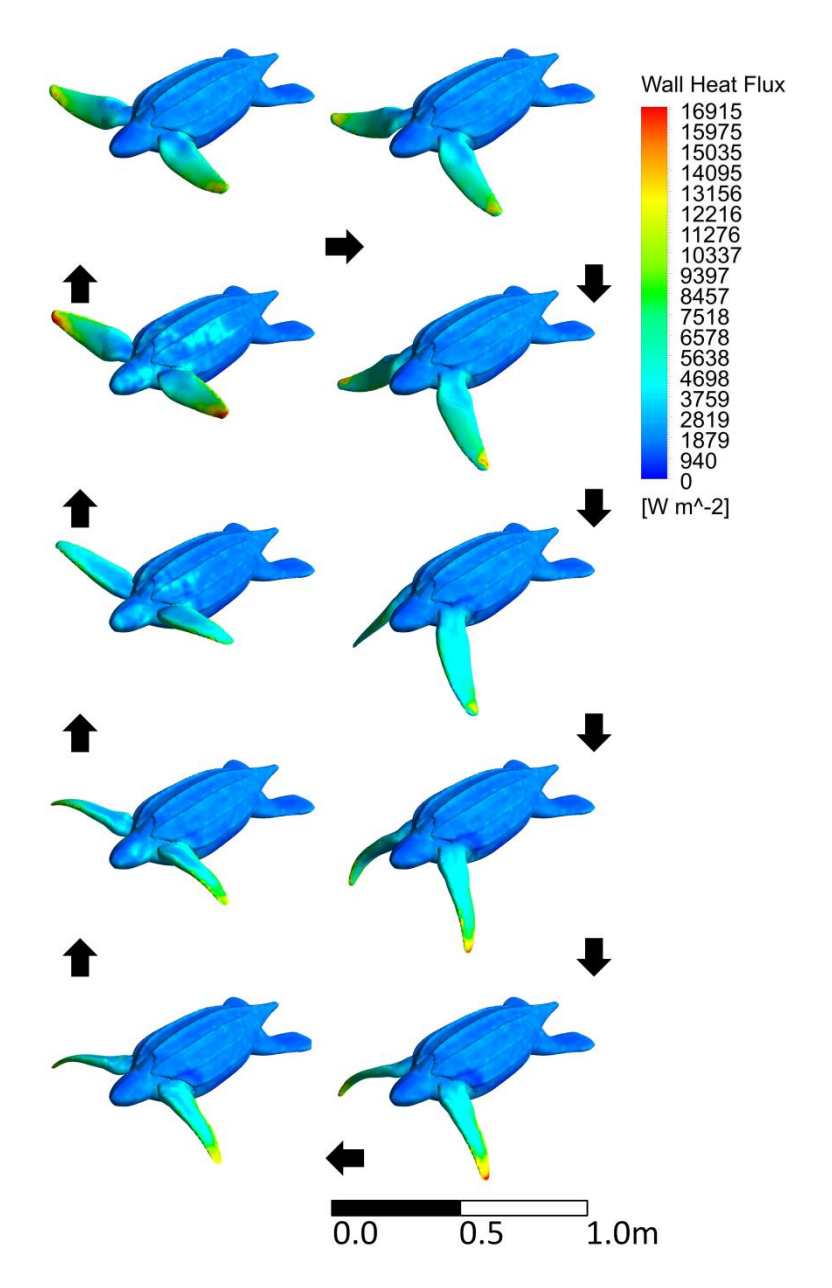


Figure 18. The heat flux contours on the juvenile turtle as it moves through one stroke period. Black arrows indicate the direction of the image sequence. This is an orthographic projection.

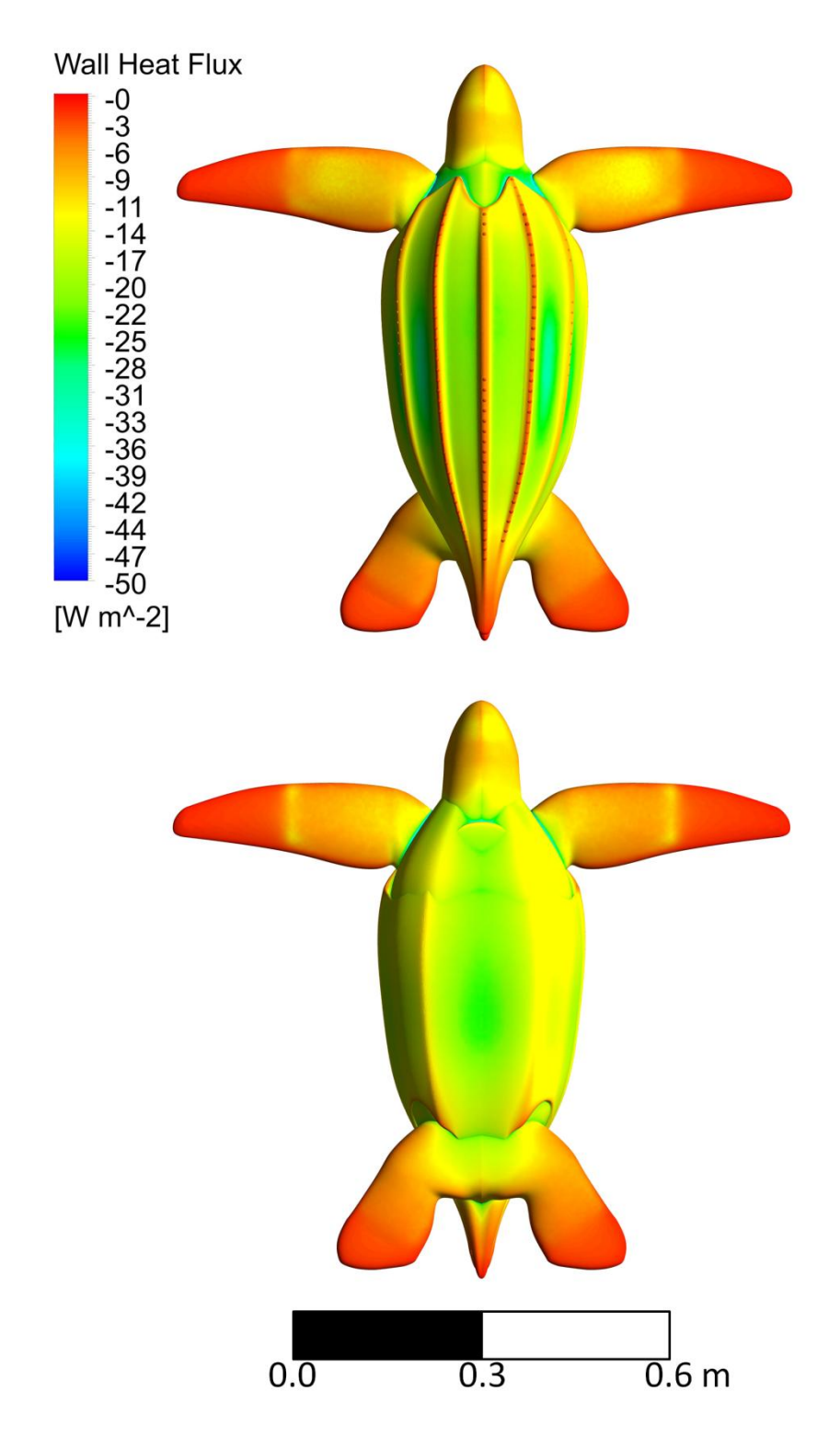


Figure 19. The heat flux contours on the internal conduction model of the juvenile turtle.

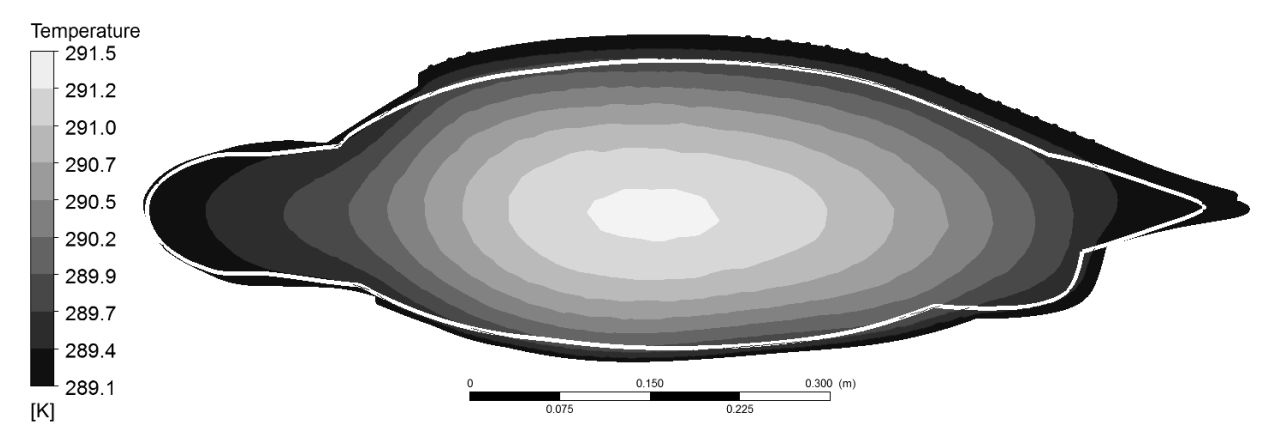
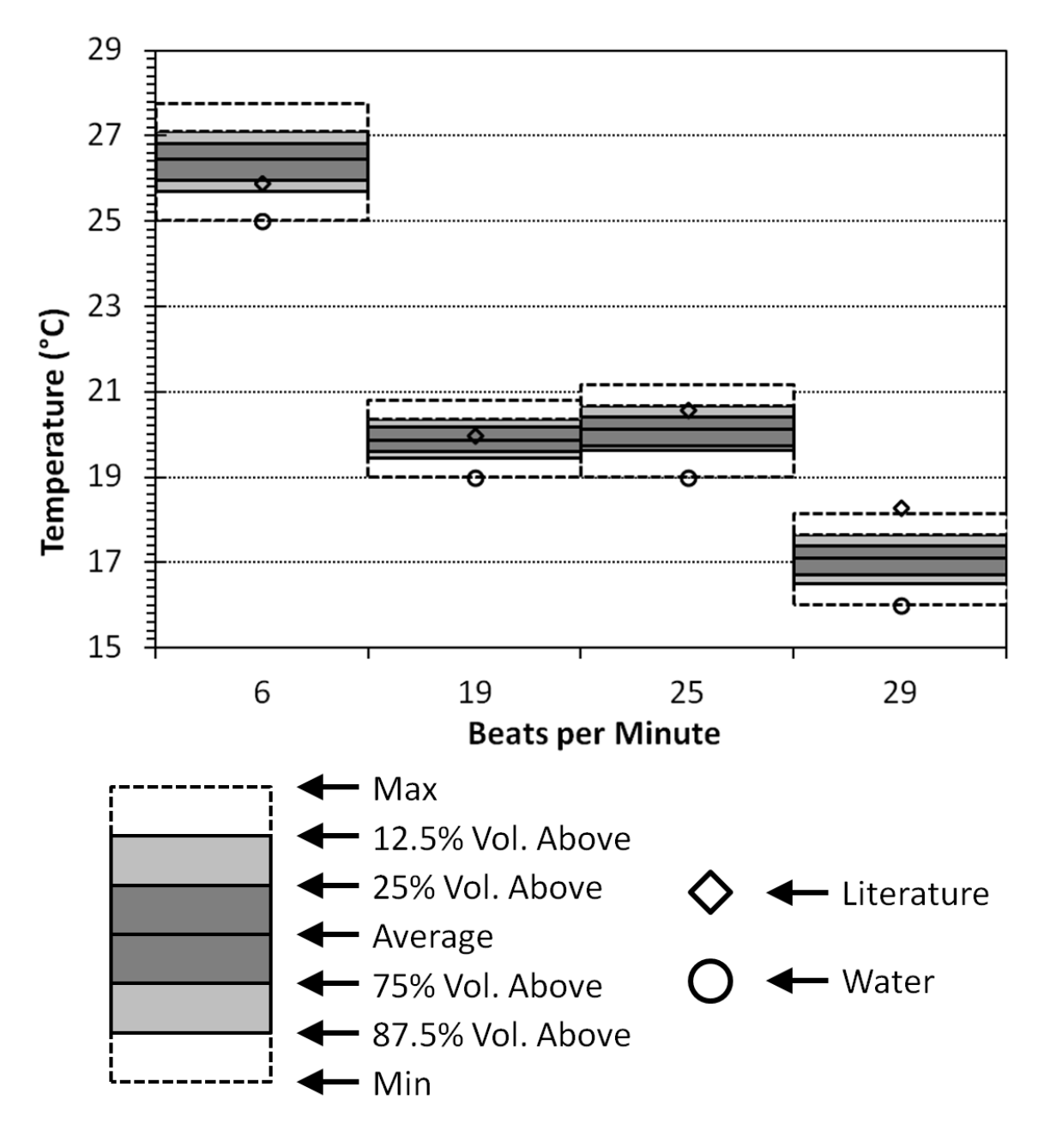


Figure 20. The temperature contours on the symmetry plane through the juvenile turtle. The white line demarks the separation between the core region and the insulating shell.



% Vol. Above = Percent of turtle core volume above given temperature

Figure 21. A comparison between the simulated and experimental internal temperatures. The dotted boxes contain the range of temperatures inside the simulated turtle's core region. The light gray region bounds the 75th temperature percentile of the turtle's core volume and the dark gray box bounds the 50th Temperature percentile of the turtle's core volume. Experimental data from literature (Bostrom, Jones, Hastings, & Jones, 2010).

References

- Bagge LE, Koopman HN, Rommel SA, McLellan WA, Pabst DA (2012) Lipid class and depth-specific thermal properties in the blubber of the short-finned pilot whale and the pygmy sperm whale. J Exp Biol 215:4330–9
- Blake RW, Chan KHS (2007) Swimming in the upside down catfish synodontis nigriventris: It matters which way is up. J Exp Biol 210:2979–89
- Boisclair D, Tang M (1993) Empirical analysis of the influence of swimming pattern on the net energetic cost of swimming in fishes. J Fish Biol 42:169–183
- Bostrom BL, Jones TT, Hastings M, Jones DR (2010) Behaviour and physiology: The thermal strategy of leatherback turtles. PLoS One 5:e13925
- Cedeno FO, Prieto MM, Xiberta J (2000) Measurements and estimate of heat capacity for some pure fatty acids and their binary and ternary mixtures. 45:64–69
- Chang C, Jang C, Cheng Y (2003) The latest record of the leatherback sea turtle (*Dermochelys coriacea*) from eastern Taiwan. Collect Res 16:17–27
- Cheng H-LM, Plewes DB (2002) Tissue thermal conductivity by magnetic resonance thermometry and focused ultrasound heating. J Magn Reson Imaging 16:598–609
- Davenport J, Fraher J, Fitzgerald E, McLaughlin P, Doyle T, Harman L, Cuffe T (2009) Fat head:
 An analysis of head and neck insulation in the leatherback turtle (*Dermochelys coriacea*). J Exp Biol 212:2753–9
- Davenport J, Holland DL, East J (1990) Thermal and biochemical characteristics of the lipids of the leatherback turtle Dermochelys coriacea: Evidence of endothermy. J Mar Biol Assoc United Kingdom 70:33–41
- Dormann CF (2007) Promising the future? Global change projections of species distributions. Basic Appl Ecol 8:387–397
- Drucker E, Lauder G (1999) Locomotor forces on a swimming fish: Three-dimensional vortex wake dynamics quantified using digital particle image velocimetry. J Exp Biol 202:2393–2412

- Dudley PN, Bonazza R, Porter WP (2013) Consider a non-spherical elephant: computational fluid dynamics simulations of heat transfer coefficients and drag verified using wind tunnel experiments. J Exp Zool A Ecol Genet Physiol 319:319–27
- Gillooly JF, Brown JH, West GB, Savage VM, Charnov EL (2001) Effects of size and temperature on metabolic rate. Science 293:2248–51
- Goff G, Stenson G (1988) Brown adipose tissue in leatherback sea turtles: A thermogenic organ in an endothermic reptile? Copeia 1988:1071–1075
- Greer AE, Lazell JD, Wright RM (1973) Anatomical evidence for a counter-current heat exchanger in the leatherback turtle (*Dermochelys coriacea*). Nature 244:181
- Hutchinson EG (1957) Concluding remarks. In: Cold Spring Harbor Symposia on Quantitative Biology.p 415–42782
- Jones TT, Hastings MD, Bostrom BL, Pauly D, Jones DR (2011) Growth of captive leatherback turtles, *Dermochelys coriacea*, with inferences on growth in the wild: Implications for population decline and recovery. J Exp Mar Bio Ecol 399:84–92
- Kearney M, Phillips B, Tracy C, Christian K (2008) Modelling species distributions without using species distributions: The cane toad in Australia under current and future climates. Ecography (Cop):1–12
- Kearney M, Porter W (2009) Mechanistic niche modelling: combining physiological and spatial data to predict species' ranges. Ecol Lett 12:334–50
- Kvadsheim PH, Folkow LP, Blix a. S (1996) Thermal conductivity of minke whale blubber. J Therm Biol 21:123–128
- Liu H, Wassersug R, Kawachi K (1997) The three-dimensional hydrodynamics of tadpole locomotion. J Exp Biol 200:2807–19
- Low K, Zhou C, Ong T, Yu J (2007) Modular design and initial gait study of an amphibian robotic turtle. Proc 2007 IEEE Int Conf Robot Biomimetics:535–540
- Marom S, Korine C, Wojciechowski MS, Tracy CR, Pinshow B (2006) Energy metabolism and evaporative water loss in the European free-tailed bat and Hemprich's long-eared bat (*Microchiroptera*): species sympatric in the Negev Desert. Physiol Biochem Zool 79:944–56
- Miller DL, Wyneken J, Rajeev S, Perrault J, Mader DR, Weege J, Baldwin C a (2009) Pathologic findings in hatchling and posthatchling leatherback sea turtles (*Dermochelys coriacea*) from Florida. J Wildl Dis 45:962–71

- Parmesan C, Yohe G (2003) A globally coherent fingerprint of climate change impacts across natural systems. Nature 421:37–42
- Parry D a (1949) The structure of whale blubber, and a discussion of its thermal properties. Q J Microsc Sci 90:13–25
- Pavlov V V., Rashad AM (2012) A non-invasive dolphin telemetry tag: Computer design and numerical flow simulation. Mar Mammal Sci 28:E16–E27
- Phillips B, Chipperfield J, Kearney M (2008) The toad ahead: Challenges of modelling the range and spread of an invasive species. Wildl Res 35:222
- Porter WP, Kearney M (2009) Size, shape, and the thermal niche of endotherms. Proc Natl Acad Sci U S A 106 Suppl :19666–72
- Schultz W, Webb P (2002) Power requirements of swimming: Do new methods resolve old questions? Integr Comp Biol 1025:1018–1025
- Skrovan RC, Williams TM, Berry PS, Moore PW, Davis RW (1999) The diving physiology of bottlenose dolphins (*Tursiops truncatus*). J Exp Biol 202:2749–2761
- Tieleman B, Williams J, Buschur M, Brown CR (2003) Phenotypic variation of larks along an aridity gradient: are desert birds more flexible? Ecology 84:1800–1815
- Tobalske B, Peacock W, Dial K (1999) Kinematics of flap-bounding flight in the zebra finch over a wide range of speeds. J Exp Biol 202:1725–39
- Usherwood JR (2003) The aerodynamics of avian take-off from direct pressure measurements in Canada geese (*Branta canadensis*). J Exp Biol 206:4051–4056
- Wallace BP, Jones TT (2008) What makes marine turtles go: A review of metabolic rates and their consequences. J Exp Mar Bio Ecol 356:8–24
- Ward S, Rayner J, MOLler U, Jackson D, Nachtigall W, Speakman J (1999) Heat transfer from starlings sturnus vulgaris during flight. J Exp Biol 202:1589–602
- Weber PW, Howle LE, Murray MM, Fish FE (2009) Lift and drag performance of odontocete cetacean flippers. J Exp Biol 212:2149–58
- Woledge R (1968) The energetics of tortoise muscle. J Physiol 197:685-707
- Wright PG (1984) Why do elephants flap their ears? South African J Zool 19:266-269

Chapter 4: Where the leatherbacks roam: Using a novel method to create a biophysical

fundamental niche model for the leatherback sea turtle under global warming

Authors: Peter N. Dudley¹, Riccardo Bonazza², and Warren P. Porter¹

¹Department of Zoology, University of Wisconsin-Madison

²Engineering Physics, University of Wisconsin-Madison

Abstract

Shifting suitable range limits under global warming will threaten many species. Modeling and mapping these potential range shifts is important for conservation. For marine species that are difficult to niche map we use a novel technique using 3D digital design, computational fluid dynamics, and finite volume heat transfer modeling to find animal core temperatures. We use this method to build a fundamental niche map for internesting leatherback sea turtles. We show that global warming threatens leatherbacks, particularly in Souteast Asia, with overheating. We also show that the impact may be less on leatherbacks that shift their nesting season or location or who are smaller. Methods such these are important to efficiently and economically produce accurate maps of regions that will become inhospitable to species under global warming conditions.

Introduction

Global warming poses a large extinction risk for many species (Thomas et al. 2004). A species' inability to shift its current range to match the future suitable range accounts for much of the extinction risk (Parmesan & Yohe 2003). Therefore, mangers and conservationists

require accurate range shift predictions to successfully address the global warming threat to their focal species. For leatherback sea turtles (*Dermochelys coriacea*) estimating new suitable ranges is quite complex. The first difficulty is that leatherbacks are gigantotherms, endothermic poikilotherms, whose large body size traps waste heat thus elevating their core temperature (Paladino et al. 1990). This effect means that leatherbacks are neither thermal conformers nor regulators and thus makes predicting their core body temperature difficult. The second difficulty is their complex life history. They have the largest range of any reptile (Saba 2013) and are biphasic (nesting on land and living in the water). Thus, global warming will affect leatherbacks over a wide geographic range as well as in two distinct environments. Hence, there is not only a need to determine the leatherback's marine distribution (National Marine Fisheries Service and U.S. Fish and Wildlife Service 1992) but also potential future nesting locations (Fuentes et al. 2012).

As the leatherbacks pelagic life makes them hard to track and global warming will introduce new sets of abiotic conditions, the best method to model their projected fundamental niche may be a biophysical mechanistic niche model (Porter et al. 2002, Kearney & Porter 2009, Bartelt et al. 2010). However, this class of model requires many physiological parameters which are difficult to measure for leatherbacks as they are not easily kept in captivity (Jones et al. 2011). Since leatherbacks are marine species, it is also difficult to estimate these parameters given the interaction between their in-water motion, metabolism, and heat transfer (Boisclair & Tang 1993).

We attempt to overcome these difficulties by using a 3D moving computational fluid dynamics (CFD) simulation and a numerical internal heat transfer model. We have shown in

our previous work that using only stroke frequency and an allometric relation for resting metabolic rate (RMR) this method is able to accurately predict leatherback core temperatures (Dudley et al.). Thus, by combining the data from our CDF model (power, heat transfer coefficients, infrared (IR) absorption and radiation, and internal temperature profiles) with global climate models (GCMs) we can accurately predict regions within the leatherback's current marine and terrestrial range which may become inaccessible under global warming conditions. We examine potential shifts in nesting time, range, as well as body geometry and size. To our knowledge, this is the first projection of the fundamental niche of an organism using this high level of accuracy, which can only come from CFD and numerical heat transfer models (Dudley et al. 2013).

Methods

Marine Fluid Simulation

We drew five different anatomically realistic adult leatherbacks in a non-uniform rational basis splines (NURBS) format using commercial 3D design software (MoI) (Fig. 1). The five different models are: one with the highest curved carapace length (CCL) to curved carapace width (CCW) ratio (1.5) and the longest CCL (171 cm) (called long narrow (LN)), one with the lowest ratio (1.2) and the longest CCL (called long wide (LW)), one with the highest ratio and the shortest CCL (128) (called short narrow (SN)), one with the lowest ratio and the shortest CCL (called short wide (SW)), and one which had an average ratio (1.4) and an average CCL (150 cm) (called average (Av)) (Fig. 2 and Table 1). These leatherbacks would weigh approximately 477 kg, 633 kg, 201 kg, 266 kg, and 337 kg respectively. The ratios and lengths are based on

data from three sources (James et al. 2007, Médicci et al. 2011, "Jupiter Island sea turtle taging project (JISTTP)" 2012). This size range more than covers the typical standard deviation observed in CCLs of sampled leatherbacks (typically less than 10 cm). The flipper length scaled with CCL and not with CCW (Walker 2010). We placed the virtual leatherbacks inside a virtual half cylinder enclosure with buffer distances of approximately 4 m. This resulted in volumes ranging from 440 to 1450 m³. We meshed all the fluid domains with tetragons. All domains contained approximately 150,000 elements (Fig. 3).

We wrote a supplemental program, which describes the leatherbacks' swimming motion. To measure the flipper motion, we used ImageJ software to analyze frames from publicly available video of leatherbacks freely swimming. The flipper had four zones. The 14% of the flipper closest to the shoulder was the transition zone from no motion to steady roll (flipper moving dorsally to ventrally) and yaw (flipper moving posteriorly to anteriorly). The next 22% of the flipper was the transition zone from steady roll and yaw to steady roll, yaw, and pitch (flipper twisting). The next 21% of the flipper was a zone of constant roll, yaw, and pitch. The last 43% of the flipper was the transition zone from steady roll, yaw, and pitch to roll, yaw, pitch, and bend (flexing of the flipper in the roll plane). The stroke had four phases. There was a down stroke (32.3% of stroke period), a turn at the bottom and at the top of the stroke (17.0% of stroke period for each), and an up stroke (33.7% of stroke period). To prevent discontinuities in the motion, we programmed smooth transitions into the top and bottom phases. To correctly position the flipper, there was also a 0.5 s setup time. We fine-tuned each of the leatherbacks stroke period so each morphology had the average internesting swim speed for a leatherback (0.53 m/s) (Hughes et al. 1998, Eckert 2002, Luschi et al. 2003, Lambardi et al.

2008, Shillinger et al. 2008, Byrne et al. 2009). As leatherbacks orient randomly with respect to current, we did not consider its effects (Galli et al. 2012). The stroke periods for the leatherbacks were 2.01 s, 2.19 s, 1.63 s, 1.72 s, and 1.81 s for LN, LW, SN, SW, and Av respectively.

The simulation used the k- ω shear stress transport (SST) model in the commercial CFD program, ANSYS Fluent, with a constant velocity inlet (0.53 m/s) and a zero pressure outlet. The plane dividing the leatherback had a symmetry boundary condition. We set the time step to 0.001 s and ran the simulation for one full period. In all analysis, we removed the initial 500 setup steps. We calculated average thrust, work, and flipper and body heat transfer coefficients. To translate the work done on the fluid into expended energy, we used the aerobic efficiency of tortoise muscle (35% (Woledge 1968)). Considering the propeller efficiency, the efficiency of converting energy to useful work is 16.7% which is similar to other studies (Webb 1971, Feldkamp 1987).

Marine Internal Simulation

The internal model is the same model we used in our previous work except scaled to each leatherback's size (Dudley et al.). The resting metabolic rate (RMR) scales with core temperature and we are attempting to determine actual core temperature, therefore assigning a metabolic rate to the internal simulation is problematic. Therefore, we ran several simulations for a single ambient temperature. Each of these simulations had a different metabolic rate corresponding to a different thermal gradient (ranging from 2°C to 18°C). For each set of simulations we then have two lines. One line is the guessed thermal gradients and one line is the actual simulated thermal gradients. The point where the guessed thermal

gradients cross the simulated thermal gradients is the actual thermal gradient and actual core temperature.

Marine Niche Map

Using the relations between ambient water temperature and core leatherback temperature from the internal swimming simulation, we developed a marine niche model program for leatherback turtles. The niche-modeling program uses the relations we found in the CFD simulations to determine the core temperature based on the ambient water temperature. The leatherback was able to decrease its ambient temperature by diving deeper, longer and more frequently up to a limit. Based on the extensive literature on leatherback dive profiles we set the limits to a maximum 100 m depth, a maximum 25 minute dive time, and a minimum 2.5 minute recover time (Southwood et al. 2005, Wallace et al. 2005).

We ran this niche map using GCM data from the Met Office Hadley Centre's Hadley
Centre Global Environment Model, version 2 (Earth System) (HadGEM2-ES) from the CMIP5
multi-model ensemble. We selected the HadGEM2-ES models based on its ability to accurately
model ocean temperatures and important ocean temperature oscillations (Atlantic

Multidecadal Oscillation and Central and Eastern Pacific El Niño-Southern Oscillation) (Kim & Yu
2012, Chiang et al. 2013). The resolution of the ocean model is 1° latitude by longitude 1° by 10
m depth. We selected the monthly average data sets for relative concentration pathway (RCP)
4.5 (a stabilizing scenario) (Smith & Wigley 2006, Clarke et al. 2007, Wise et al. 2009) and 8.5
('business as usual') (Riahi et al. 2007) and the historical simulation. We averaged the ocean
temperature by month over a 5 year window (2095-2100 for RCP8.5/4.5 and 2005-2010 for the
historical)

Terrestrial Fluid Simulation

We setup the land model's fluid dynamics component to calculate the heat transfer coefficients of the leatherback's body and flipper at different wind speeds. For this model, we added a plane below the plastron of the leatherback to simulate the ground. The ground covered 24% of the leatherback's surface area. We enclosed this geometry in a half pipe with a 5 m buffers around the leatherback. We meshed the leatherback with 1.2 million elements using a combination of tetrahedrons, pyramids and wedges (Fig. 4). The simulation used the k- ω SST model with a variable velocity inlet (0.1 to 20.0 m/s) and a zero pressure outlet.

Terrestrial Internal Model

The internal land model geometry was similar to the swimming geometry with the exception that we divided the surface area into three areas. The bottom area exchanged heat with the ground by conduction. This portion of the plastron and the bottom of the flipper accounted for 33% of the leatherback's surface area. The middle area exchanged heat by convection with the air and infrared (IR) radiation with the ground and accounted for 22% of the surface area. The top portion exchanged heat through convection with the air and IR radiation with the sky and accounted for the remaining 55% of the surface area. We set the IR temperature of the ground to that of the ambient temperature multiplied by sand's emissivity. We set the IR temperature of the sky using the Swinbank relation (Swinbank 1963). Our previous more simplified model had demonstrated that evaporative cooling has little effect, thus we neglected it (Dudley & Porter 2014). The internal heat generation was based on metabolic rates of nesting leatherbacks (1.05 W/kg when crawling (Paladino et al. 1990, 1996), 1.38 W/kg when digging and covering (Paladino et al. 1990), and 0.15 when laying (Lutcavage et

al. 1990, Paladino et al. 1996)). The nesting time table was 3 minutes to crawl up, 22 minutes to dig, 15 minutes to lay, 45 minutes to cover, and 8 minutes to return (Carr & Ogren 1959). We set the initial temperature of all leatherbacks to 29.85 °C and set other temperatures relative to this initial temperature. Preliminary runs showed that core temperature on an absolute scale made little difference in temperature increase and that difference between the initial core temperature and ambient was the important factor. We ran the Av internal model for five different air temperatures, five different wind speeds, and nine different land temperatures for a total of 225 combinations. This number of points proved to give excessive resolution and so we ran the remaining four leatherbacks with three different air temperatures, three different wind speeds, and three different land temperatures for a total of 27 combinations.

Terrestrial Niche Model

The land niche model used the 255/27 element matrix to interpolate the temperature increase a leatherback would experience in a given region. We again used the HadGem2-ES model taking monthly averages for soil temperature, daily minimum temperature, and wind velocity. The resolution of the atmosphere data sets and land data sets are 1.875° longitude by 1.25° degree latitude. We averaged the marine core temperatures that overlapped each of the atmosphere/land cells. We only examined land areas that directly bordered water.

Results

Marine Simulation

From the marine CFD simulation we calculate power and heat transfer coefficients. The power profile was similar for all five morphologies. There was a rise in power output during the down phase, a spike in power in the middle of the bottom phase, a spike followed by a plateau during the up phase, and a spike in power in the middle of the top phase (Fig. 5). For the average power during the stroke, the LN had the highest while the SW had the smallest (Fig. 6). Note that LN and SN used more power to swim at the same speed as LW and SW respectively. This difference is because the narrowing of the carapace moves the flippers closer together and reduces their propeller efficiency (useful power/ available power). Also note that attempting to calculate power by using the force necessary to overcome static drag would have underestimated power output by 60% even given a low 20% propeller efficiency. Figure 7 shows the Av leatherback's pressure profile during the stroke. It is evident that most of the power comes from the flipper's distal region.

For the heat transfer coefficient, there is a relatively stable coefficient for the body and a changing coefficient on the flipper (Fig. 8). The flipper heat transfer coefficient is highest during the down stroke and lowest during the bottom portion of the stroke. The Av leatherback had the highest coefficients while the SN had the lowest (Fig. 6). Figure 9 shows the heat flux through the skin as the Av leatherback moves through its stroke. Note the higher heat fluxes of the flipper's distal region and the lateral portion of the carapace posterior to the flipper. Since these simulations only get the heat transfer coefficient, the leatherback skin is set at a constant temperature and the actual leatherback's heat flux (below) will differ.

The internal simulation produced a relation for each of the five leatherbacks between ambient temperature and leatherback core temperature (Fig. 10). SN and SW had the lowest

core temperature for a given ambient temperature, Av was slightly above them, and LW and SN were warmer still and close together. The shallow slope of the graphs around 20 °C is due to the leatherback controlling its core conduction through vasoconstriction and dilation. Figure 11 shows the heat flux contour map for the Av leatherback at 23 °C. The highest heat flux is around the soft tissue of the shoulder regions.

The Marine niche model produces 12 maps (one for each month) for a given set of conditions. We use the maps for the Av leatherback in June as an example (Fig. 12.), and the remaining maps are in appendix 1. The orange to red areas on the map indicate regions where the leatherbacks are within one standard deviation of their critical thermal maximum (CTM) $(40.2 \pm 1.3 \, ^{\circ}\text{C})$ and the black areas are where they are above one standard deviation of their CTM. Solely from the maps, it is evident that Av leatherbacks are under no thermal distress anywhere under current conditions (except a narrow band near Sumatera, Western Indonesia), but will be under some distress in South East Asia under RCP4.5, and under severe distress in South East Asia under RCP8.5.

Looking at the condition of the Av leatherback during local nesting seasons at some specific areas with large leatherback nesting populations (French Guiana and Suriname (FG&S) (nesting March-July), Gabon and Congo (G&C) (nesting November-February), and West Papua, Indonesia (WP) (nesting May-September)), we see that leatherback core temperatures will increase fairly similarly. Only WP under RCP8.5 will have significant portions of its water inaccessible to leatherbacks in 2095-2100 (Fig. 13). Three strategies leatherback populations in WP could use as refuges are changing location, changing nesting time, or changing size.

location change (nesting in Vietnam instead of WP) provides some relief (a decrease from 85% of near shore area inaccessible to 35% inaccessible); and size change (moving from Av to SN) provides the most relief, and makes all of WP accessible (Fig. 14).

The LW leatherback is in distress in places outside of WP. The LW has 10% of near shore area over one standard deviation above the CTM in FG&S under RCP4.5, 73% in FG&S under RCP8.5, and 2% in G&C under RCP 8.5 (Fig. 15).

Terrestrial Simulation

The terrestrial niche model produces 12 maps (one for each month) for a given set of conditions. We show two maps of the Av leatherback under RCP4.5 in June as an example; one is for the core temperature increase during nesting and one is for the actual temperature after nesting (Fig. 16.). The remaining Av maps are in appendix 2. A leatherback heats up while nesting except during the laying portion where the low metabolic rate allows it to cool (Fig 17). Figure 18 shows a typical heat flux map for a leatherback nesting. Again, the high heat flux was around the shoulder area. Our terrestrial data in our three regions of interest yields similar results to the marine niche map. The leatherbacks are most in danger in WP (Fig. 19) and changing size is the best option (Fig 20). The nesting phase has a higher percent of area above one standard deviation of the CTM in WP (increasing from ~20% to ~70% even considering refuges)

Discussion

This study shows that using 3D CFD in conjunction with a biophysical niche model is an accurate method to model current ranges and future ranges under projected global climate

change scenarios. For animals with complex and difficult-to-measure physiologic characteristics, or for animals whose physiological data is expensive to collect, this method proved a useful alternative for gathering highly accurate physiological data. In comparison to an empirical niche model this method is superior especially considering global warming because forming an empirical niche map for novel conditions requires complex statistical methods and may still be inappropriate or inaccurate (Dormann 2007, Phillips et al. 2008). Using the leatherback sea turtle, we then showed how this physiological data can be used to predict an animal's future fundamental niche and projected range shift under global warming conditions.

Our results show that global warming, especially if mitigation efforts are not successful, will be quite damaging for leatherbacks particularly in South East Asia. While all leatherback internesting core temperatures will increase, only those in South East Asia will rise above their CTM. For larger leatherbacks, FG nesting populations will experience some thermal distress especially under RCP 8.5. While the body size of the population could decrease in respones to increased temperatures, observed cases of rapid decreases in body size are in species with shorter generation times (Jackson et al. 2001, Grant & Grant 2002, Heimsath et al. 2003, Shackell et al. 2010).

These predictions are conservative, particularly in the terrestrial phase. Our model used the average monthly minimum temperature, and an efficient nesting schedule. If leatherbacks nest slower or at a warmer time of day, especially if the sun is up, they are facing more thermal risk than our model considers.

Several other works address the question of modeling sea turtle ranges, habitats, or niches. Pike uses a model that mapped a suitability index onto current nesting sites for all sea

turtle species. While the work is limited to current conditions this approach could perhaps be expanded to make future projections (2013). Hawkes et al. used loggerhead tracking data off the U.S. east coast to make a suitability index considering preferred temperature (2007, 2011), and Pikesley et al. have done similar work with olive ridley sea turtles off the coast of west Africa (2013). Our paper is the first to use a biophysical model to map on a global scale and consider global warmings effects.

Comparing this to our earlier work (Dudley & Porter 2014), we see that that research underestimated the threat global warming poses to leatherbacks, particularry in South East Asia. Most likely this underestimate is due to the lower field metabolic rate we used which came from a doubly labeled water (DLW) study (Wallace et al. 2005). Our metabolic rate is higher and their results may suffer from the difficulties of conducting DLW experiments on a marine vertebrate (Jones et al. 2009).

The data from this research will help managers and conservationists, particulary in South East Asia, predict when leatherbacks may stop nesting at local beaches to seek more hosptitable waters. Our next phase of this project will be to complete the maps and data sets for each half decade up to 2100 and make them pubically available.

Acknolgements

We acknowledge the World Climate Research Programme's Working Group on Coupled Modelling, which is responsible for CMIP, and we thank the Met Office Hadley Centre's for producing and making available their model output. For CMIP the U.S. Department of Energy's Program for Climate Model Diagnosis and Intercomparison provides coordinating support and

led development of software infrastructure in partnership with the Global Organization for Earth System Science Portals.

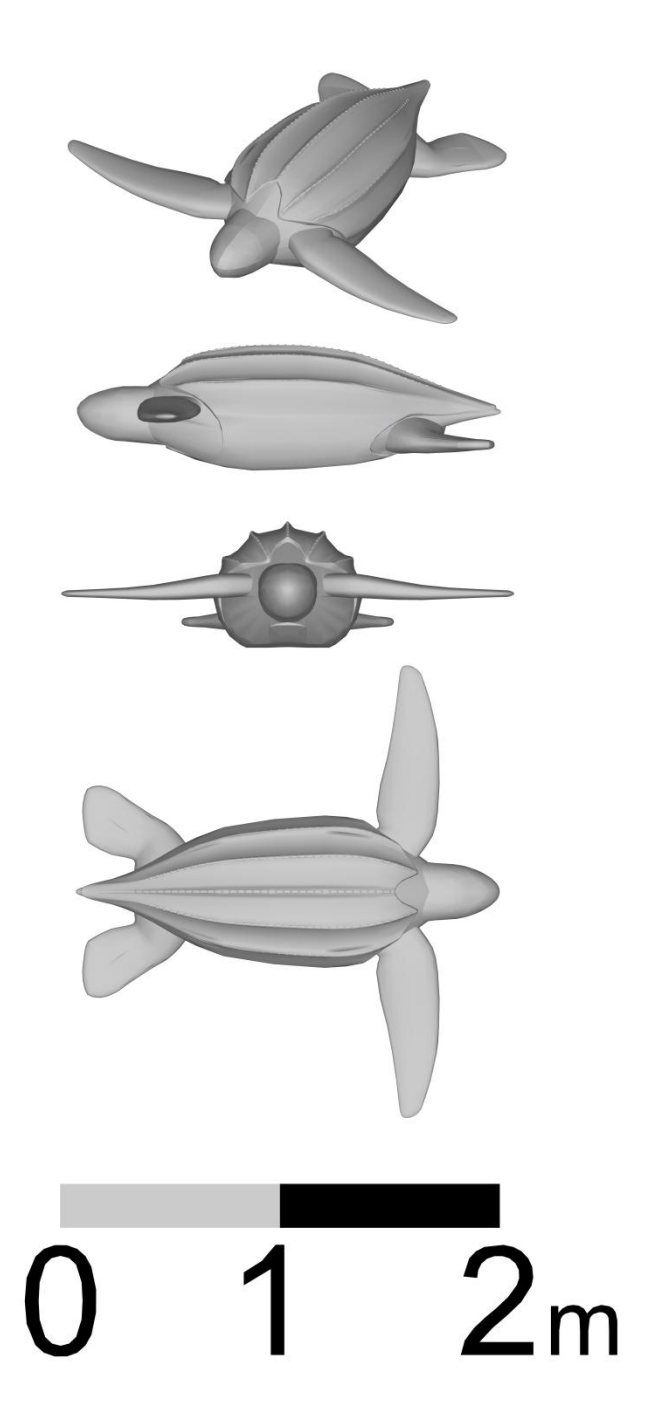


Figure 1. The 3D NURBS model of the average leatherback morphology.

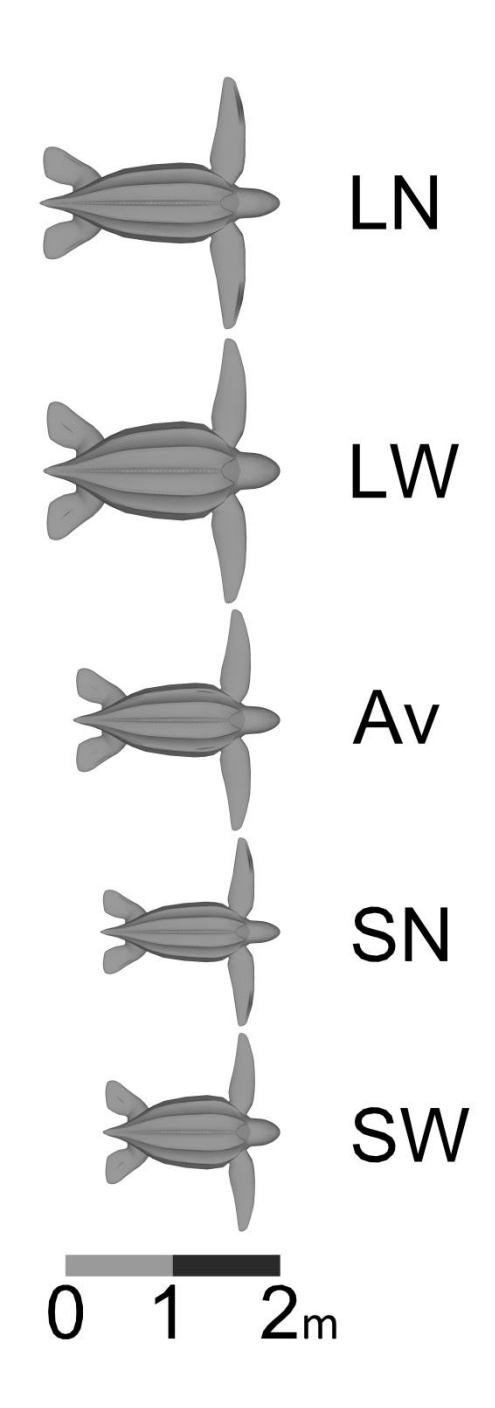


Figure 2. The five different leatherback morphologies we modeled are long narrow (LN), long wide (LW), average (Av), short narrow (SN), and short wide (SW). These turtles would weigh approximately 477 kg, 633 kg, 337 kg, 201 kg, and 266 kg respectively.

Table 1. The curved carapace length, volume, mass, and surface area for the long wide (LW), long narrow (LN), short wide (SW), short narrow (SN), and average (Av) leatherbacks

Morphology	CCL (m)	Volume (m³)	Mass (kg)	Surface Area (m²)
Av	1.5	0.332	338	3.90
LW	1.71	0.624	636	5.72
LN	1.71	0.472	482	5.00
SN	1.28	0.262	268	3.20
SW	1.28	0.198	202	2.80

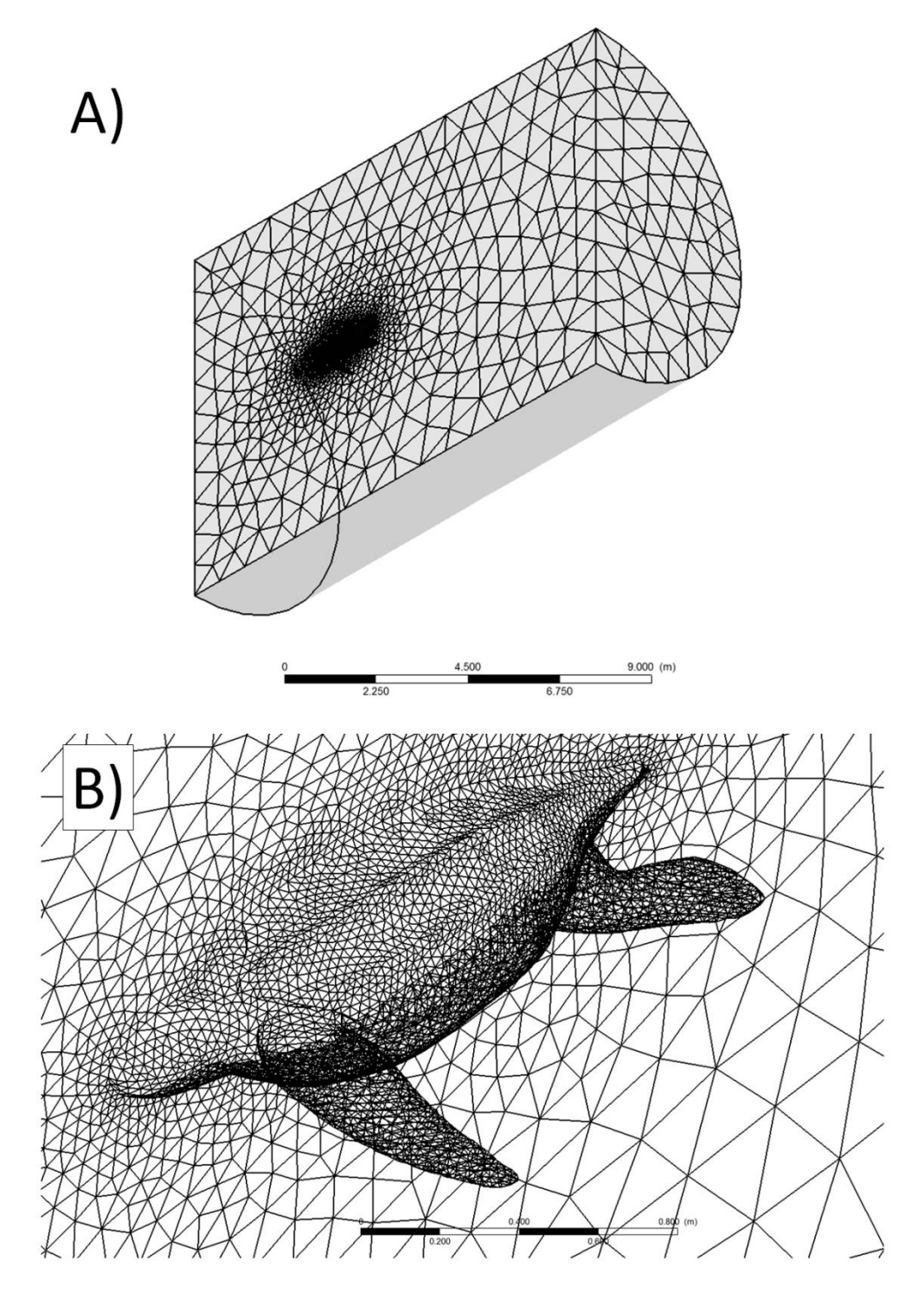


Figure 3. A) The full fluid domain of the Av leatherback. The plane bisecting the leatherback's midline is a symmetry boundary condition. B) A close up of the meshing around the turtle body.

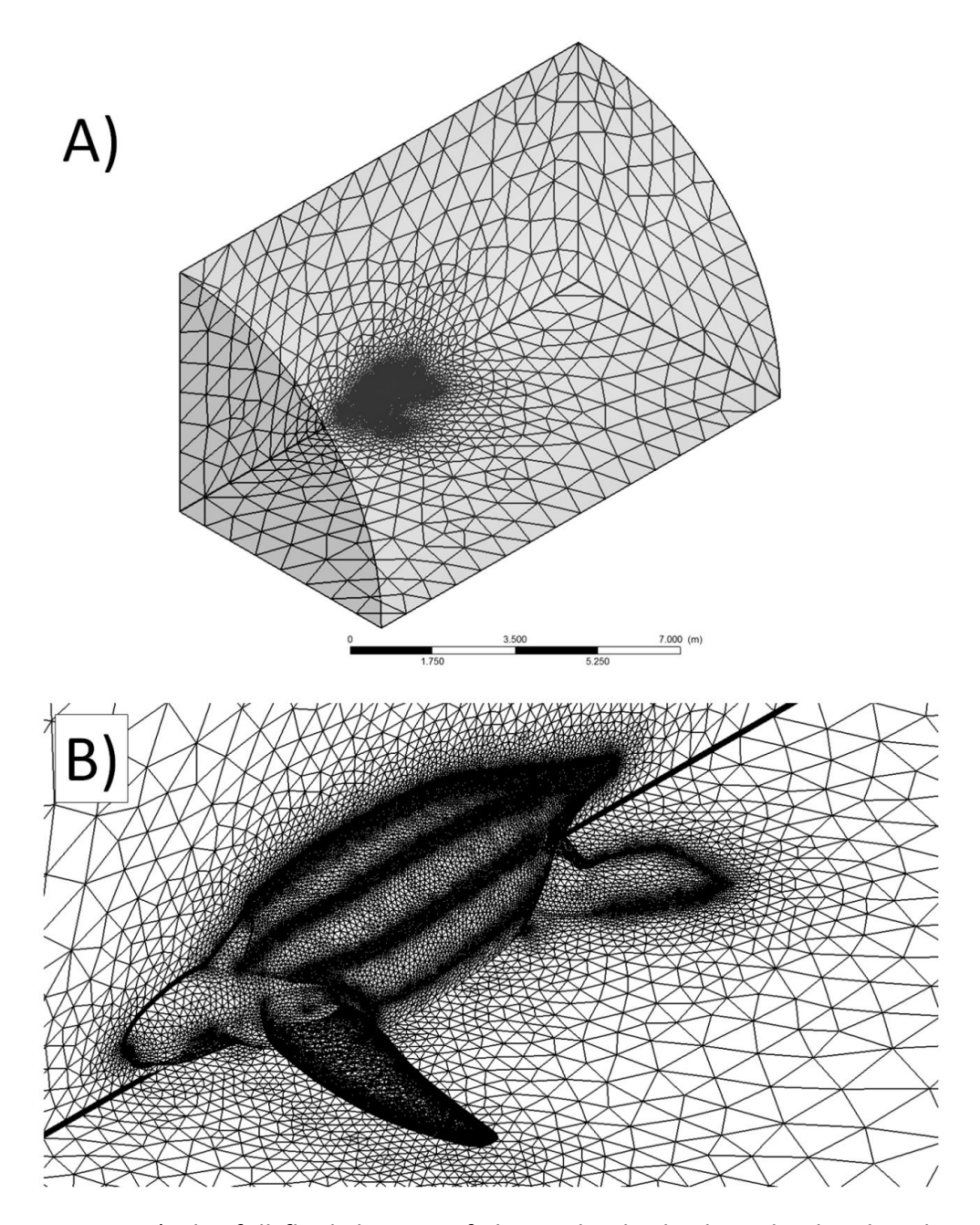


Figure 4. A) The full fluid domain of the Av leatherback on land. The plane bisecting the leatherback's midline is a symmetry boundary condition. B) A close up of the meshing around the turtle body.

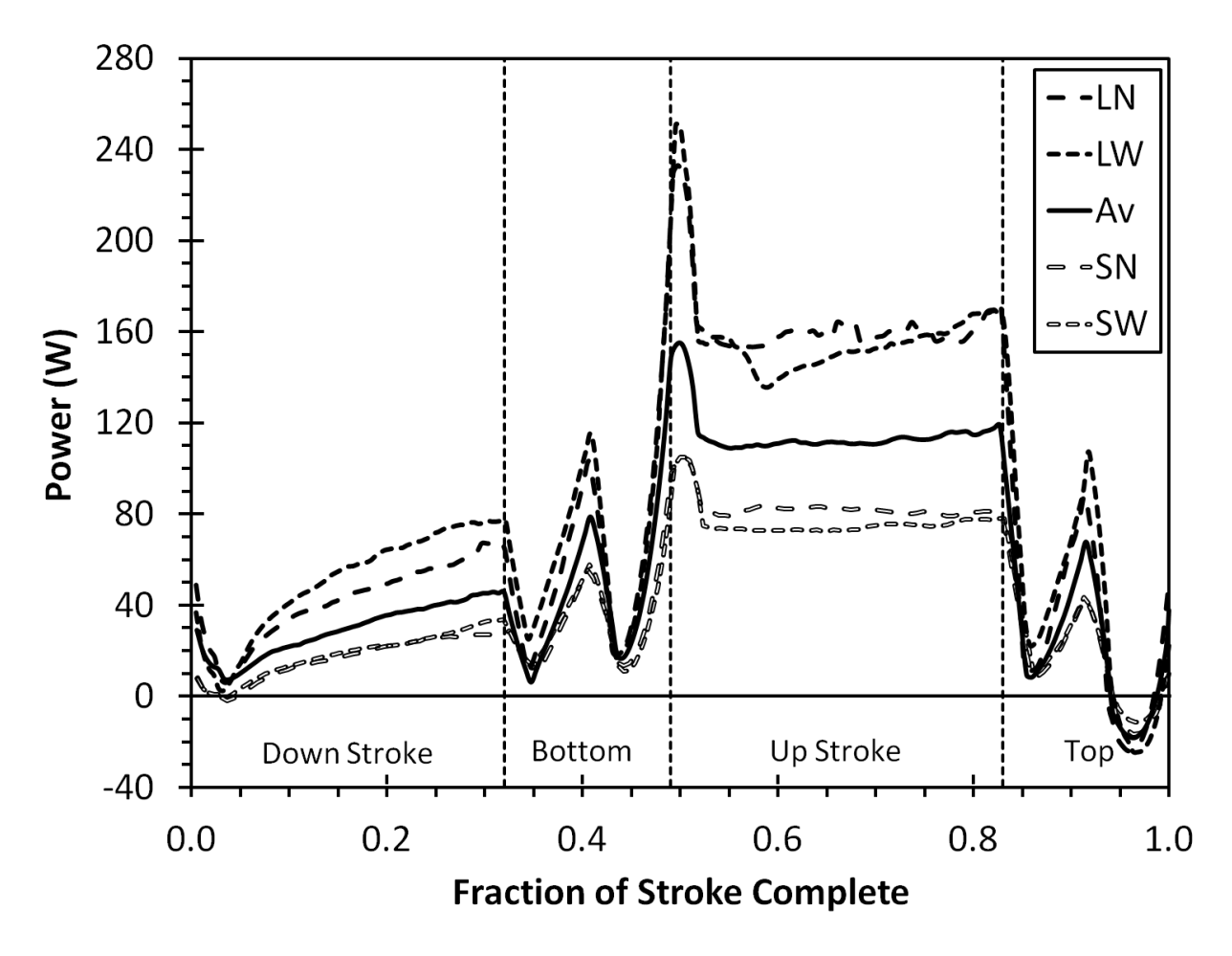


Figure 5. The power the leatherback's flippers put into the water as a function of fraction of stroke complete. The vertical lines separate each portion of the stroke (down stroke, bottom, up stroke, top). We fine tuned the leatherback's stroke period so that forces in the swimming direction summed to zero over one stroke period.

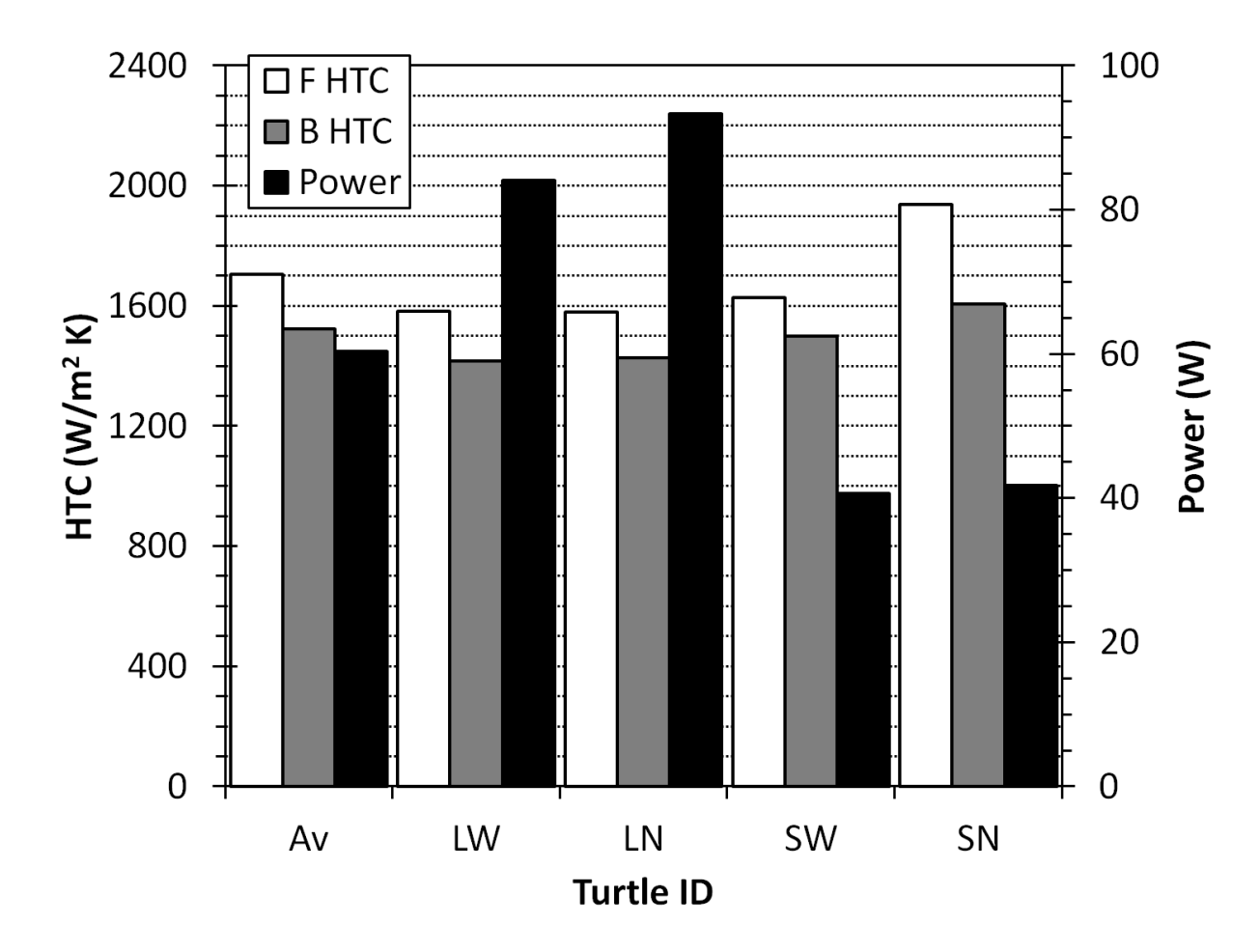


Figure 6. The average data from the five leatherback morphologies. The graph shows power, flipper heat transfer coefficient (F HTC), and body heat transfer coefficient (B HTC). A smaller propeller efficiency makes the LN and SN require more power than the LW and SW respectively.

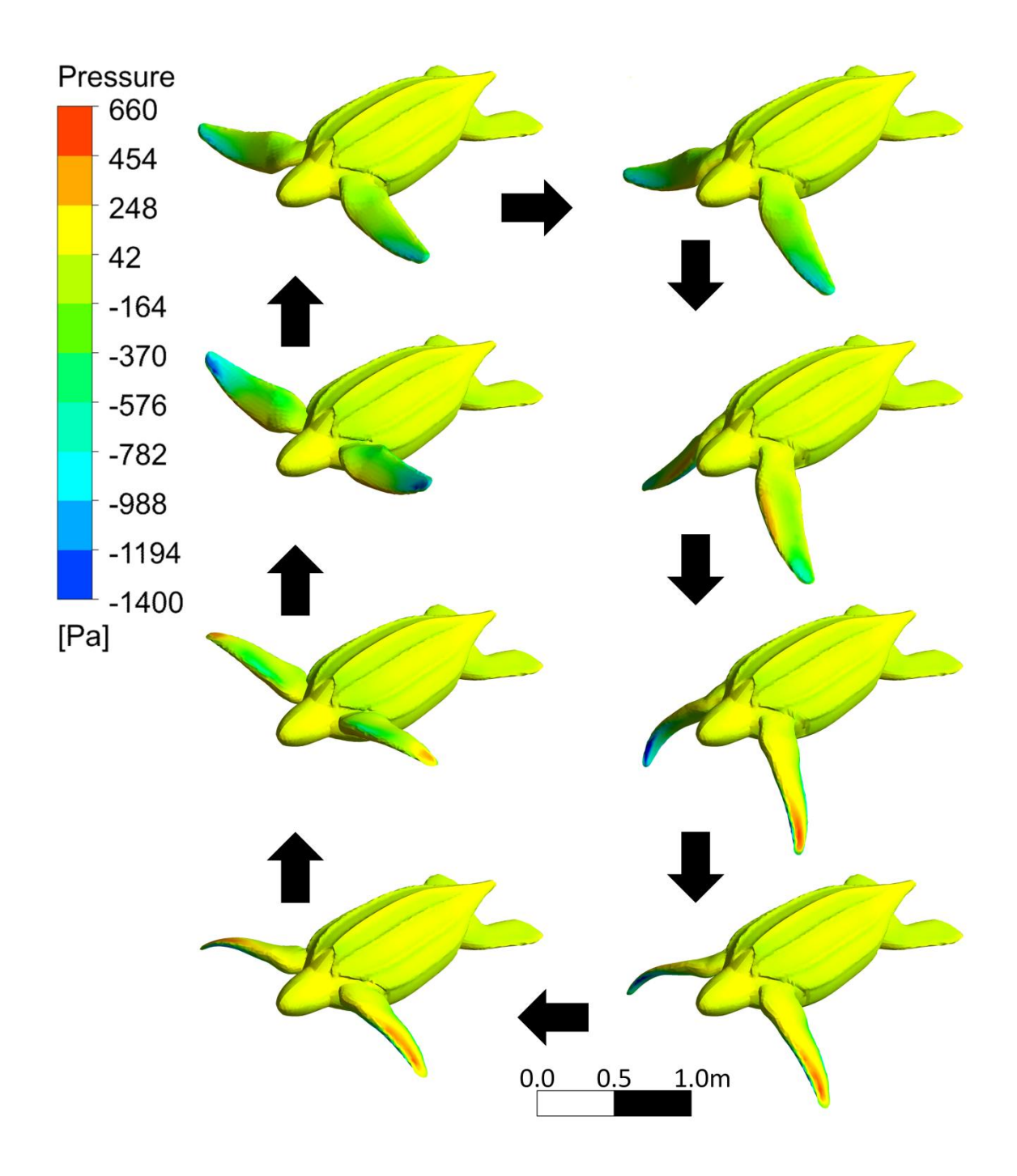


Figure 7. The pressure contours on the Av leatherback as it moves through one stroke period. Black arrows indicate the direction of the image sequence.

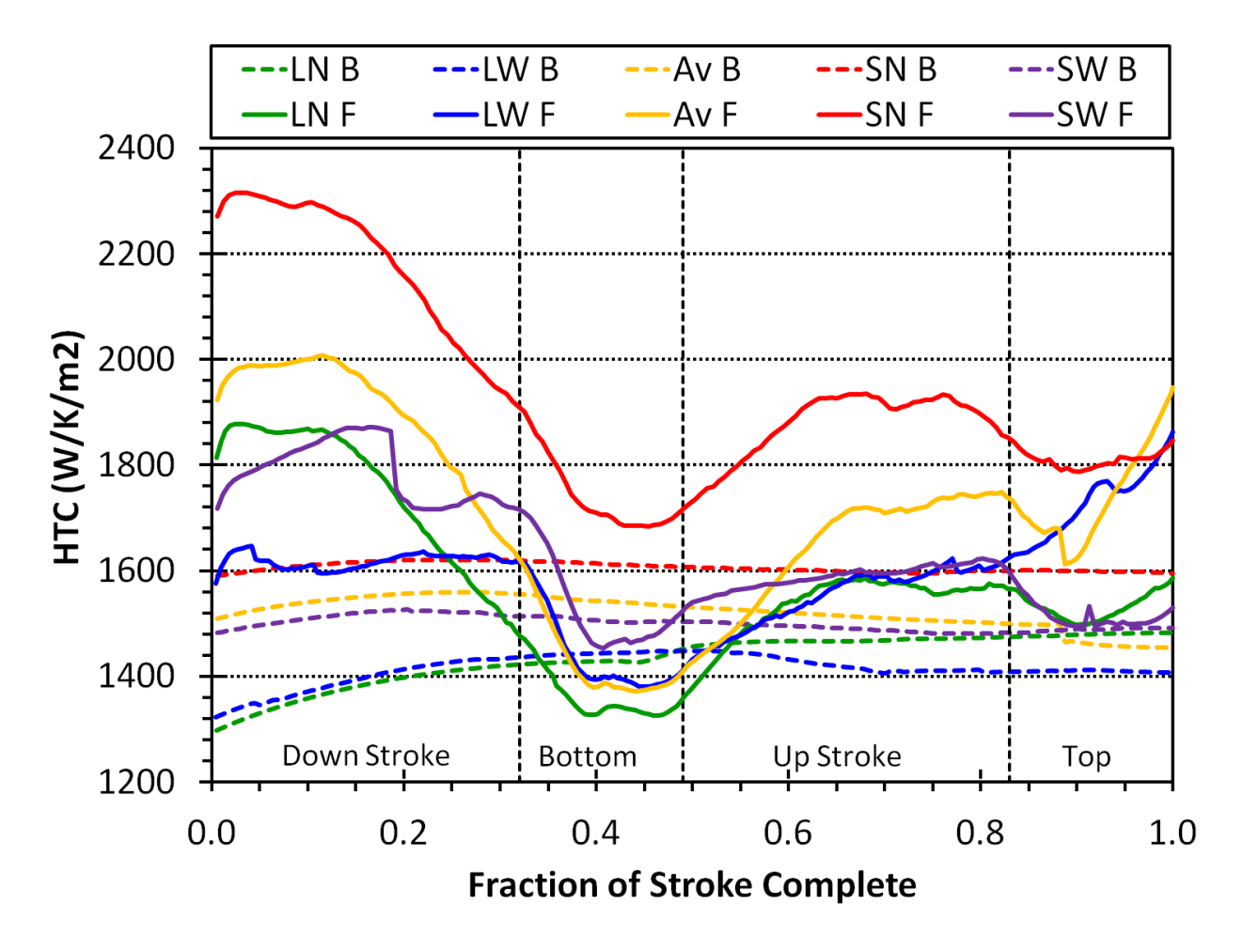


Figure 8. The heat transfer coefficients of our five simulated leatherbacks as they went through one stroke period. B and F stand for the heat transfer coefficient on the body and flipper, respectively. The vertical black lines demark the four different stroke phases (down, bottom, up, and top). Since each swimming frequency has its own period, the x-axis is percent of stroke completed.

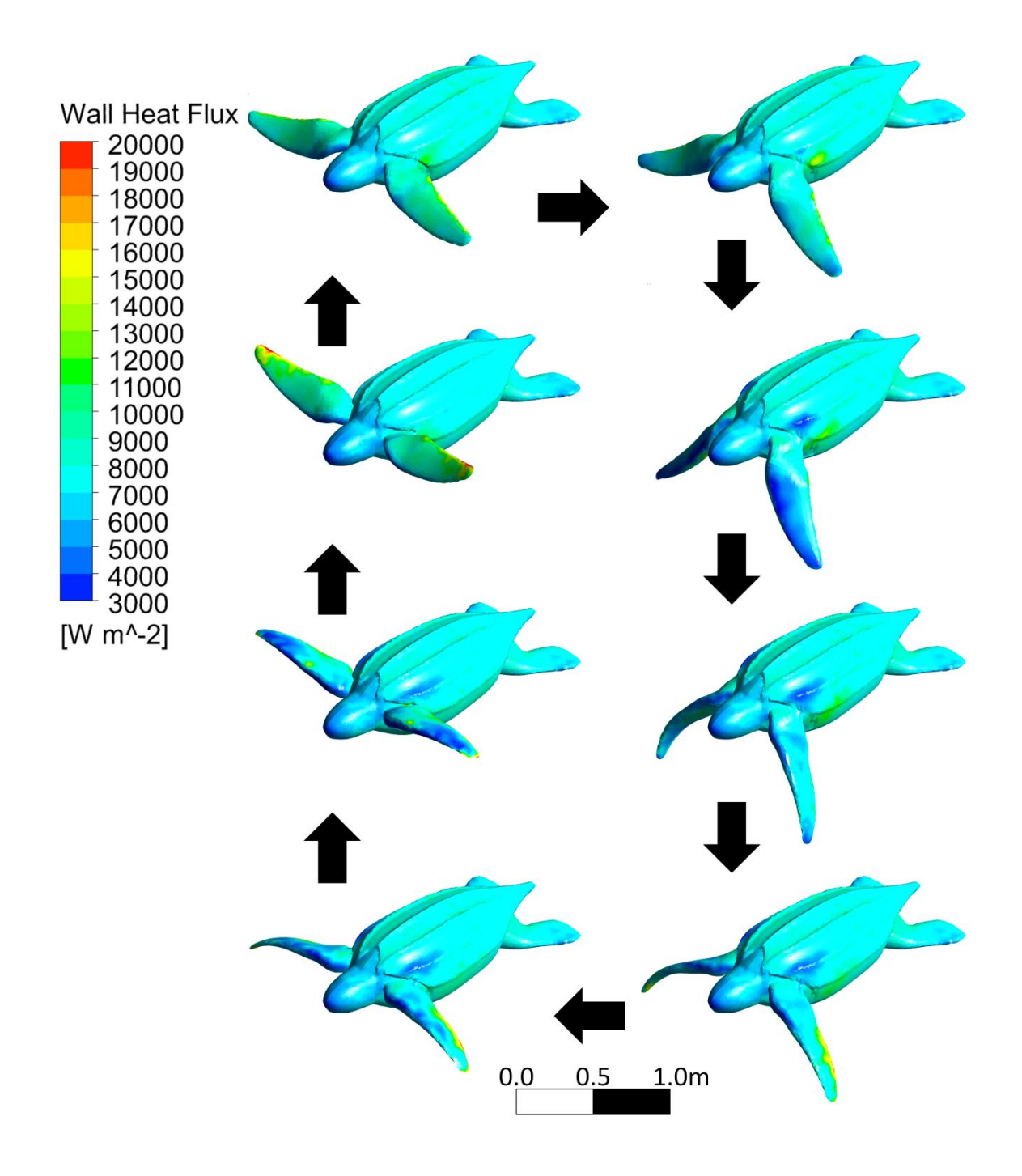


Figure 9. The heat flux contours on the Av leatherback as it moves through one stroke period. Black arrows indicate the direction of the image sequence.

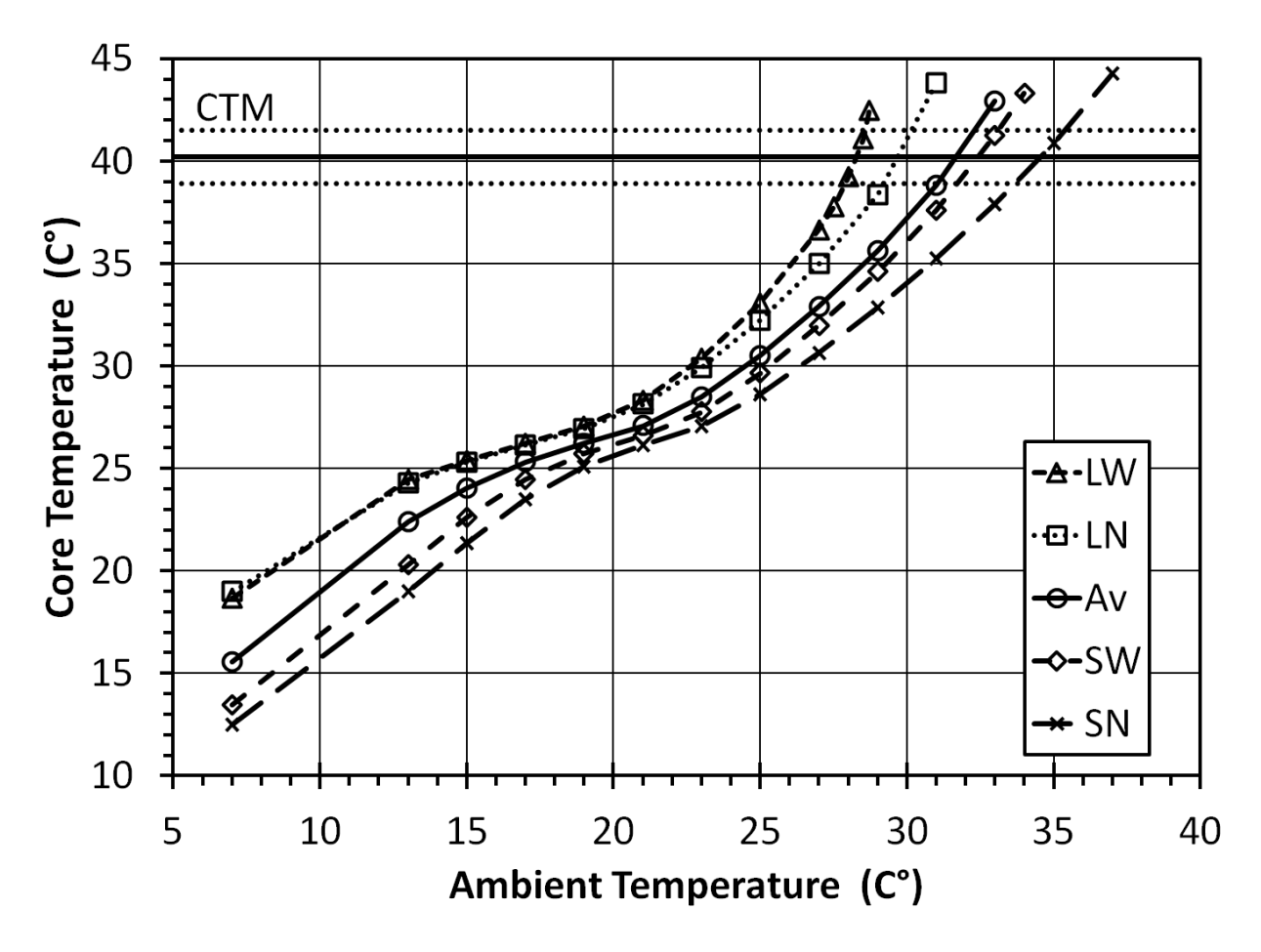


Figure 10. The core body temperature of a leatherback given the ambient water temperature. The bold, horizontal, black line demarks the critical thermal maximum (CTM) while the dotted lines demark the standard deviation in the CTM measurement.

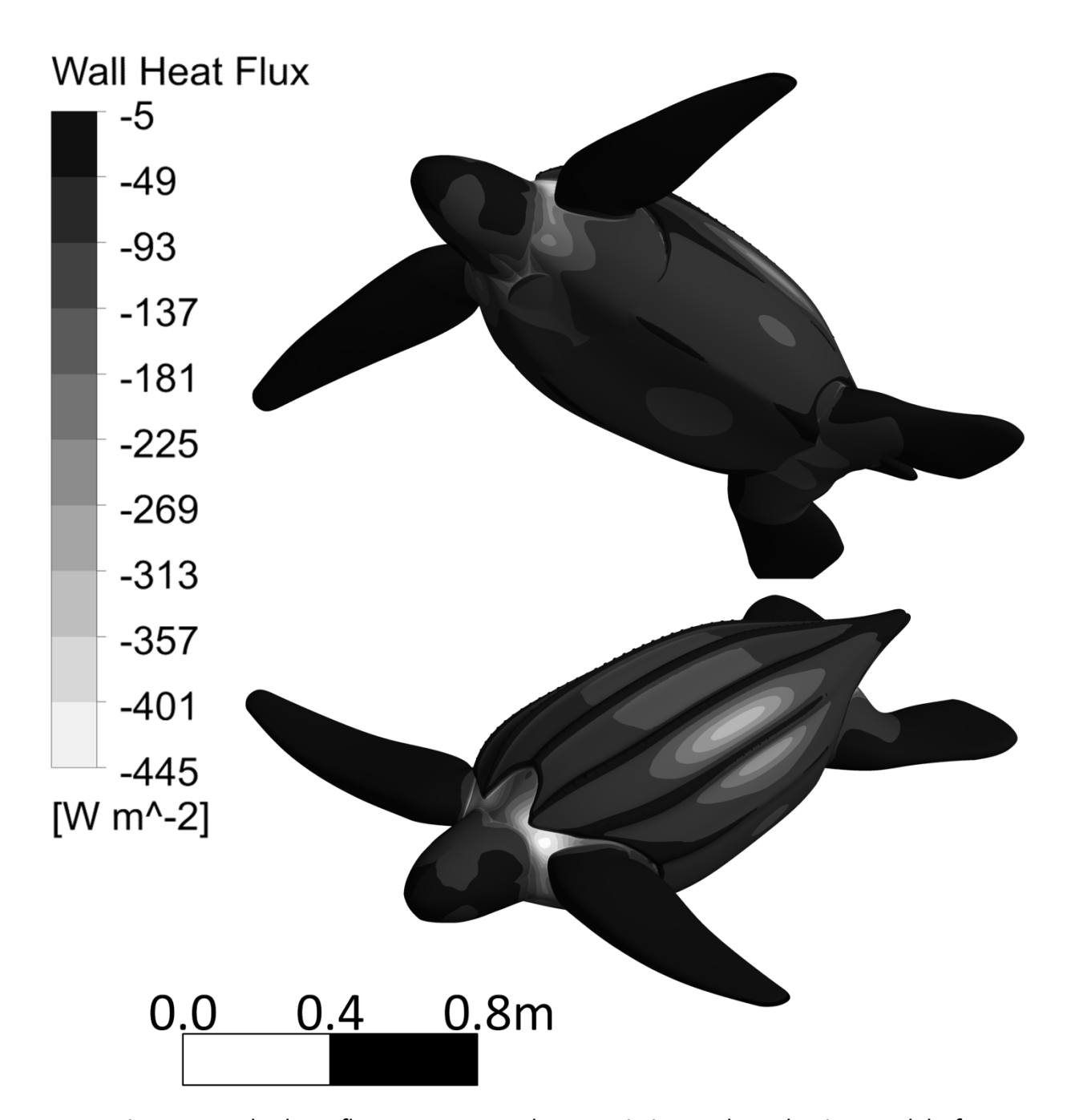


Figure 11. The heat flux contours on the aquatic internal conduction model of the Av leatherback.

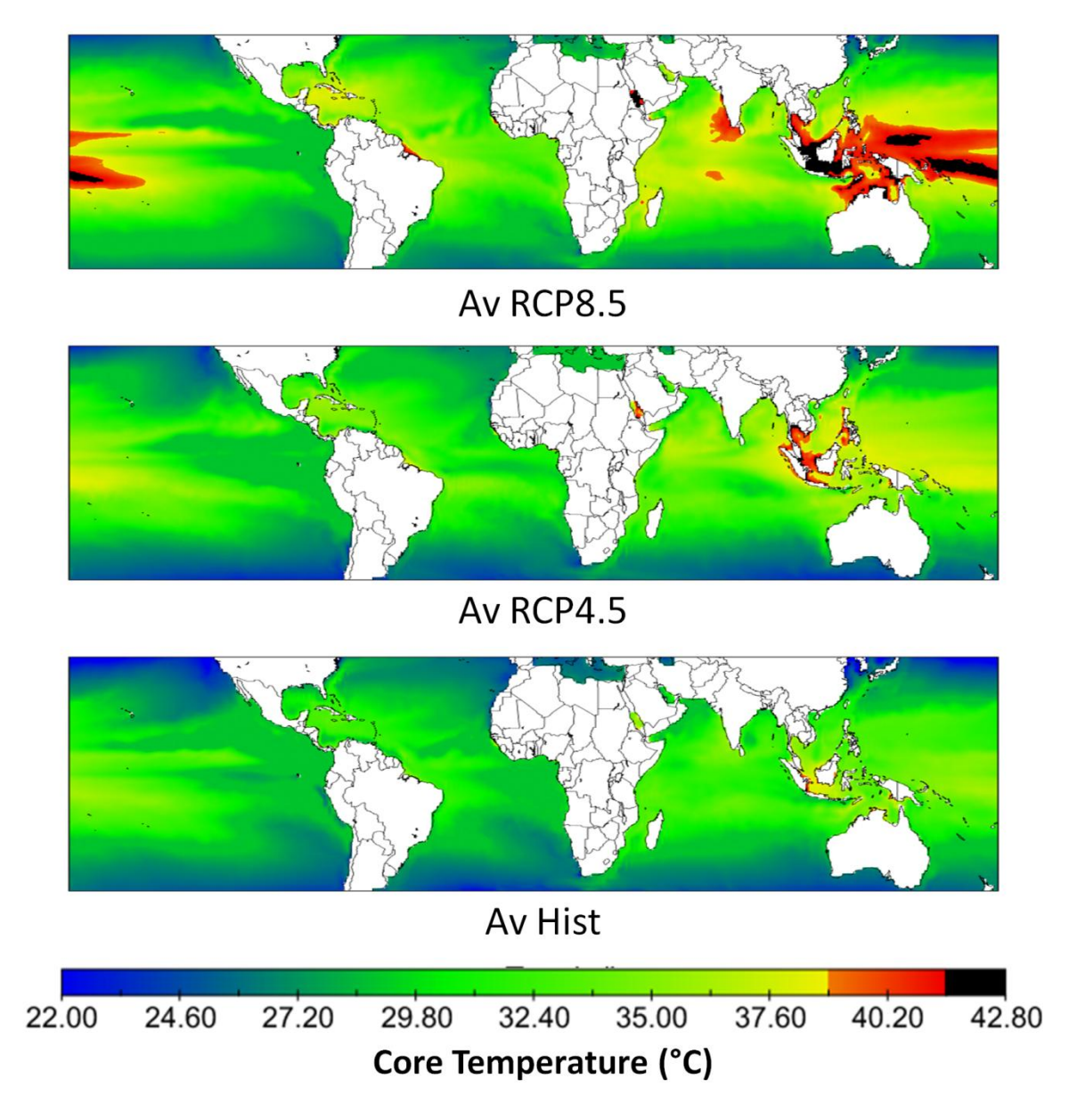


Figure 12. The average core temperature of an Av leatherback in June for 2095-2100. Areas in orange to red are areas where the leatherback's core temperature is within one standard deviation of the CTM. Areas in black are where the leatherback's core temperature is above one standard deviation of the CTM.

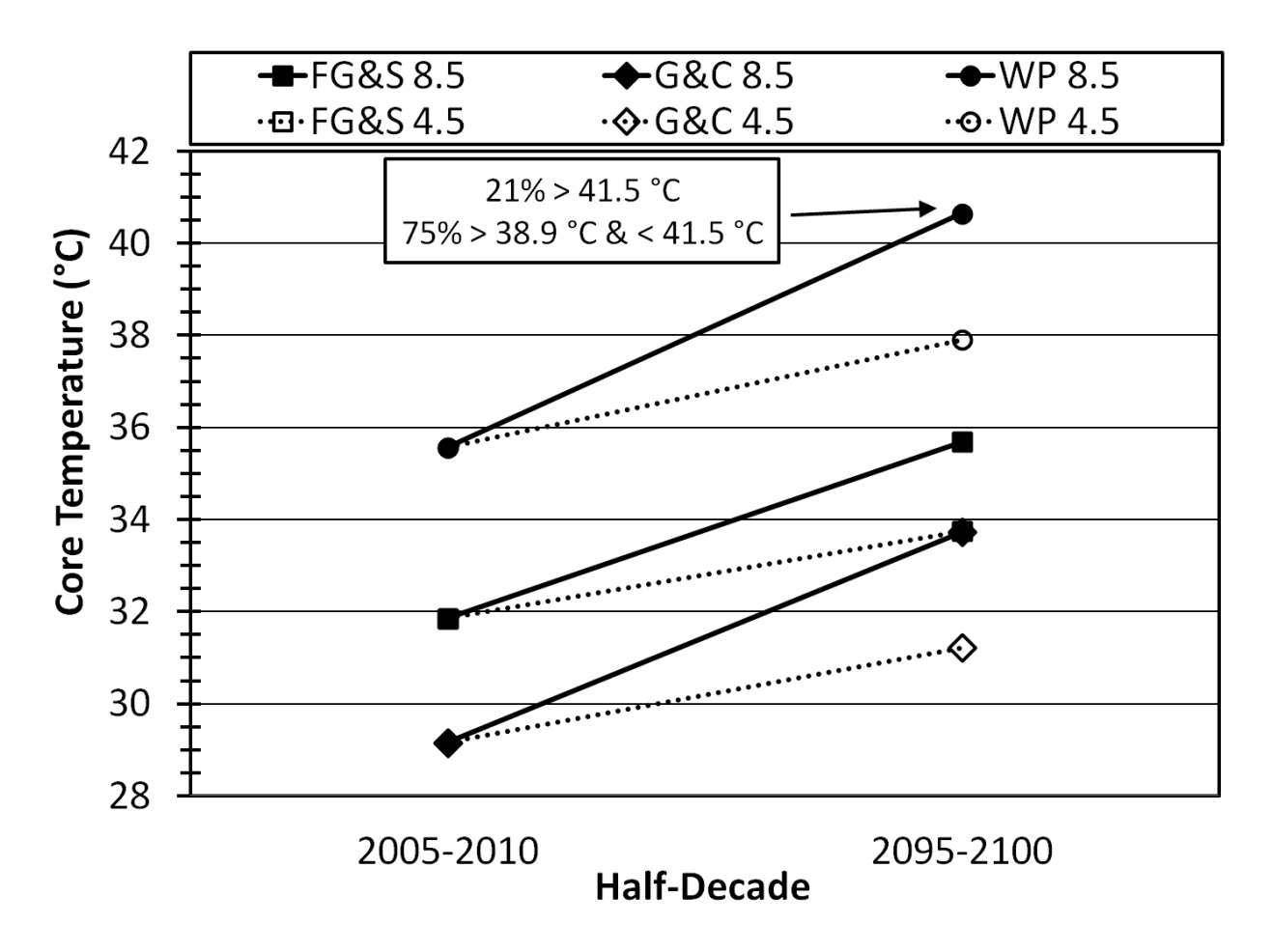


Figure 13. The change in the Av leatherback's core temperature in a given region for 2005-2010 vs. 2095-2100. Averages are for the relevant nesting months at each location (French Guiana and Suriname (FG&S) (nesting March-July), Gabon and Congo (G&C) (nesting November-February), and West Papua (WP) (nesting May-September)). In WP 2095-2100 75% of the area will push the leatherback's core temperatures within one standard deviation of the CTM (39.8 to 41.5 °C). 21% of the area will push the leatherback's core temperature above one standard deviation of the CTM (above 41.5 °C).

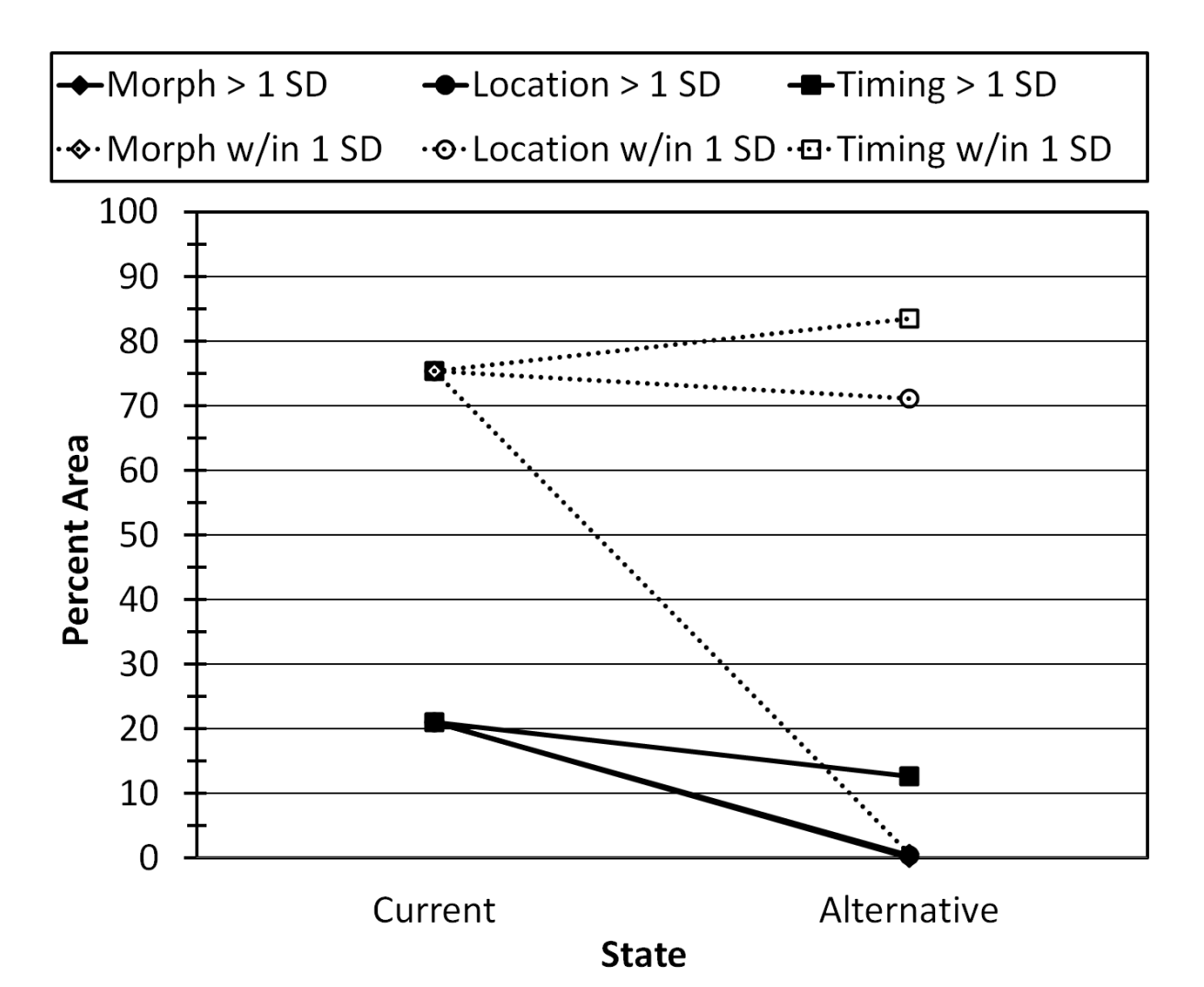


Figure 14. The change in the Av leatherback's percent of marine area where its core temperature is within (w/in 1 SD) or above (> 1 SD) one standard deviation of the CTM (39.8 to 41.5 °C and above 41.5 °C respectively) for its current nesting behavior vs. an alternative nesting behavior in the WP region under RCP8.5. Averages are for the relevant nesting months at each location. The alternatives are to change nesting location (location), change in nesting seasonal timing (timing), or change in morphology (morph) (i.e. going from Av to SN leatherback). Note: Morph > 1 SD and Location > 1 SD overlap.

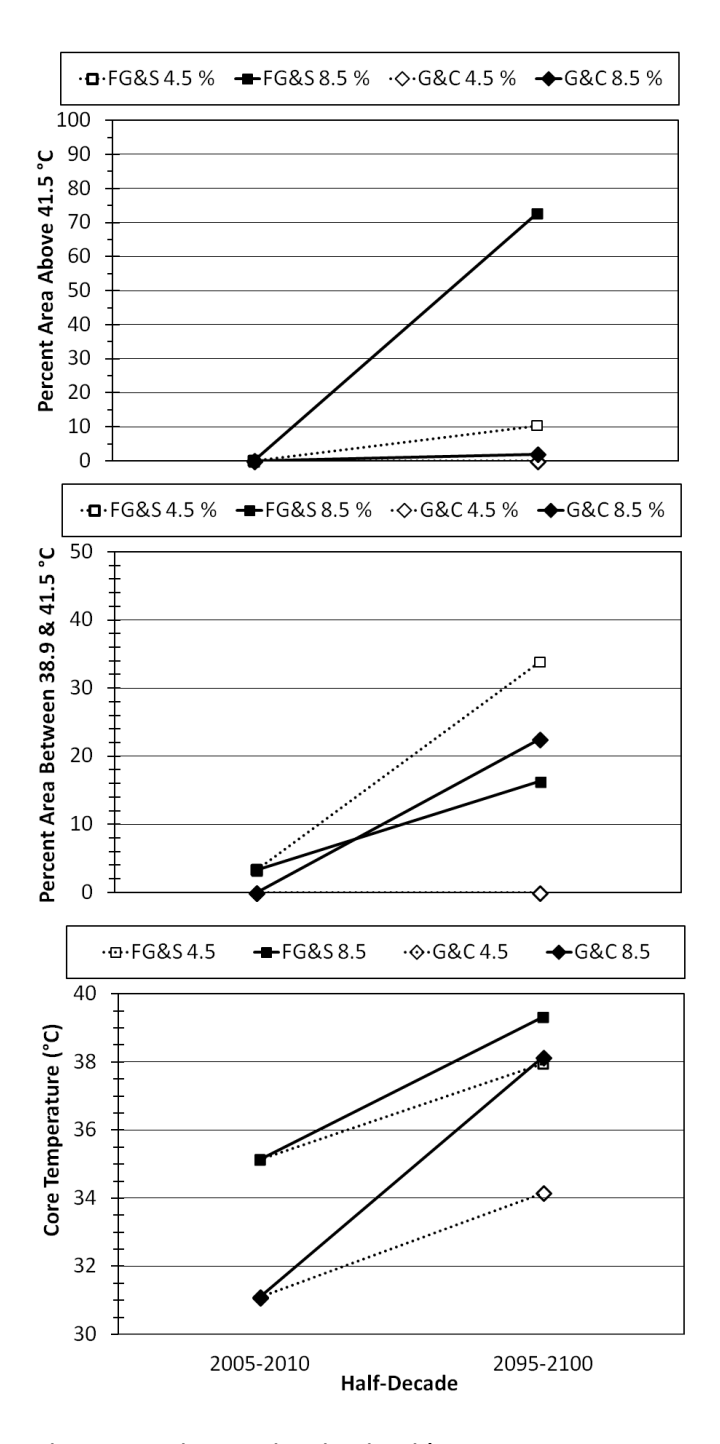


Figure 15. The change in the FW leatherback's core temperature and percent of marine area where its core temperature is within or above one standard deviation of the CTM (39.8 to 41.5 °C and above 41.5 °C respectively) for 2005-2010 to 2095-2100. Averages are for the relevant nesting months at each location (French Guiana and Suriname (FG&S) (nesting March-July), Gabon and Congo (G&C) (nesting November-February), and West Papua (WP) (nesting May-September)).

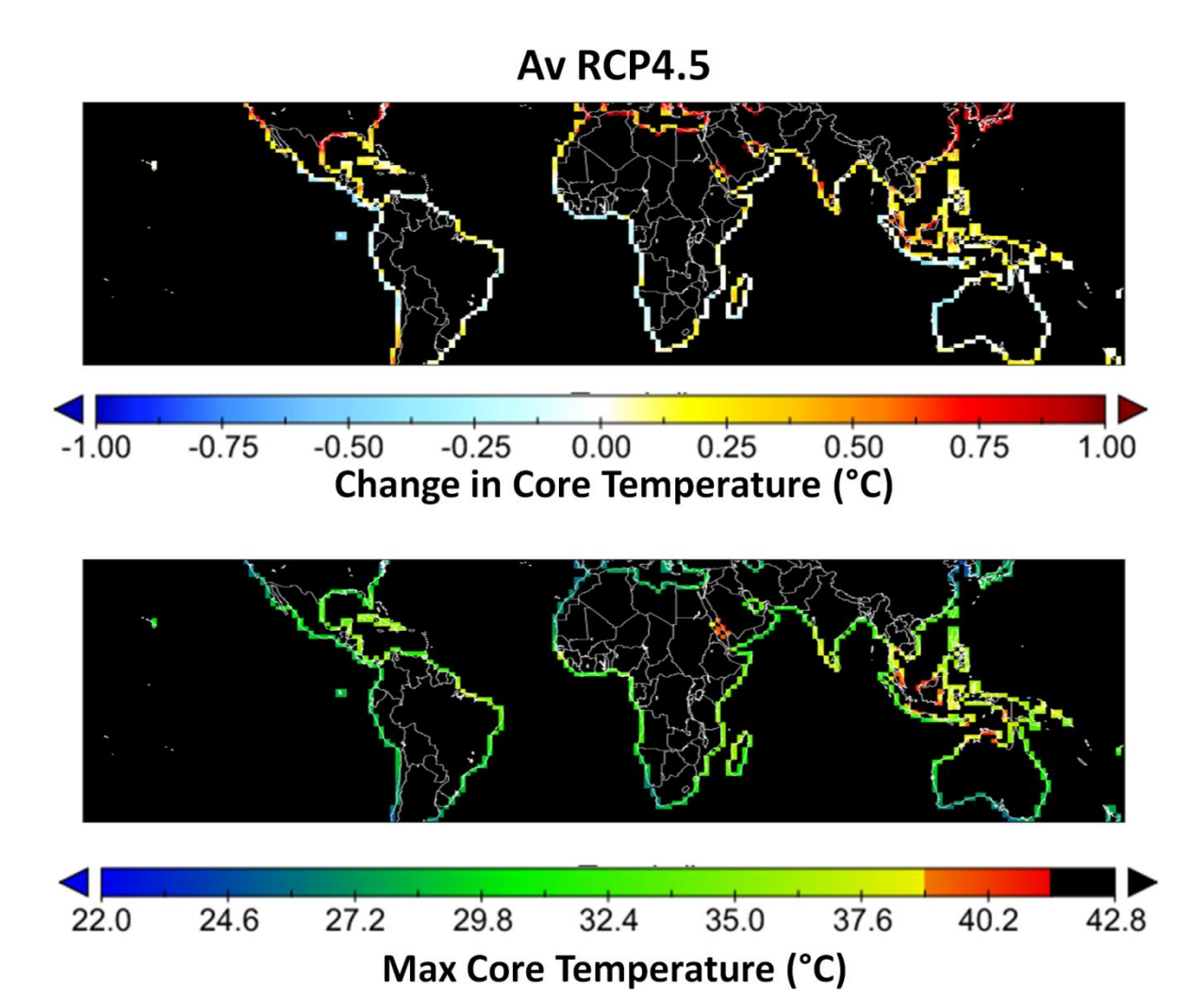


Figure 16. (Top) The maximum increase in core temperature of an Av leatherback in June for 2095-2100 during the nesting phase. (Bottom) The maximum core temperature of an Av leatherback in June for 2095-2100 during the nesting phase. Areas in orange to red are areas where the leatherback's core temperature is within one standard deviation of the CTM. Areas in black are where the leatherback's core temperature is above one standard deviation of the CTM.

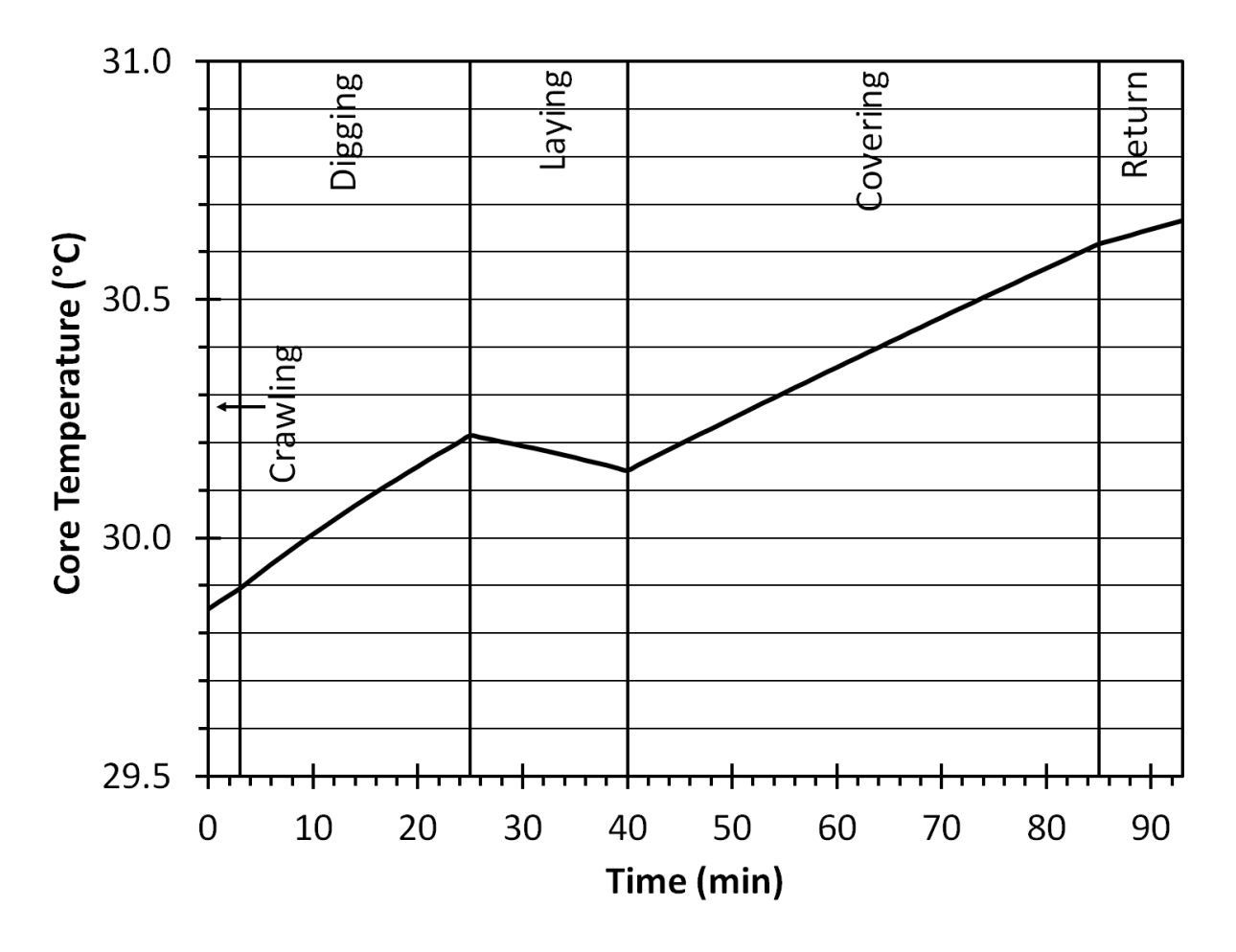


Figure 17. An example of the core temperature of a leatherback as a function of time during the nesting phase. Vertical lines demarcate separate parts of the nesting phase. Conditions for the following run were wind = 7.25 m/s, air temperature = 24.85 °C, and land temperature = 23.85°C.

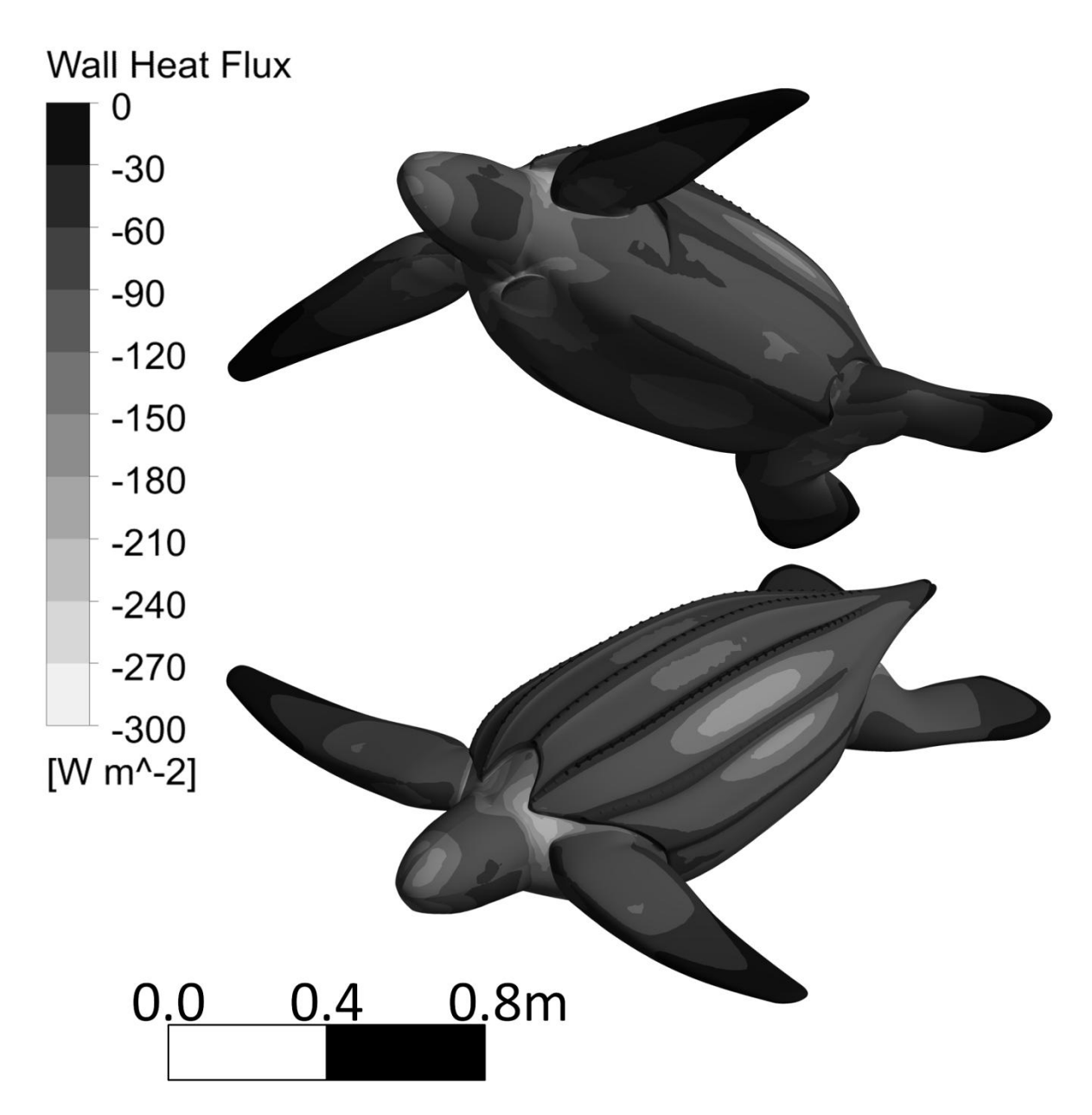


Figure 18. The heat flux contours on the terrestrial internal conduction model of the Av leatherback.

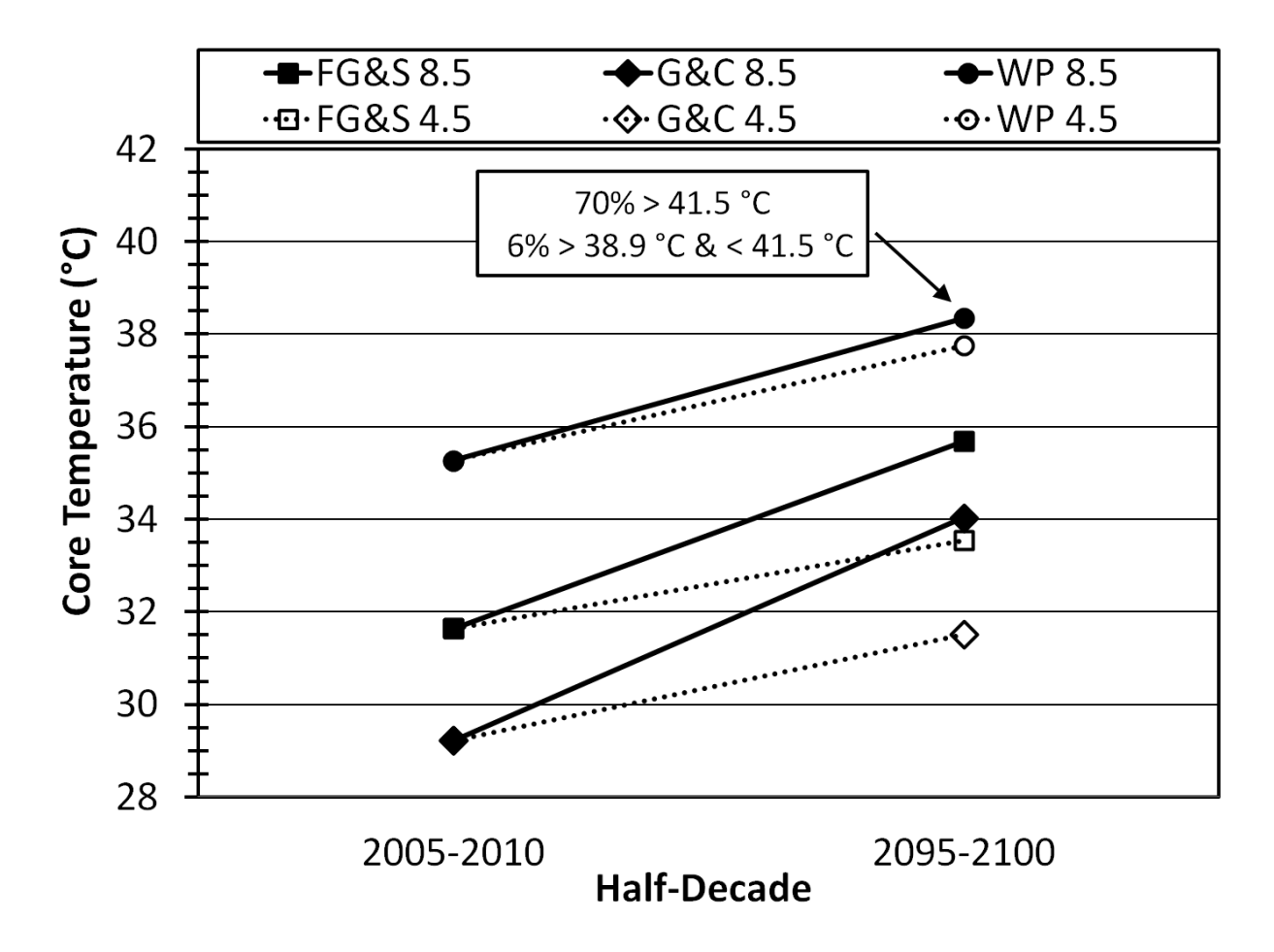
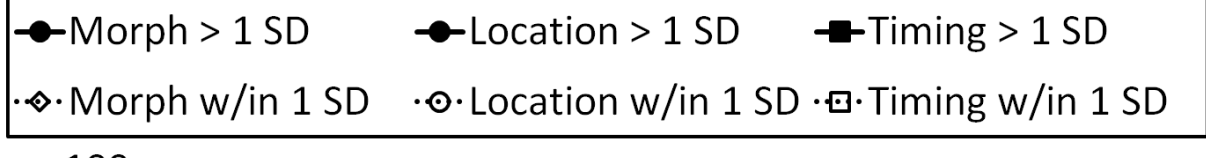


Figure 19. The change in the leatherback's core temperature and percent of land area inaccessible during the nesting phase in a given region for 2005-2010 to 2095-2100. Averages are for the relevant nesting months at each location (French Guiana and Suriname (FG&S) (nesting March-July), Gabon and Congo (G&C) (nesting November-February), and West Papua (WP) (nesting May-September)). In WP 2095-2100 6% of the area will push the leatherback's core temperatures within one standard deviation of the CTM (39.8 to 41.5 °C). 70% of the area will push the leatherback's core temperature above one standard deviation of the CTM (above 41.5 °C).



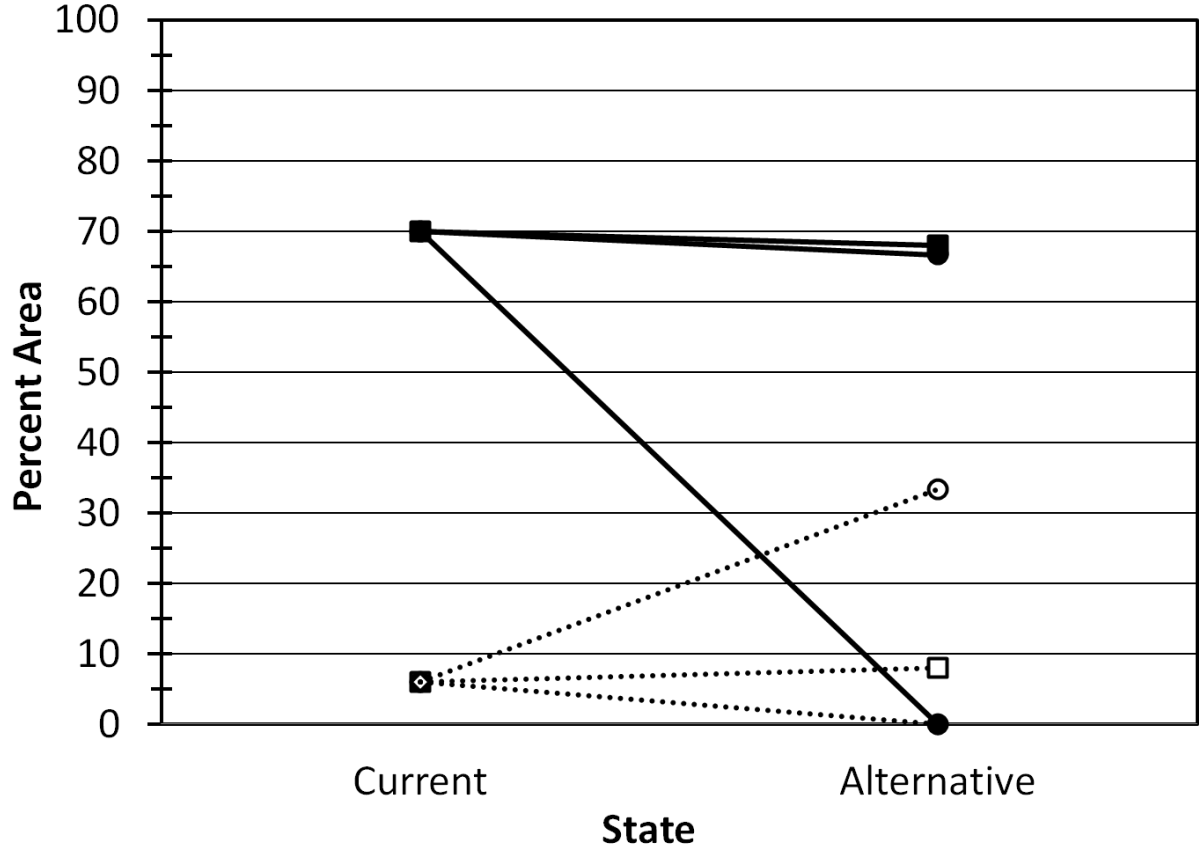


Figure 20. The change in the Av leatherback's percent of land area where its core temperature is within (w/in 1 SD) or above (> 1 SD) one standard deviation of the CTM (39.8 to 41.5 °C and above 41.5 °C respectively) for its current nesting behavior (current state) vs. an alternative nesting behavior in the WP region under RCP8.5. Averages are for the relevant nesting months at each location. The alternatives are to change nesting location (location), change in nesting seasonal timing (timing), or change in morphology (morphology) (i.e. going from Av to SN leatherback).

References

- Bartelt PE, Klaver RW, Porter WP (2010) Modeling amphibian energetics, habitat suitability, and movements of western toads, Anaxyrus (=Bufo) boreas, across present and future landscapes. Ecol Modell 221:2675–2686
- Boisclair D, Tang M (1993) Empirical analysis of the influence of swimming pattern on the net energetic cost of swimming in fishes. J Fish Biol 42:169–183
- Byrne R, Fish J, Doyle TK, Houghton JDR (2009) Tracking leatherback turtles (Dermochelys coriacea) during consecutive inter-nesting intervals: Further support for direct transmitter attachment. J Exp Mar Bio Ecol 377:68–75
- Carr A, Ogren L (1959) The Ecology and Migrations of Sea Turtles, 3 *Dermochelys* in Costa Rica.

 Am Museum Novit
- Chiang JCH, Chang C-Y, Wehner MF (2013) Long-Term Behavior of the Atlantic Interhemispheric SST Gradient in the CMIP5 Historical Simulations. J Clim 26:8628–8640
- Clarke LE, Edmonds JA, Jacoby HD, Pitcher HM, Reilly JM, Richels RG (2007) Scenarios of greenhouse gas emissions and atmospheric concentrations: U.S. climate change science program synthesis and assessment product 2.1a.
- Dormann CF (2007) Promising the future? Global change projections of species distributions. Basic Appl Ecol 8:387–397
- Dudley PN, Bonazza R, Porter WP (2013) Consider a non-spherical elephant: computational fluid dynamics simulations of heat transfer coefficients and drag verified using wind tunnel experiments. J Exp Zool A Ecol Genet Physiol 319:319–27
- Dudley PN, Bonazza R, Wyneken J, Jones TT, Porter WP Leatherbacks in silico: Modeling the core temperature of a sea turtle using computational fluid dynamics. Prep
- Dudley PN, Porter WP (2014) Using empirical and mechanistic models to assess global warming threats to leatherback sea turtles. Mar Ecol Prog Ser 501:265–278
- Eckert S a (2002) Swim speed and movement patterns of gravid leatherback sea turtles (*Dermochelys coriacea*) at St Croix, US Virgin Islands. J Exp Biol 205:3689–97
- Feldkamp SD (1987) Swimming in the California sea lion: morphometrics, drag and energetics. J Exp Biol 131:117–35
- Fuentes M, Fish M, Maynard J (2012) Management strategies to mitigate the impacts of climate change on sea turtle's terrestrial reproductive phase. Mitig Adapt Strateg Glob Chang

- Galli S, Gaspar P, Fossette S, Calmettes B, Hays GC, Lutjeharms JRE, Luschi P (2012) Orientation of migrating leatherback turtles in relation to ocean currents. Anim Behav 84:1491–1500
- Grant PR, Grant BR (2002) Unpredictable evolution in a 30-year study of Darwin's finches. Science 296:707–11
- Hawkes L a., Broderick AC, Coyne MS, Godfrey MH, Godley BJ (2007) Only some like it hot quantifying the environmental niche of the loggerhead sea turtle. Divers Distrib 13:447–457
- Hawkes L a., Witt MJ, Broderick AC, Coker JW, Coyne MS, Dodd M, Frick MG, Godfrey MH, Griffin DB, Murphy SR, Murphy TM, Williams KL, Godley BJ (2011) Home on the range: spatial ecology of loggerhead turtles in Atlantic waters of the USA. Divers Distrib 17:624–640
- Heimsath A, Lave J, Whipple K, Koons P, Brandon M (2003) Undesirable evolutionary consequences of trophy hunting. 426:655–658
- Hughes G., Luschi P, Mencacci R, Papi F (1998) The 7000-km oceanic journey of a leatherback turtle tracked by satellite. J Exp Mar Bio Ecol 229:209–217
- Jackson JB, Kirby MX, Berger WH, Bjorndal K a, Botsford LW, Bourque BJ, Bradbury RH, Cooke R, Erlandson J, Estes J a, Hughes TP, Kidwell S, Lange CB, Lenihan HS, Pandolfi JM, Peterson CH, Steneck RS, Tegner MJ, Warner RR (2001) Historical overfishing and the recent collapse of coastal ecosystems. Science 293:629–37
- James MC, Sherrill-Mix SA, Myers RA (2007) Population characteristics and seasonal migrations of leatherback sea turtles at high latitudes. Mar Ecol Prog Ser 337:245–254
- Jones TT, Hastings MD, Bostrom BL, Andrews RD, Jones DR (2009) Validation of the use of doubly labeled water for estimating metabolic rate in the green turtle (Chelonia mydas L.): a word of caution. J Exp Biol 212:2635–44
- Jones TT, Hastings MD, Bostrom BL, Pauly D, Jones DR (2011) Growth of captive leatherback turtles, *Dermochelys coriacea*, with inferences on growth in the wild: Implications for population decline and recovery. J Exp Mar Bio Ecol 399:84–92
- Jupiter Island sea turtle taging project (JISTTP) (2012) Arch Carr Cent Sea Turt Res Leg Database Initiat
- Kearney M, Porter W (2009) Mechanistic niche modelling: combining physiological and spatial data to predict species' ranges. Ecol Lett 12:334–50
- Kim ST, Yu JY (2012) The two types of ENSO in CMIP5 models. Geophys Res Lett 39:1-6

- Lambardi P, Lutjeharms J, Mencacci R, Hays G, Luschi P (2008) Influence of ocean currents on long-distance movement of leatherback sea turtles in the Southwest Indian Ocean. Mar Ecol Prog Ser 353:289–301
- Luschi P, Sale a, Mencacci R, Hughes GR, Lutjeharms JRE, Papi F (2003) Current transport of leatherback sea turtles (Dermochelys coriacea) in the ocean. Proc Biol Sci 270 Suppl :S129–32
- Lutcavage ME, Bushnell PG, Jones DR (1990) Oxygen transport in the leatherback sea turtle Dermochelys coriacea. Physiol Zool 63:1012–1024
- Médicci MR, Buitrago J, Guada H, Eckert K (2011) Estimación poblacional, rutas migratorias y características morfométricas de la tortuga cardón (Dermochelys coriacea, Vandelli 1761) en las playas de Cipara y. 40:309–326
- National Marine Fisheries Service and U.S. Fish and Wildlife Service (1992) Recovery plan for leatherback turtles in the U.S. Caribbean, Atlantic, and Gulf of Mexico. Washington, D.C.
- Paladino FV, O'Connor MP, Spotila JR (1990) Metabolism of leatherback turtles, gigantothermy, and thermoregulation of dinosaurs. Nature 344:858–860
- Paladino FV, Spotila JR, O'Connor MP, Gatten, Robert E. J (1996) Respiratory physiology of adult leatherback turtles (*Dermochelys coriacea*) while nesting on land. Chelonian Conserv Biol 2:223–229
- Parmesan C, Yohe G (2003) A globally coherent fingerprint of climate change impacts across natural systems. Nature 421:37–42
- Phillips B, Chipperfield J, Kearney M (2008) The toad ahead: Challenges of modelling the range and spread of an invasive species. Wildl Res 35:222
- Pike D a. (2013) Climate influences the global distribution of sea turtle nesting. Glob Ecol Biogeogr 22:555–566
- Pikesley SK, Maxwell SM, Pendoley K, Costa DP, Coyne MS, Formia A, Godley BJ, Klein W, Makanga-Bahouna J, Maruca S, Ngouessono S, Parnell RJ, Pemo-Makaya E, Witt MJ (2013) On the front line: integrated habitat mapping for olive ridley sea turtles in the southeast Atlantic (R Loyola, Ed.). Divers Distrib 19:1518–1530
- Porter WP, Sabo JL, Tracy CR, Reichman OJ, Ramankutty N (2002) Physiology on a landscape scale: plant-animal interactions. Integr Comp Biol 42:431–53

- Riahi K, Grübler A, Nakicenovic N (2007) Scenarios of long-term socio-economic and environmental development under climate stabilization. Technol Forecast Soc Change 74:887–935
- Saba V (2013) Oceanic Habits and Habitats Dermochelys coriacea. In: The Biology of Sea Turtles.p 163–188
- Shackell NL, Frank KT, Fisher J a D, Petrie B, Leggett WC (2010) Decline in top predator body size and changing climate alter trophic structure in an oceanic ecosystem. Proc Biol Sci 277:1353–60
- Shillinger GL, Palacios DM, Bailey H, Bograd SJ, Swithenbank AM, Gaspar P, Wallace BP, Spotila JR, Paladino F V, Piedra R, Eckert SA, Block BA (2008) Persistent leatherback turtle migrations present opportunities for conservation. PLoS Biol 6:e171
- Smith SJ, Wigley TML (2006) Multi-Gas Forcing Stabilization with Minicam. Energy J SI2006:373–392
- Southwood AL, Andrews RD, Paladino F V, Jones DR (2005) Effects of diving and swimming behavior on body temperatures of pacific leatherback turtles in tropical seas. Physiol Biochem Zool 78:285–297
- Swinbank WC (1963) Long-wave radiation from clear skies. Q J R Meteorol Soc 89:339–348
- Thomas CD, Cameron A, Green RE, Bakkenes M, Beaumont LJ, Collingham YC, Erasmus BFN, Siqueira MF De, Grainger A, Hannah L, Hughes L, Huntley B, Jaarsveld AS Van, Midgley GF, Miles L, Ortega-Huerta M a, Peterson a T, Phillips OL, Williams SE (2004) Extinction risk from climate change. Nature 427:145–8
- Walker G (2010) The influence of morphology and artificial light on terrestrial transit of the leatherback turtle (*Dermochelys coriacea*)
- Wallace BP, Williams CL, Paladino F V, Morreale SJ, Lindstrom TR, Spotila JR (2005)

 Bioenergetics and diving activity of internesting leatherback turtles *Dermochelys coriacea* at Parque Nacional Marino Las Baulas, Costa Rica. J Exp Biol 208:3873–84
- Webb PW (1971) The swimming energetics of trout. J Exp Biol 55:521–540
- Wise M, Calvin K, Thomson A, Clarke L, Bond-Lamberty B, Sands R, Smith SJ, Janetos A, Edmonds J (2009) Implications of limiting CO2 concentrations for land use and energy. Science 324:1183–6
- Woledge R (1968) The energetics of tortoise muscle. J Physiol 197:685-707

Conclusion

We have shown that modern CFD techniques can accurately model both static and dynamic animals as well as the internal thermal environment. We demonstrated that this information combined with GCMs could produce fundamental niche maps of a species (assuming that species is thermally limited and not resource limited). We used leatherback sea turtles as an example species for our method because of their complex physiology and life history, and that IUCN considers them a threatened species.

By creating a biophysically based fundamental niche model for the leatherback sea turtle, we found that the average-sized leatherbacks will be in thermal distress in Southeast Asia under projected global warming scenarios. We also found that larger leatherbacks will be in thermal distress in other world regions if global warming is not mitigated.

We hope to conduct further analysis to produce a complete set of maps spanning 2010 to 2100. These maps and their raw data could provide managers and conservationists with a valuable tool in leatherback conservation.